Spring 2013

Pulsating aurora: Source region & morphology

Allison Jaynes

PULSATING AURORA: SOURCE REGION & MORPHOLOGY

BY

ALLISON JAYNES

B.S. in Physics, University of North Carolina at Greensboro 2006

DISSERTATION

Submitted to the University of New Hampshire
in Partial Fulfillment of
the Requirements for the Degree of

Doctor of Philosophy

in

Physics

May, 2013

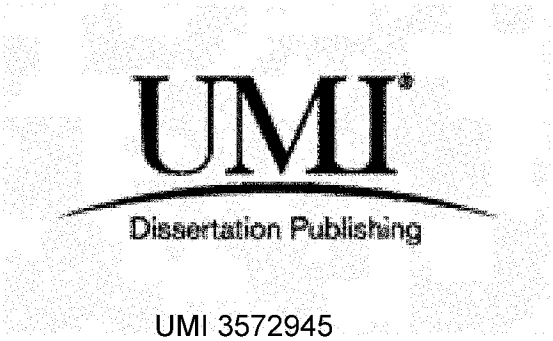

ProQuest LLC
789 East Eisenhower Parkway
P.O. Box 1346
Ann Arbor, MI 48106-1346

This dissertation has been examined and approved.

Dissertation Director, Marc Lessard, Associate Professor of Physics

Lynn Kistler, Professor of Physics

Dawn Meredith, Associate Professor of Physics

Eberhard Moebius, Professor of Physics

Thomas Moore, Senior Project Scientist, NASA Goddard

2/1/2013

Date

ACKNOWLEDGMENTS

Every dissertation acknowledgements page begins by thanking the student's research advisor. This is not, however, a perfunctory gesture of gratitude. I wish to wholeheartedly express my appreciation towards my advisor, Marc Lessard, not just for being a great scientific advisor, but for being a role model, an understanding leader, a cheerleader when I needed one, and even a little bit of a life coach. I could not have hoped for a better advisor to guide me through grad school and prepare me for a career in the physics world.

A big thanks is extended to my UNH thesis committee: Professor Lynn Kistler, Professor Dawn Meredith, and Professor Eberhard Moebius. Your suggestions and edits to this document have resulted in a great improvement over its original form. And thanks is due to Dr. Thomas Moore of NASA Goddard Space Flight Center, for agreeing to be a long-distance member of my committee, and for acting as my NASA-based advisor during my three-year Graduate Student Research Fellowship tenure. On that note, I wish to thank the New Hampshire Space Grant Consortium and NASA GSRP for the generous amounts of funding invested in my graduate education.

I can't forget to thank the supportive group of engineers and scientists that worked on the various rocket launches in which I participated. First and foremost is Paul Riley of UNH; the best electrical engineer and arctic traveling partner ever. Also, many thanks to the engineers at Wallops Flight Facility, the staff at Poker Flat Research Range and Andøya Rocket Range, and the scientists I had the great pleasure of working with at UNIS (The University Centre in Svalbard), Norway.

Thanks to graduate school support staff and professors, fellow grad students - network of positivity.

An enormous thank you goes to Dr. Sarah Jones. I honestly have no idea what I would have done without you. You have been an insightful mentor and true friend through it all.

Thanks to the following collaborators and co-conspirators (by no means an exhaustive list): Juan Rodriguez and Paul Loto'aniu of NOAA, Eric Donovan and Dave Knudsen of the University of Calgary, Robert Michell and Marilia Samara of SwRI, Hans Stenbaek-Nielsen of University of Alaska - Fairbanks, and Kristina Lynch of Dartmouth College.

I also need to give thanks to the panoply of supporting characters in the field that have all inadvertently helped to cement my enthusiasm for the space sciences and have honestly shown me that there is a community of great people that have the same curiosities as I do. Thanks to all my graduate school professors, the support staff, and my fellow grad students for fostering a network of positivity.

Thanks to the past and present occupants of Room 426 AB (aka the Bomb Shelter). It's not easy to share an office space with a complete stranger and have that turn into lasting professional and personal relationships. The office has been my safe haven of support and solace through a lot of life experiences - so thanks to everyone who was around. Edith and I are both very grateful!

A great debt is owed to Professor Steve Danford, Professor Ed Hellen and Professor Alice Haddy for being my undergraduate physics support team (more than they perhaps realize) and providing the catalyst for my enthusiasm to develop into a real passion and eventually a career.

Lastly, overwhelming gratitude is due to my close friends and family for putting up with this entire process, including Matthew most of all. I'm not sure how he managed to bear the brunt of my stress and frustration, but I'm very glad he did. Now, hopefully, he can share in my elation as we both move on to a new chapter in our lives.

Table of Contents

List of Figures

ABSTRACT

PULSATING AURORA: SOURCE REGION & MORPHOLOGY

by

Allison Jaynes

University of New Hampshire, May, 2013

Pulsating aurora, a common phenomenon in the polar night sky, offers a unique opportunity to study the precipitating particle populations responsible for this subtle yet fascinating display of lights. The conjecture that the source of these electrons originates near the equator, made decades ago, has now been confirmed using *in-situ* measurements. In this thesis, we present these results that compare the frequencies of equatorial electron flux pulsations and pulsating aurora luminosity fluctuations at the ionospheric footprint. We use simultaneous satellite-based data from GOES 13 and ground-based data from the THEMIS allsky imager array to show that there is a direct correlation between luminosity fluctuations near the ground and particle pulsations in equatorial space; the source region of the pulsating aurora.

Pulsating aurora almost exclusively occurs embedded within a region of diffuse aurora. By studying the two particle populations, one can contribute to the theory behind auroral pulsations. The interplay between the two auroral types, and the systems that control them, are not yet well known. We analyze ground optical observations of pulsating aurora events to attempt to characterize the relationship between the two types of auroral precipitation.

Pulsating aurora is a significant component of energy transfer within the framework of magnetosphere-ionosphere coupling. Further study of the morphology, total energy deposition, and the pulsation mechanism of pulsating aurora is key to a better understanding of our earth-sun system.

CHAPTER 1

INTRODUCTION

The northern lights have fascinated mankind for centuries. The nightly dance of light emissions excited by charged particles originating from the sun is one of the truly awesome natural wonders of the world. As charged particles, originating from the sun and the earth's atmosphere, are accelerated by changes in magnetospheric electric and magnetic fields into the earth's upper atmosphere, they collide with atmospheric atoms, molecules and ions to create the dramatic natural light display we call aurora. Since these precipitating particles are confined to move along magnetic field lines, the study of the structure and dynamics of the aurora allows us a chance to study the near-earth plasma environment and to investigate the plasma populations in the magnetosphere that ultimately give rise to the aurora.

Kristian Birkeland, a Norwegian auroral researcher, and the first scientist to link the northern lights to the particles streaming from the sun, wrote:

> "It seems to be a natural consequence of our points of view to assume that the whole of space is filled with electrons and flying electric ions of all kinds. We have assumed that each stellar system in evolutions throws off electric corpuscles into space. It does not seem unreasonable therefore to think that the greater part of the material masses in the universe is found, not in the solar systems or nebulae, but in 'empty' space." (excerpt from The Norwegian Aurora Polaris Expedition 1902-1903)

It is this study of plasmas in 'empty space' that bring us a deeper understanding of our natural world.

The aurora is the visible component of the complex and extensive system referred to as space weather. Space weather encompasses the entire near-earth space environment and the changing conditions of this expanse. The study of these evolving conditions has consequences of great import for our current civilization on earth. Charged particles gaining entry to our atmosphere can affect or permanently damage our communications, GPS and weather satellites. Electric power lines and transformers can be impaired during high geomagnetic activity, disrupting power transmission to potentially significant population sizes. In addition, the enhanced radiation is unsafe for airline pilots and passengers traveling through the polar cap during strong magnetic storms. Degradation to pipelines at high latitudes has also been widely reported, as a result of ground currents induced by storm activity. These health, safety and commercial issues all benefit from a higher understanding of space weather, magnetosphere-ionosphere coupling and the aurora.

Pulsating aurora, in particular, offers a unique opportunity to study the source of the precipitating particle populations responsible for this subtle yet fascinating display of lights, due to its frequency and duration. To fully understand this phenomenon and its generation mechanisms, a survey of all the magnetospheric and ionospheric components is necessary. This requires the use of ground instrumentation, such as optical measurements from allsky cameras and photometers, as well as observations using riometers (which measure ionosphere absorption)and incoherent scatter radar (which measure the conductivity of the ionosphere), and magnetic field measurements from magnetometer arrays. A complete comprehension also necessitates above ground measurements, both *in-situ* data in the auroral altitudes using sounding rockets and in the magnetosphere domain using satellite experiments. Pulsating aurora is a visual manifestation of large-scale, sustained coupling

between the magnetosphere and ionosphere. Thorough study of the specific transport and energization mechanisms involved will help us to understand this coupling more completely.

The source region for the energetic modulated particles that make up pulsating auroral forms has been a debated topic for some time. Sounding rocket studies from as early as the 1970's have determined, by and large, that the source region lies in the equatorial magnetosphere. This conclusion was reached by analyzing velocity dispersion between higher and lower energy electrons responsible for the auroral pulsations. Inter-hemisphere research of magnetically conjugate auroral forms (occurring at the two opposite ends of the same magnetic field line) have chiefly aided in confirming this premise, although a few studies show a distinct lack of conjugacy. The mechanism implicated in the generation of these modulations is VLF pitch-angle scattering of particle populations. VLF chorus has been shown to share the same temporal occurrence domain as pulsating aurora, as well as the same spatial extent in the magnetosphere.

The relationship between diffuse particle precipitation and pulsating aurora particles contains quite a few unknowns. The particles appear to be two separate particle populations, yet pulsating aurora is almost always found embedded in a background of diffuse aurora. The precipitations may also dwell at entirely different altitudes, with little to no overlap. There is, however tenuous or substantial, some connection between processes that exhibit each auroral form, as we will see in the course of this dissertation. Exploring these processes has implications for both types of aurora. The diffuse background and pulsating aurora are generally described in the literature as two disparate phenomena, with separate generation theories for each. Yet, the particles responsible for both diffuse and pulsating are theorized to come from the same region (the equatorial plane near geosynchronous orbit), and conjectured to occur from the same mechanism (pitch-angle diffusion via wave-particle interactions). A study of the interaction between these two not-so-distinct particle

precipitations will help to formulate a more coherent theory behind the pulsating aurora modulations.

This dissertation tackles the two outstanding questions mentioned above, namely: 1) *Where does the source region for the modulated pulsating aurora electrons originate?* and 2) *What is the link between the diffuse population and pulsating aurora, in the context of the theories behind the pulsations?*

Chapters 2 through 5 serve primarily to set the stage for the dissertation research, although some smaller studies conducted are contained within these sections. Chapter 2 begins with the basics of space plasma, to provide a general framework for the discussions ahead. Chapter 3 presents a quick overview of the earth's magnetosphere and the structure within. Chapter 4 is a treatise on the physics of the aurora, including energy spectrum, physical characteristics, the current systems that govern the paths of charged particles and an explanation of auroral substorms. Chapter 4 also includes a section on observational techniques for remote and *in-situ* sensing of the aurora; of particular note is research we conducted on designing an auroral imager (Sec. 4.5.1).

Chapter 5 delves deeper into a specific auroral form: pulsating aurora. In this chapter, the features of pulsating aurora are outlined, including the temporal and spatial distinctions, and precipitation features. Previous ground- and space-based determinations of a source region for the energetic electron modulations that characterize this type of aurora are covered as well. To finish, we present a study we completed on widespread, persistent pulsating aurora that highlights the importance of pulsating aurora in large-scale energy deposition in the ionosphere (Sec. 5.5). The work centers on a pulsating aurora event that spans the entire nightside, persisting for many hours, and even extending into the dayside in MLT (magnetic local time). While substorms come and go throughout the interval, the pulsating aurora does not appear to be a result of the substorm injections, since it pre-exists

the substorms and lasts longer than what would be considered a recovery phase. However, the brightness of the pulsations may be briefly enhanced by the substorms.

The study detailed in Chapter 6 concerns conjugate satellite and ground observations of electron flux modulations. Here, we present first results of *in-situ* magnetospheric particle flux pulsations that correlate directly with visible pulsating aurora. Using a particle detector on the GOES 13 satellite, energetic electrons are observed with a periodic modulation pattern in equatorial space at geosynchronous orbit. At the same time, auroral pulsations are seen from the ground using a THEMIS allsky imager, along the magnetic footpoint of the satellite. The two periodic fluctuations correlate very well, insinuating a location of the source region for the pulsating aurora electrons out in the equatorial magnetosphere. This equatorial source region of pulsating aurora has been a long-standing conjecture based on earlier sounding rocket experiments, but had not been confirmed until now. Cross-correlation coefficients were plotted for each pixel in the allsky imager with the electron flux to create contour plots of highly correlated pulsating patches. The results also show that at times several pulsating patches are correlated at once. This study has implications for the theoretical pulsation mechanisms, as well as perhaps putting constraints on magnetic field line mapping. The major success of the investigation is the determination of the source region of pulsating aurora electrons.

Chapter 7 explores the relationship between diffuse aurora and pulsating aurora, by offering preliminary results from filtered allsky images taken of pulsating events at both 4278 Å and 5577 Å from near Poker Flat, Alaska. The ratio of the two emissions can communicate information about the characteristic energy of the pulsations. A decrease in this ratio has often been reported during the maxima of the auroral pulsation. Additionally, data from an observation period of pulsations observed over Churchill, Manitoba is analyzed. The pulsations show a peculiar feature from time to time: a sudden intensification of the

pulsation followed by a complete erasure of the aurora (including the diffuse background). This "diffuse aurora eraser" is likely a quenching of the pulsation mechanism by as-yet-unknown means.

The main conclusions of the dissertation are summarized in Chapter 8. This body of work is presented as a further step towards understanding the physical processes behind pulsating aurora, and the impact it has on the larger magnetosphere-ionosphere coupling system. Much attention is given to the discrete aurora, especially the magnetic substorm process that is intimately involved; diffuse aurora, including pulsating aurora, has largely been overlooked in the scope of auroral research. Here, we strive to understand this less-studied auroral component; from the source region of modulated particles, to the visible aurora in the ionosphere. Each bit of knowledge gained is a piece of the puzzle, whether it fits into the ionospheric picture or the magnetospheric one. Only with contributions from both ends, and consideration of the full extent of auroral precipitation, will the picture be eventually complete.

CHAPTER 2

SPACE PLASMA

2.1 Overview of Plasmas

The form that matter takes in the realm of space physics is not simply solid, liquid or gas, but instead plasma - a fourth state of matter that consists of a sparse, tenuous "gas" of charged particles. In a plasma, the ions and electrons react to electromagnetic fields in such a way that their behavior may often be described using fluid motion equations. A space plasma is rarefied enough to where interactions between particles can be considered non-existent and only the effects of the relevant fields needs to be accounted for. This leads to elegant equations that exclusively consider average collective motions of and forces on many particles at once, imitating a fluid flow.

Not every low-density gas of particles can be considered a true plasma. One requirement the gas must meet is overall charge neutrality:

$$n \simeq n_e \simeq n_i \tag{2.1}$$

This is an approximation on a large scale, of course, since if $n_e = n_i$ entirely everywhere, there would be no charge separation and thus no electrostatic fields would exist. Instead, we consider the space plasma to be quasi-neutral; electrically neutral on large spatial scales, but locally able to deviate from this state for short durations. A fundamental parameter

of a plasma, based on this idea of neutrality, can be derived starting with the electrostatic potential of a lone particle (say, a proton):

$$\phi = \frac{q}{4\pi\epsilon_0 r} \tag{2.2}$$

Dropping this proton into an electron-proton plasma alters its potential since the particles will be attracted to or repelled by the added charge. In this case, we consider electrons as the only moving particles; the ions are heavy and slow-moving, and therefore have negligible displacement relative to the mobile electrons. The distorted potential must satisfy Poisson's equation

$$\nabla^2\phi = -\frac{e}{\epsilon_0}(n_i - n_e) \tag{2.3}$$

Here, $n_e = n$ due to our quasi-neutral constraint. And n_e will have to include the distortion introduced by the additional proton, but can be described using Boltzmann's law for a Maxwellian distribution, where $q = -e$

$$n_e = n_0 \exp\left[\frac{e\phi}{k_B T_e}\right] \tag{2.4}$$

This can then be expanded into a Taylor series within Poisson's equation, assuming weak potentials, $|e\phi| \ll k_B T_e$,

$$\nabla^2\phi = -\frac{n_0 e}{\epsilon_0}\left(1 - \exp\left[\frac{e\phi}{k_B T_e}\right]\right), \tag{2.5}$$

$$\nabla^2\phi = \frac{n_0 e^2}{\epsilon_0 k_B T_e}\phi, \tag{2.6}$$

with keeping only first-order terms of the series. We can assume a spherically symmetric

potential,

$$\frac{\partial^2}{\partial r^2}(r\phi) - \frac{n_0 e^2}{\epsilon_0 k_B T_e}(r\phi) = 0, \tag{2.7}$$

to obtain a differential equation with a known solution,

$$\phi = \frac{const.}{r}\, e^{-r/\lambda_D}, \tag{2.8}$$

where r is the radius from the center of the test proton. It is easily seen that

$$\lambda^2{}_D = \frac{\epsilon_0 k_B T_e}{n_0 e^2} \tag{2.9}$$

The *Debye length*, λ_D, describes the radius of a sphere of influence around the particle, wherein the proton is affecting the plasma distribution, and outside of which the plasma is unperturbed.

The number of particles within this Debye sphere, can be represented as $N_D = n_0 \lambda_D^3$, where N_D is often called the *plasma parameter*. We can think of this as an additional constraint on a plasma; it is necessary that this number density is much greater than identity, $N_D \gg 1$, in order for the plasma to behave ideally.

Another defining parameter of a plasma is the frequency with which it oscillates. Again, assuming the ions are relatively static within the plasma, if we start with a volume of electrons and displace it by a small amount, δx, an electric field arises from charge displacement. The field pulls back on the electrons with a force described by Hooke's Law

$$\mathbf{F} = -k\ \delta\mathbf{x}, \tag{2.10}$$

where k is known as the spring constant. The inertial electrons move back towards their initial position, yet overshoot their starting point, and the system behaves as a harmonic

oscillator,

$$-eE = m_e \frac{d^2\,\delta x}{dt^2} = -\frac{n_0 e^2}{\epsilon_0}\,\delta x \tag{2.11}$$

Simplifying to,

$$\frac{d^2\,\delta x}{dt^2} + \left(\frac{n_0 e^2}{\epsilon_0 m_e}\right)\,\delta x = 0, \tag{2.12}$$

we end up with the equation for a simple harmonic oscillator, where the parenthetical expression is the angular frequency of said oscillation. This plasma frequency, ω_p, is an inherent characteristic of a space plasma. Other frequencies exist, such as the cyclotron frequency of a charge in a uniform magnetic field, and the frequency of collisions between different particles; these quantities will be discussed in the next sections.

2.2 Single Particle Motion

A particle within an electric field and magnetic field experiences a force referred to as the *Lorentz force*

$$\mathbf{F} = q\mathbf{E} + q\mathbf{v} \times \mathbf{B} \tag{2.13}$$

In potential form,

$$\mathbf{B} = \nabla \times \mathbf{A},\ \mathbf{E} = -\nabla\phi - \frac{\partial \mathbf{A}}{\partial t} \tag{2.14}$$

We can get the particle's motion using Newton's Law

$$m\frac{d\mathbf{v}}{dt} = q\mathbf{E} + q\mathbf{v} \times \mathbf{B}, \tag{2.15}$$

where we are neglecting gravitational forces for this analysis. We can now demonstrate one of the significant repercussions of this equation of motion; a magnetic field affects the particle motion only in the direction *perpendicular to* its original motion.

In a uniform magnetic field with $\mathbf{B} = B\hat{\mathbf{z}}$, and no electric field, $\mathbf{E} = 0$, we get components

$$m\dot{v}_x = qBv_y \tag{2.16}$$

$$m\dot{v}_y = qBv_x \tag{2.17}$$

$$m\dot{v}_z = 0 \tag{2.18}$$

Taking the second derivative, and substituting, gives

$$\ddot{v}_x = -\Omega_c^2 v_x \tag{2.19}$$

$$\ddot{v}_y = -\Omega_c^2 v_y \tag{2.20}$$

which insinuates circular motion of the particle around the magnetic field direction, with angular frequency $\Omega_c = \frac{qB}{m}$, which we dub the *cyclotron frequency* or *gyrofrequency* (Fig. 2-1). From this we can get the *gyroradius*,

$$r_c = \frac{m\ v_\perp}{|q|\ B}\ v_\parallel, \tag{2.21}$$

also known as the *Larmor radius* or *cyclotron radius.*

Now we need to consider what happens when the particle has a velocity parallel to the magnetic field, when the electric field is non-zero or when the magnetic field contains a gradient, as is often the case. With a constant parallel velocity, $v_\parallel$, the circular motion described above becomes a helical trajectory, with a *pitch angle* defined as

$$\alpha = \tan^{-1}\left(\frac{v_\perp}{v_\parallel}\right) \tag{2.22}$$

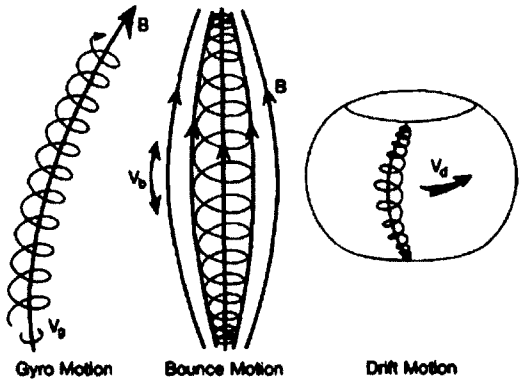

Figure 2-1: Schematic of the three particle motions within the earth's magnetic field. The first diagram shows gyromotion around a field line. The second represents trapped particles engage in bounce motion. And the third depicts any of the potential drift motions, while the particle undergoes both gyro and bounce motion. Reprinted with permission from *Kivelson and Russell* (1995).

Adding an electric field changes the particle path as well. We can break up the field into components and examine what happens in each case. First, let's assume an electric field parallel to the magnetic field. This parallel $E_{\|}$ will accelerate the particle along the direction of $\mathbf{B}$; one direction if it's an electron, another if it's an ion. Add in enough particles and the resulting field induced by charge separation will cancel out $E_{\|}$, so we can therefore consider this E-field direction to be irrelevant in a general plasma population. The perpendicular electric field component is a different story entirely. Consider an electric field in the x direction. The resulting components of $E_{\perp}$, from Eq. 2.15, are

$$\dot{v}_x = \Omega_c v_y + \frac{q}{m} E_x \tag{2.23}$$

$$\dot{v}_y = -\Omega_c v_x \tag{2.24}$$

Continuing as before, the second derivatives are

$$\ddot{v}_x = -\Omega_c^2 v_x \tag{2.25}$$

$$\ddot{v}_y = -\Omega_c^2 \left(v_y + \frac{E_x}{B} \right) \tag{2.26}$$

Notice that Eq. 2.26 is similar to our original motion without an electric field, Eq. 2.20, but with an offset in the y direction. This is easy to picture. As the particle goes along its helical orbit, it will be accelerated during part of an orbit and decelerated during another part of an orbit. So one portion of the orbit will have a larger radius of curvature and one portion will have a smaller radius. The result is a sort of "stretched slinky" path, with a quantifiable *drift velocity*

$$\mathbf{v}_E = \frac{\mathbf{E} \times \mathbf{B}}{B^2} \tag{2.27}$$

The above is often referred to as $E \times B$ *drift.* This motion is independent of charge, therefore both ions and electrons drift in the same direction as they move along the earth's magnetic field lines, as we will discuss later. Now we turn to the treatment of magnetic field gradients and curvature. If a gradient in the magnetic field exists perpendicular to that field, the particle will drift in another way, perpendicular to both ∇B and $\mathbf{B}$. As the particle's trajectory goes towards the direction of a weaker B-field, the radius of curvature will grow smaller. Similarly, as the trajectory goes in the direction of the stronger field, the radius will increase. This results in a *gradient drift velocity*

$$\mathbf{v}_\nabla = \frac{m v_\perp^2}{2q} \frac{\mathbf{B} \times \nabla B}{B^3} \tag{2.28}$$

Unlike the $E \times B$ drift, the gradient drift is charge dependent, and will cause ions and electrons to drift in opposite directions, creating electric currents that play a large role in

the structure of the earth's ionosphere. The curvature of the earth's magnetic field lines cause particles to experience a centrifugal force as they move along their paths, which induces yet another type of drift motion: *curvature drift*. If we define $\mathbf{R}_c$ as the local radius of curvature, we can show the centrifugal force to be

$$\mathbf{F}_{centrif} = m v_{\parallel}^2 \frac{\mathbf{R}_c}{R_c^2} \tag{2.29}$$

Analogously to the above drift velocities, we can obtain an expression for the curvature drift velocity (Fig. 2-1)

$$\mathbf{v}_c = \frac{m v_{\parallel}^2}{q} \frac{\mathbf{R}_c \times \mathbf{B}}{R_c^2 B^2}, \tag{2.30}$$

which will also factor into the discussion of the currents in the ionosphere.

2.3 Adiabatic Invariants & Trapped Particles

In the preceding section, we showed that particles can drift due to different electromagnetic field configurations, and at times drift in opposite directions due to their charge. This opposing movement leads to the generation of transverse currents, whose strengths are impacted by the energy of the particles. Of particular interest is a quantity known as the *magnetic moment*

$$\mu = \frac{\frac{1}{2} m v_{\perp}^2}{B} \tag{2.31}$$

which is the ratio between the perpendicular component of the particle energy and the strength of the magnetic field. The magnetic moment is considered the first of three *adiabatic invariants* considered in the earth's magnetic domain. The quantity, μ, remains constant in this system, as long as the magnetic field changes adiabatically - that is, if the field changes slowly enough relative to the starting condition, within one gyroperiod.

As a particle travels in the earth's magnetosphere through regions of changing B, it must undergo some acceleration if μ is to remain constant. We can examine μ in terms of pitch angle, by substituting for $v_\perp$ using Eq. 2.22

$$\mu = \frac{\frac{1}{2}mv^2 \sin^2 \alpha}{B} = \frac{W \sin^2 \alpha}{B} \tag{2.32}$$

Since μ and the total energy are constants, the only thing that can change with B is the pitch angle, α. As B increases, α increases as well. Though the total energy remains unchanged, the components will vary with the magnetic field: in regions of increasing field strength, $v_\perp$ will increase as $v_\parallel$ dwindles. In a converging magnetic field geometry, like the earth's magnetosphere, the particle will reach a point where the parallel velocity disappears; here, $\sin \alpha$ must be at a maximum, which occurs at $\alpha = 90°$. This point along the field line is called the *magnetic mirror point*, B_m, and it is the point where the particle will be reflected back in the other direction. A *trapped* particle may bounce back and forth between mirror points in a dipole-like field (Fig. 2-1), until there is some change in the magnetic topology, or in the pitch angle itself, drastic enough to break one or more adiabatic invariants.

A second adiabatic invariant is related to this periodic bounce motion. For the parallel motion of a particle moving between two mirror points we can write

$$J = \oint m v_\parallel \, ds \tag{2.33}$$

and using energy conservation,

$$J = \sqrt{2\mu m} \oint \sqrt{B_m - B(s)} \, ds \tag{2.34}$$

where s is the distance along the field line (in the guiding center of the particle trajectory),

ds is an element of that length, the closed-path integral is taken over the entire period between the mirror points, and J is referred to as the *bounce invariant.* This quantity is invariant for field changes much slower than the bounce period. The consequence of Eq. 2.34 is that the parallel component of the particle energy increases as the length of the bounce path is decreased.

A trapped particle will drift azimuthally in an axisymmetric magnetic field, according to the parameters listed in the previous section, tracing out a "shell" as it completes one full revolution around the planet. This surface is called an *L-shell* and any particle in a constant L-shell will have a third adiabatic invariant called the *drift invariant.* This invariant, Φ_B, is the conserved magnetic flux enclosed by the drift shell of a particle and is written as

$$\Phi_B = \oint v_d r \, d\varphi \tag{2.35}$$

where v_d is the sum of all $v_\perp$, φ is azimuthal angle, and the closed-path integral is taken over an entire drift period. Again, this quantity is only constant if the changes in the fields are much slower than the drift period. The third invariant follows directly from the adiabatic invariance of μ. The consequence of Eq. 2.35 is that as the particle moves towards a stronger magnetic field, such as near the earth's poles, the gyroradius will decrease in step, such that the enclosed magnetic flux remains constant.

In an azimuthally symmetric magnetic field, particles that are mirrored on the same field line at one local time, will still occupy the same field line as they drift into other local times. The earth, however, does not possess a symmetric magnetic field. In fact, there is significant azimuthal asymmetry between the day and night side, even in the trapped region of the magnetosphere, due to magnetospheric currents. This results in particles with different pitch angles to drift closer to or farther from the earth and thus end up on different drift shells at later local times. This *drift shell splitting* results in the outer radiation belt

having small equatorial pitch angles on the nightside and larger equatorial pitch angles on the dayside.

In the portion of earth's magnetic field that approximates a dipole (under ~6.6 R_E), there exists trapped populations of particles (including a portion of highly energetic particles that constitute the *radiation belts*). These collections of trapped particles undergo bounce motion as well as drift motion, with ions drifting westward and electron drifting eastward. The current created by this differential drift is called the *ring current*, an important component of the larger magnetospheric current system.

In a natural system, with all its myriad complexities at play, all three invariants mentioned here can be violated. Electromagnetic field variations on short enough timescales can violate one or more adiabatic invariants, based on the criteria already mentioned. Temporal changes are not the only such perturbation to consider. Sudden spatial changes in the magnetic field configuration can cause disturbances as well. When one or more of the invariants are in violation, the gyration, bounce and/or drift motions can no longer be described in the simple system we have laid out.

2.4 The Loss Cone & Pitch Angle Scattering

One pertinent process that contributes significantly to the loss of magnetospheric particles into the earth's atmosphere is pitch angle scattering. As long as a particle's pitch angle is known at one location along a field line, it can be determined at any other point. Therefore, for a trapped particle we can write

$$\sin\alpha = \sqrt{\frac{B}{B_m}} \tag{2.36}$$

If the magnetic field in the ionospheric end of the field line is less than B_m, the particle will often precipitate into the earth's atmosphere. This conceptual pictures gives the following condition

$$\mu < \frac{W}{B_i} \tag{2.37}$$

where B_i is ~100 km above the surface of the earth. In terms of equatorial pitch angle and the equatorial magnetic field,

$$\sin \alpha_e < \sqrt{\frac{B_e}{B_i}} \tag{2.38}$$

Any particle for which this condition holds true is considered to be within the *loss cone.* The difference in magnetic field magnitude between the equatorial region and the ionosphere is several orders of magnitude, which means the solid angle of the loss cone is quite small. In fact, it is under 3° for the geostationary orbit L-shell. All particles with pitch angles within that limit will precipitate in the atmosphere, however, auroral precipitation occurs at a greater rate than one would expect for an isotropic distribution of pitch angles. The difference is due to plasma waves, with higher frequencies than bounce or gyro periods, interacting with magnetospheric particles through a process called *pitch angle scattering.* Each bounce period is another chance for a particle to precipitate, and particles with a mirror point over 500 km are not likely to precipitate, while those with mirror points near 200 km are more likely to be lost. The violation of adiabatic invariants essentially widens the loss cone and keeps the loss cone about half full for electrons within the inner plasma sheet. If this scattering rate is great enough that the pitch angle distribution is able to return to an isotropic distribution within one particle bounce period, we can consider this *strong pitch angle diffusion.* Here, the particles diffuse rapidly from the edges of the loss cone through the center, and the precipitation rate depends entirely on the size of the loss cone. The probability of loss within one bounce period would then be equal to $\Omega_L/2\pi$,

where Ω_L is the solid angle of the loss cone.

The in-depth study of wave-particle interactions is vast and very relevant to the process of auroral precipitation. For a circularly polarized transverse wave (the type of waves that interact with auroral particles, discussed further in Sec. 5.4), its frequency will be Doppler shifted from the point of view of a trapped particle. If that Doppler shifted frequency is equal to the gyrofrequency of the particle, such an interaction will take place. If we consider a wave with angular frequency, ω, and propagation constant, k, we can show the relation to the particle's gyrofrequency and parallel velocity by

$$\omega = \Omega_c - kv_{\|} \tag{2.39}$$

Electrons will interact with right-hand polarized waves, for electron energies of 100's of eV to 1000 keV. These pertinent frequencies are in the range of 3-30 kHz, and are referred to as *very-low-frequency* (VLF) waves. This range includes electron cyclotron harmonic (ECH) and whistler-mode chorus waves. Wave energy will grow, at the expense of particle energy, therefore wave growth leads to decreases of particle pitch angle and subsequent diffusion into the loss cone. As electrons are lost, the waves will damp; and thus continues a cyclical process that requires periodic injections of particles and wave energy.

CHAPTER 3

THE MAGNETOSPHERE

EARTH'S MAGNETIC FIELD AND ITS INTERACTION WITH THE SUN

The sun emits a constant stream of charged particles called the *solar wind*, as well as a magnetic field that gets pulled around with the sun's rotation and extends its spiral shape into interplanetary space. The plasma streaming out radially from the surface of the sun eventually reaches the earth's magnetic field; this bombardment works to create the distorted magnetic configuration around our planet. As a rock in a fast-flowing river warps the current that sweeps past and over the obstacle, so the earth's magnetic enclosure is reshaped from what would be a dipole field in the absence of the solar wind. Fig. 3-1 depicts the major features of the magnetosphere discussed in this chapter.

3.1 Structure of Earth's Magnetosphere

The magnetosphere is an intricate system of fields, currents and processes that all influence the way that solar wind particles enter and interact with our earth's magnetic field and atmosphere. As the bulk of the solar plasma begins to come in contact with the earth's field, a substantial deceleration occurs and the particles go from supersonic to subsonic

speeds at a boundary defined by a shock front. Inside this *bow shock*, the *magnetopause* exists as the outer boundary which contains the entirety of the distorted terrestrial magnetic field. This field appears as a compressed dipole configuration on the dayside of the earth (the degree of compression depending on the immediate solar wind pressure). On the nightside, the topology is referred to as a stretched tail configuration, where the *magnetotail* extends far downstream in the direction of the solar wind flow. The magnetopause itself is a thin current sheet. To satisfy current closure for the open field lines in the tail, there must be a central current sheet flowing through the center of the magnetotail. We call this the *neutral sheet current* in the region of the *central plasma sheet* (CPS). The CPS contains the bulk of the magnetotail plasma, with electron densities averaging $\sim$0.5 cm^3. The tail lobes are regions on the outer edges of the tail that contain significantly lower densities than the midsection.

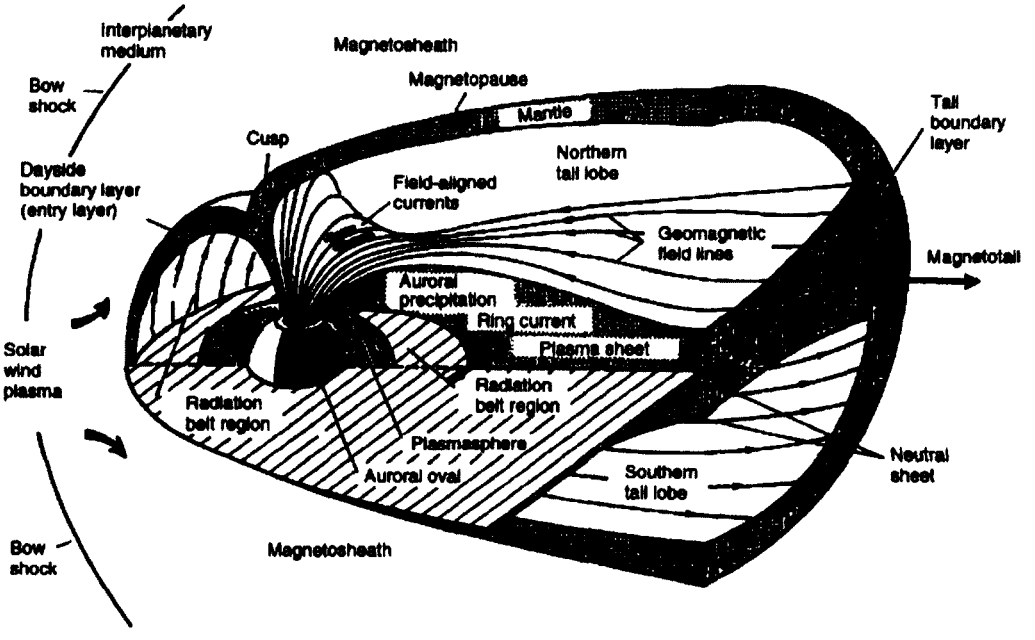

Figure 3-1: A schematic showing the major features of the earth's magnetosphere. Reprinted from *Kelley* (2009), with permission.

Generally, for space plasmas, we can invoke the *frozen-in flux* property. This condition states that for an arbitrary surface, the group of field lines intersecting that surface will stick with the surface, even as it moves or changes shape; therefore, the flux through that surface remains constant as well. The field lines may twist or move closer together or further apart, but they stay bound tightly to the surface, which we can extend into a cylindrical volume that we call a *flux tube.* This concept can be applied to the *interplanetary magnetic field* (IMF) that originates at the sun and pervades the solar system, with a field strength on the order of 5 nT at 1 AU (the distance from the earth to the sun). Near the sun, the magnetic field is radial and varies as $1/r^2$. As the sun rotates, this field becomes spiral shaped (dubbed the *Parker Spiral*) like a garden hose sprinkler, instead of a symmetric, radially expanding formation over long distances. At these distances, the magnetic field is azimuthal and falls off by $1/r$. The exact orientation of the ever-changing IMF angle has serious implications on the amount of solar plasma that gains entry into the magnetosphere. When the IMF has a strong southward component, the field is able to merge more successfully to the terrestrial field lines and a temporary conduit is formed for particles to leak in, instead of being deflected around the magnetopause. During such a magnetic merging, or *reconnection*, event, the frozen-in flux law breaks down. Nightside reconnection is an explosive process that is the genesis for *magnetospheric substorms*, a topic discussed more in-depth later.

3.2 Plasma Convection & Magnetic Reconnection

Two major drivers of the dynamic magnetic field lines and movement of plasma in the magnetosphere are: energy input from the solar wind and the rotation of the earth. This circulation of plasma is referred to as *convection.* Magnetic reconnection allows a direct injection of momentum into the magnetosphere and sets up a convection pattern, as outlined here. A southward IMF will merge with the earth's magnetic field, along a line referred

to as an *X-line*, and the merging lines will create two new open field lines each with one footprint on the dayside earth and the other end stretching into the solar wind (Fig. 3-2). These two newly created field lines will be swept tailward along with the bulk of the IMF draping over the volume of the magnetosphere. The sections of the field lines that still remain within the magnetopause will move over the polar cap during this process. Next, the stretched field lines will continue downtail on the nightside, eventually meeting each other far into the magnetotail (100-200 R_E). At this meeting point, the two open field lines will reconnect again to form a highly stretched closed field line. The magnetic tension of this topology serves to pull the new closed field line towards earth and sweeps plasma along with it; thus creating the earthward convective flow of plasma on the nightside. The field line will then often continue back over the polar caps and regain its place in the dayside magnetosphere, ready to continue the cycle if a southward IMF persists. The requirement

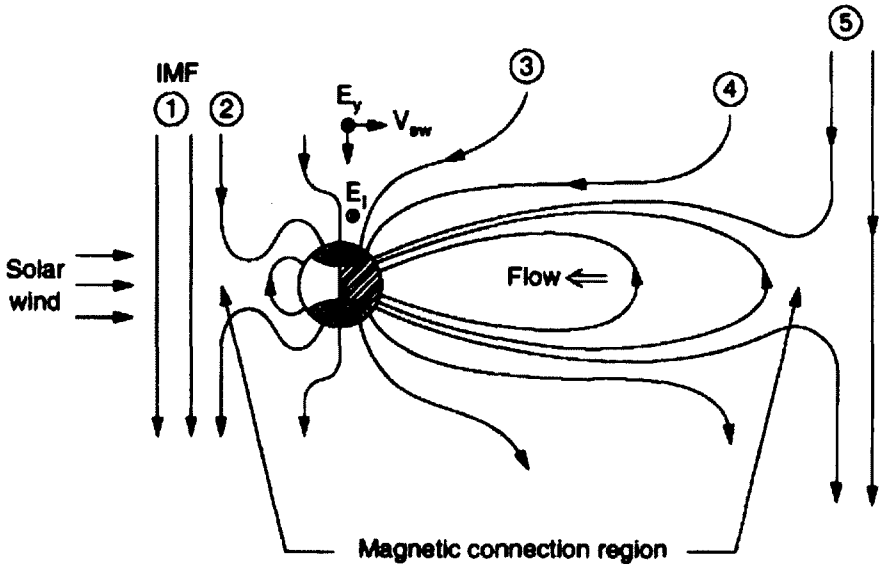

Figure 3-2: Side-view illustration of reconnection in the magnetosphere. The (2) represents an southward IMF merging with the terrestrial field, and the (5) represents a later point in the process, after the merged field line is swept tailward. Tail reconnection happens within this region, just after the configuration of field line (5) shown here. Reprinted from *Kelley* (2009), with permission.

for current closure during this (oversimplified) picture of large-scale plasma convection and transport gives rise to multiple current systems and $\mathbf{E} \times \mathbf{B}$ drift patterns across the polar cap. These will be investigated in the next chapter.

3.3 The Plasmasphere

Another force exerts control on the plasma motion nearer to earth. The corotation of plasma with the earth's rotation is dominant from the ionosphere to within an upper boundary occurring anywhere between 3-5 R_E. At the upper boundary of this range, the solar wind convective flow contributes to corotation, creating a new set of equipotential lines. This is approximately the region that the radiation belts inhabit, and is called the *plasmasphere*. The field lines within the *plasmapause* are entirely closed and therefore populated by ionospheric particles. This region contains a cold and dense plasma population (few eV and several 10^3 cm^{-3}), with a "trough" of low densities occurring just outside the plasma-

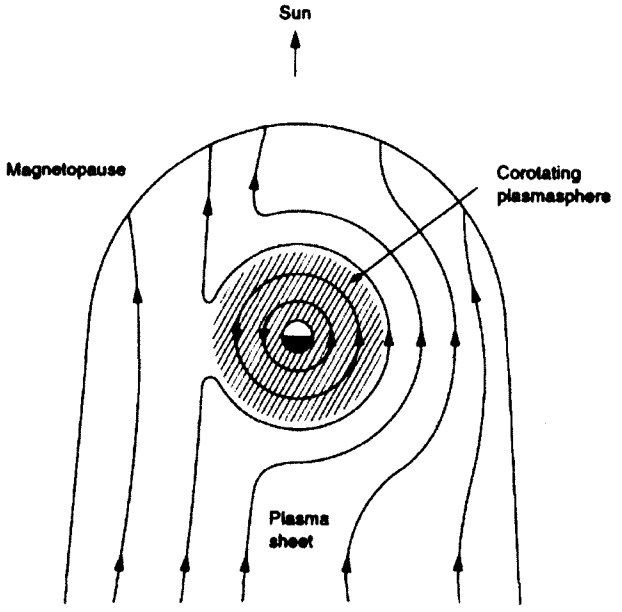

Figure 3-3: The corotating plasmasphere (shaded area) shown within contours of plasma flow. Reprinted from *Kelley* (2009), with permission.

pause. During higher geomagnetic activity, the plasmapause moves closer to earth, as the solar wind driven convection dominates down to lower L-shells. The plasmasphere field lines have their footprints in the mid- to low-latitudes, since the polar cap zones are also controlled more by the solar wind convection.

3.4 The Big Picture

The magnetic cloak draped around our planet acts as a line of defense against the near-constant barrage of pervasive and destructive solar particles. Without a magnetosphere, life as we know it on earth would not exist. For the nearly 10% of the total solar wind plasma that breaches the outer magnetopause, other systems come into play that further buffer the earth's surface from the damaging particles. A delicate balance between accumulation and loss of energetic particles is maintained by the earth's Van Allen belts. Near the poles, in what is known as the *auroral oval*, there are avenues open to those particles with the correct pitch angles, such that they penetrate all of earth's defenses and finally precipitate in the upper atmosphere. In this same vicinity, acceleration mechanisms also act to precipitate auroral particles.

Thus we begin to see the larger picture that ultimately causes the awesome display of the northern and southern lights. Solar wind particles that find conduits into our magnetosphere will drift around, and follow convective flows, and eventually become energized or scattered before finding entry into the earth's ionosphere. The study of auroral displays is essential to understanding the magnetosphere as a whole, and expanding our knowledge on the entire sun-earth system.

CHAPTER 4

THE AURORAL IONOSPHERE

The *ionosphere* is the domain of the earth's atmosphere that consists of neutral particles that have become ionized by solar UV radiation on the dayside and through direct impact by energetic particles from the magnetosphere primarily on the nightside. This latter process creates visible light emissions as a byproduct, which we call the *aurora*. The ionosphere acts as a sort of television screen through which we can view a one-sided picture of magnetospheric developments. The plasma that reaches our ionosphere originated from the sun at some point, embarking on a dynamic odyssey - and as we observe the displays dance overhead, we can piece together a story about that journey.

4.1 The Aurora

The auroral oval is defined to be the roughly oval-shaped ring outlining the majority of auroral precipitation that sits centered just a few degrees tailward of the magnetic pole. It can be up to 20° in latitude, but is generally agreed to be between 60° and 75° MLAT (*magnetic latitude*), and is in a constant state of flux. The interior of this ring contains the polar cap, where the field lines are all open field lines connecting directly to the solar wind. Thus the auroral oval overlaps with the *open-closed field line boundary*, the precise location of which is highly dynamic. Auroral emissions, created through collisions with atmospheric constituents, consist of a whole zoo of spectral lines and bands. (The other effects that the

bombarding particles have are: heating of the atmosphere, production of Bremsstrahlung x-rays and dissociating atmospheric molecules, but we will focus on ionization/excitation mechanisms.)

4.1.1 Auroral Energies & Classifications

The bulk of auroral particles have energies in the range of 100's of eV to a few 100 keV. The very lowest range, < 1 keV, makes up the dayside portion of the auroral oval. This soft precipitation enters the dayside ionosphere from the *cusp region* of the magnetosphere, the funnel-shaped corridor between the sunward closed field lines and the open field lines emanating out into the solar wind. This aurora is considered *diffuse aurora*, and exists throughout the auroral oval. The low-energy auroral particles "drizzle" into this direct access point, and reach the ionosphere with minimal energy. Within this low range, there also exists *Alfvénic aurora*; precipitated particles that are accelerated via Alfvén waves in the ionosphere. The medium-range energies, $\sim$1-30 keV, originate on higher-latitude, draped magnetic field lines, on the tailward side of the magnetosphere. The spatial distribution of this precipitation in the ionosphere is a tailward tipped ring, with a much higher precipitation occurrence on the nightside, but still some emissions on the dayside ionosphere at very high geographic latitudes. This type of aurora creates the oft-photographed, dynamic light shows that popularize this natural phenomenon. We call it *discrete aurora*, as it often manifests as bright bands, veils or arcs, with sharp boundaries in the night sky. The highest-energy particles, from $\sim$30 keV to perhaps 100 keV, create a second ring-shaped precipitation distribution of constant latitude, and is more concentrated on the dawn side or morning sector of the ionosphere. The distribution occurs at lower latitudes than the discrete aurora on the dayside, but overlaps on the nightside. This precipitation picture is consistent with a population of trapped energetic particles on a constant L-shell, precipitat-

ing into the loss cone through some mechanism as they drift in a longitudinal ring current. This energetic aurora usually takes the form of a modulated, *pulsating aurora*, discussed in detail in Chapter 5. Proton aurora is much more broad and diffuse than electron aurora of the same energy, due to charge exchange by the incoming hydrogen atoms, and occurs in a oval displaced towards the dusk side, with respect to the electron auroral oval.

These classifications of aurora based on energy range seem quite separate, but in the natural world, borders blend together and forms overlap to such a degree that often the exact energies of the source particles become murky. To this end, much emphasis has been placed on attempting to observe and define many boundaries in the magnetosphere and relate them to the auroral forms we see from the ground. These boundaries include, among others: the cusp, the high- and low-latitude boundary layers, the plasma sheet boundary layer, and the open-closed field line boundary. The energy input necessary for a mid-strength visible aurora is about $10^{-3}\mathrm{W}\cdot\mathrm{m}^2$. For a typical arc formation, this translates to a total 10^6 kW of power needed. Since only approximately 1% of all the particle energy is converted to visible light, we see that the auroral oval constitutes an enormous transfer of energy from the solar wind and magnetosphere to the ionosphere daily.

4.1.2 Auroral Color & Intensities

The colors seen in auroral displays give information about the atmospheric species being excited in the atmosphere. In general, one can boil down visible aurora into three colors: red, green and blue. These emissions result from neutral or ionized molecular nitrogen, atomic oxygen, molecular oxygen and atomic nitrogen, in order of decreasing importance. There may be small contributions from nitric oxide (NO) as well. The red colors mainly come primarily from the 630-636.4 nm, which are [OI] oxygen emission lines. The green line occurs mainly at 557.7 nm and is another [OI] emission line. A blue-violet color comes

mostly from the 427.8 nm [N_+^2] nitrogen first negative band. Thermal electrons can produce the 630 nm red aurora as well - this results in *stable auroral red* (SAR) arcs, seen on the lower border of the auroral oval. Often, auroral forms appear white or grey in color, yet it is usually green aurora that is too dim to meet the color threshold of the human eye. The full auroral spectrum includes a myriad of minor emission lines and bands, and can be examined in detail within *Aurora* by Alister Vallance Jones.

Absorption within visible aurora is small enough to be ignored. So the surface brightness of the aurora is proportional to line-of-sight integrated emission per unit of volume. If we call the surface brightness I, the total integrated emission is $4\pi I$ in photons per square centimeter per second. The unit used in place of $4\pi I$ is called the Rayleigh (R). One Rayleigh equals the integrated volume emission of $10^6 \frac{\text{photons}}{\text{cm}^2 \cdot \text{s}}$. Clearly, auroral intensity depends on the viewing angle; a thin auroral form will look brighter when viewed at lower angles along the horizon, since more emission will be included in the line-of-sight. 1 kR near the 5577 Å line is the very lower limit of the human eye threshold. Therefore, an auroral form of several kR will be dimly visible (more so near the horizon) while a very bright, discrete auroral arc will be closer to 100 kR, even peaking up to many 100's of kR.

4.1.3 Spatial and Temporal Distribution of Aurora

The height of auroral forms have been studied primarily using sounding rockets and ground-based data. The lower edge is considered to be 95-105 km, depending on the type of aurora (dayside aurora has a higher average height), with a vertical extent of 10-40 km. The median height of auroral emissions is generally taken to be at 110 km. However, long rays can extend up to great heights of hundreds of kilometers. Carl Størmer's *The Polar Aurora* contains these findings and a full statistical height distribution in work done by himself and colleagues.

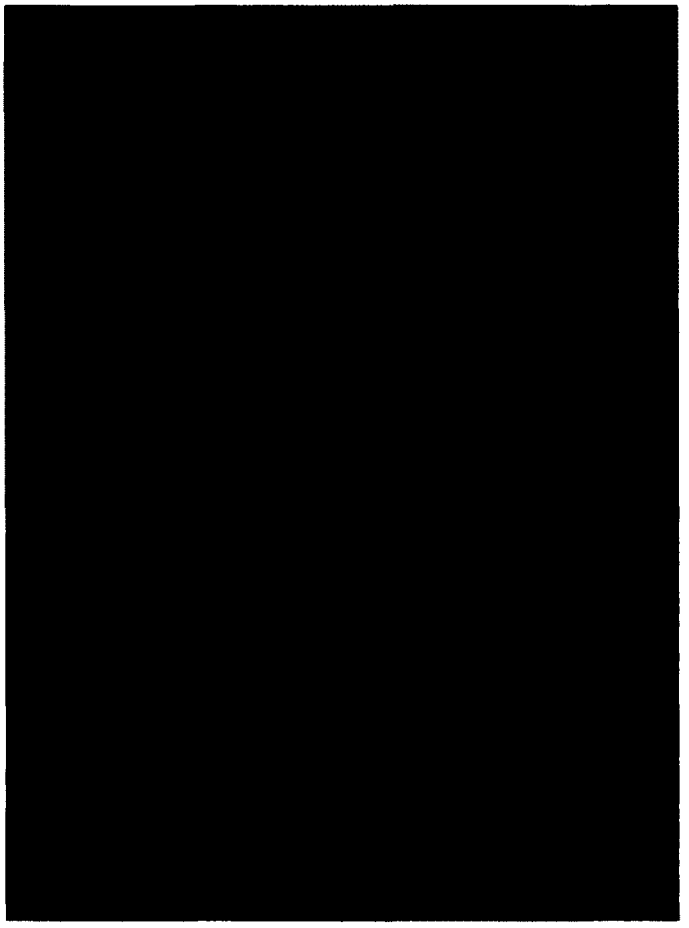

Figure 4-1: Discrete, green aurora over radar dish at Poker Flat Rocket Range, Alaska. Photographed during MICA sounding rocket launch window, 19 February, 2012.

The auroral oval is centered around 77° magnetic latitude on the dayside and around 67° on the nightside for periods of quiet to moderate geomagnetic activity. The oval expands equatorward during enhanced magnetic storms, as we will discuss shortly. The general locations for various auroral types were mentioned already, but we shall summarize the distribution once more. Discrete aurora is more prevalent on the nightside at intermediate latitudes, diffuse aurora occurs concentrated on the dayside at high latitudes, the distribution of proton aurora seems to peak on the dusk side, and pulsating aurora appears more often on the dawn side at slightly lower latitudes. Auroral forms drift westward in the pre-midnight sector and eastward in the post-midnight sector. Again, this compartmentalized view is not the real story: the regions interweave and overlap, and one can find instances

of any type of aurora appearing in an uncommon location.

When analyzing auroral morphology, a common unit of time to use is MLT (magnetic local time), which is the local reference time for an observer on earth with respect to a constant sun-earth frame. When an observer or station is directly pointed towards the sun, that is considered magnetic noon, and a full 12 hours later is magnetic midnight, with 24 magnetic local time sectors covering this entire extent. The noon-midnight plane is the plane which intersects both the magnetic axis and the spin axis of the earth. Another common convention to use in conjunction with MLT is *universal time* (UT), which is measured with respect to Greenwich, England in the westward direction with each hour covering 15° of longitude. Many types of aurora therefore have a nominal MLT range, along with an MLAT domain.

Conjugate aurora between the northern and southern hemispheres has been observed since the International Geophysical Year collaboration in 1957-1958. More recently, *Stenbaek-Nielsen et al.* (1972, 1973) has given descriptive reports of auroral observations gained from paired aircraft flights along magnetically conjugate trajectories in each hemisphere. They saw two quite distinct auroral systems; a diffuse aurora region that lies more equatorward and a region of discrete arcs that lies poleward. The equatorward diffuse system was seen to be closely conjugate, while the discrete system was conjugate unless during a time of high geomagnetic activity when displacements occurred. Also, they found the northern hemisphere aurora to be approximately 30% brighter than the southern hemisphere aurora, for both systems. Conjugate pulsating patches and flickering aurora were reported as well, though not all pulsations were conjugate. The exact relationship between magnetospheric conditions and simultaneous displays of aurora in both hemispheres is still a topic of open study.

It has already been demonstrated that the profile of the solar wind is intricately linked

to the aurora. Just how much of an effect the solar wind inputs have on auroral dynamics will be seen in Section 4.3. For now, it is sufficient to show the solar cycles intrinsic to the sun that influence auroral activity. The sun undergoes an 11 year sunspot cycle; the activity on the surface of the sun visibly declines and rises periodically on this timescale. The peak time for aurora, however, occurs 1-2 years *after* a solar maximum.

The sun has a rotational period of $\sim$ 27 days. There exists a relationship between this period and occurrence rates of aurora, simply because an active feature of the sun's surface will be rotating along with it and can have a recurring influence on the aurora, provided the feature persists for longer than a solar day. The precise nature of the relationship between flares or other solar eruptive events and the aurora is tenuous and depends mainly upon the degree of coupling possible between the IMF and the earth's magnetosphere, which is governed by the instantaneous magnetic field line geometry.

4.2 Ionospheric Current Systems

In a magnetized plasma, we can find an expression of the total current, $\mathbf{j}$, from Ohm's law

$$\mathbf{j} = \sigma \mathbf{E} - \frac{\sigma}{n_e e} \mathbf{j} \times \mathbf{B} \tag{4.1}$$

where the conductivity, σ, is given by

$$\sigma = \frac{n_e e^2}{m_e \nu_c} \tag{4.2}$$

We include ν_c as the collision frequency because we assume the particles in the ionosphere to be in the collisional domain. We can take the cross-product of Eq. 4.1 with $\mathbf{B}$ and substitute the result back into Eq. 4.1 to eliminate the $\mathbf{j} \times \mathbf{B}$ term and get the current for

an arbitrary magnetic field alignment

$$\mathbf{j} = \sigma_{\parallel}\mathbf{E}_{\parallel} + \sigma_P\mathbf{E}_{\perp} - \sigma_H\frac{\mathbf{E}_{\perp} \times B}{B} \tag{4.3}$$

From this we can see three separate current components with corresponding conductivities. The *Birkeland current* is the component parallel to **B** with conductivity $\sigma_{\parallel}$; this is also referred to as a field-aligned current. The *Pedersen current* is perpendicular to **B** but parallel to $\mathbf{E}_{\perp}$ with conductivity σ_P. And the *Hall current* component is perpendicular to both **B** and $\mathbf{E}_{\perp}$ with conductivity σ_H.

If we assume the magnetic field to be aligned with the z axis, $\mathbf{B} = B\hat{z}$, we can simplify Eq. 4.1 to

$$\mathbf{j} = \boldsymbol{\sigma} \cdot \mathbf{E} \tag{4.4}$$

We can now write the conductivities, using the definition for the electron cyclotron frequency found in Chapter 2. Note the n_e term in each definition, disclosing the collisional dependency of these conductivities (which in turn depends on altitude):

$$\begin{aligned} \sigma_{\parallel} &= \sigma = \frac{n_e e^2}{m_e \nu_c} \\ \sigma_P &= \frac{\nu_c^2}{\nu_c^2 + \Omega_{ce}^2}\sigma \\ \sigma_H &= -\frac{\nu_c \Omega_{ce}}{\nu_c^2 + \Omega_{ce}^2}\sigma \end{aligned} \tag{4.5}$$

From here, we see that if $|\Omega_{ce}| < \nu_c$, the Pedersen conductivity is the dominant feature and the electrons are scattered before they are able to even start to gyrate around the magnetic field. And if $|\Omega_{ce}| > \nu_c$, the Hall conductivity then dominates and the electrons gyrate for many cycles before a collision. However, when $|\Omega_{ce}| \approx \nu_c$ then the two conductivities are of equal import and the electrons are scattered about once per gyration period, and will have an angle of about 45° with the $\mathrm{E}_{\perp}$ and $\mathbf{E} \times \mathbf{B}$ directions. The parallel electric fields have

values on the order of 0.2 μV/m for a 30 kR discrete arc, and can range up to 20 μV/m for very active arcs. The perpendicular fields for the same arcs have values on the order of 10's of mV/m.

In addition to the Hall, Pedersen and field-aligned currents, there exists a secondary current flow (a subset of Hall/Pedersen currents) inside the auroral oval, named the *auroral electrojets.* These currents flow at auroral emission heights, a mere 100 km above the ground, and therefore have the most direct impact on the earth's surface out of all the current systems. Due to the motion of flux tube footprints up over the polar cap to the nightside and then back towards the dayside after tail reconnection (as described in Sec. 3.2), a two-cell electric field convection pattern is created in the polar cap and extends into the aurora oval. The electric field in the auroral zone of this convection E-field is nominally between 20-50 mV/m. It is often a distorted version of the figure shown here, depending on the strength and clock angle of the IMF. The auroral electrojets are eastward and westward directed in channels of high-conductivity originating in the dusk sector and dawn sector respectively. The westward electrojet can continue through midnight and into the evening sector, especially during a substorm. Current closure of these ionospheric current sheets is a requirement, which is satisfied by connection to field-aligned current (FAC) systems. These FAC's are divided into two categories: *Region 1* and *Region 2* currents. Figure 4-2 shows how the Pedersen current system connects to the larger magnetospheric current system, with Region 1 currents flowing into the high-latitude boundary layer of the plasma sheet and the Region 2 currents joining to the westward ring current in the equatorial plane. The electrojet typically causes ground magnetic field disturbances fluctuating between 100-1000 nT, shooting up to 3000 nT during exceptional geomagnetic storms. The auroral electrojet (AE) index is a measure of the total electrojet activity and is used as a proxy for geomagnetic activity. The AE index is based on the H magnetic field component from

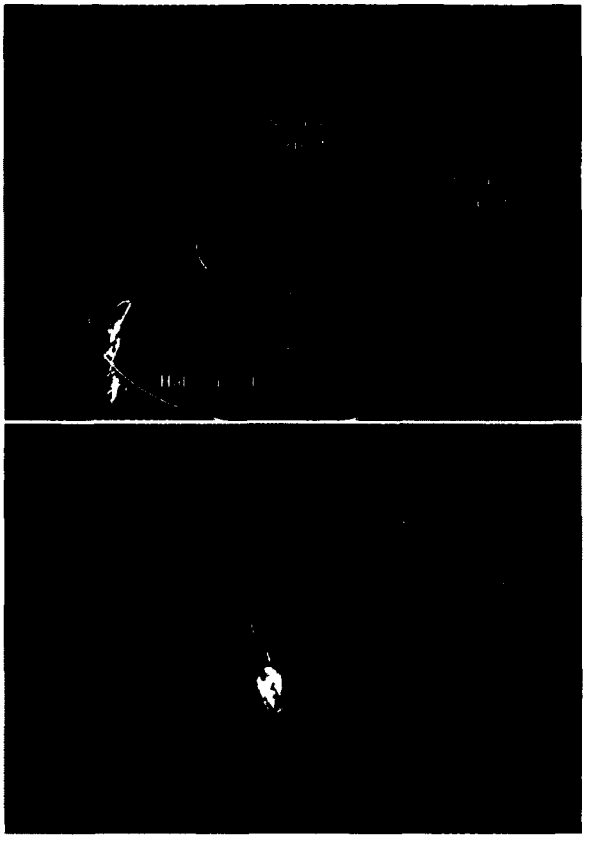

Figure 4-2: Top panel shows polar cap ionospheric current system consisting of Hall and Pedersen currents. In the bottom panel, field-aligned Region 1 and Region 2 currents are closing the ionospheric current sheet to the magnetosphere. Reprinted, with permission, from UCAR[1].

ground-based stations scattered throughout the auroral zone. The *Dst* index, another geomagnetic indicator, is based on the total ring current magnetic field and energy, determined from the H component at low-latitude stations. Recording and watching these magnetic indices gives an idea of when a *magnetic substorm* or *storm* is developing and how strong the activity will be.

---

[1]The source of this material is the COMET® Website at http://meted.ucar.edu/ of the University Corporation for Atmospheric Research (UCAR), sponsored in part through cooperative agreement(s) with the National Oceanic and Atmospheric Administration (NOAA), U.S. Department of Commerce (DOC). ©1997-2011 University Corporation for Atmospheric Research. All Rights Reserved.

4.3 Auroral Substorms

Pliny the Elder described the aurora as a "flame of bloody appearance... which falls down upon the earth..." around 77-79 CE in his *Natural Histories.* Associations between war, destruction and the northern lights were not uncommon in ancient times, persisting even up to the 19th century. In his observation, Pliny was most likely viewing a substorm from a lower latitude. The equatorward edge of the auroral oval often appears blood-red along the horizon from a mid-latitude perspective. Such a sight can mimic large fires on the horizon thus intimating war and fighting in one's imagination. These perspectives are not unfounded. When a magnetic storm or substorm takes place, intense, violent auroral displays appear, which can bring a sense of awe to the observer. A substorm is defined by *Akasofu* (1977) as "the manifestation of the process by which the energy stored in the magnetotail is sporadically and efficiently dissipated, rather than by a slow, continuous process." A magnetospheric cycle thus transpires from a favorable coupling between the solar wind and magnetosphere, most often when the IMF turns suddenly southward. If this IMF configuration endures for a significant period of time, several substorms can emerge one after the other, and the ring current grows and causes a disturbance in the surface magnetic field, known as a magnetic storm. Each phase of a substorm has specific auroral responses related to it. Here, let us break down the steps of an auroral substorm.

4.3.1 Phases of a Substorm

The timeline for a typical substorm is one to several hours. In general, one can break down a substorm cycle into three phases: the *growth phase*, the *expansion phase* (immediately preceded by the *substorm onset* itself), and the *recovery phase.* The substorm begins with the southward turning of the IMF, when the coupling is greatly increased and there is enhanced flux transport into the tail. Some of that flux is reconnected and those flux tubes

convect back towards the dayside, leading to enhance auroral electrojet currents. That flux which was not reconnected on the nightside gets piled on to the magnetotail lobes, resulting in an increased neutral sheet current. This stretches the field lines more and more in the tailward direction and is also referred to as *tail loading.* At the end of this phase, which normally lasts about one hour, the tail region is unstable due to the accumulation of magnetic energy. The growth phase is signified in the aurora by the appearance of quiet, azimuthally oriented arcs stretching across the sky. The dim arcs can be seen slowly marching equatorward for the duration of this phase.

The outlet for the buildup of magnetic tension in the tail leads to the onset and expansion phase. While the magnetospheric details are debatable, to the ground observer the process has a very clear progression (described with great detail in *Akasofu* (1964)). A brightening of the equatorward arc, typically in the just-pre-midnight sector, indicates onset. The brightening increases dramatically in a very short time and rapidly expands westward and poleward. The recently-stable arcs begin to kink and swirl, a spectacle known as *breakup aurora*, and soon fill the entire sky with a dynamic, fast-paced show of lights. The westward motion of this breakup aurora is called the *westward traveling surge.* Torch-like *omega band* auroral forms develop in the east extending poleward, so named because of their distinctive upper border shaped like the capital Ω. Rapidly pulsing and flickering patches form and disappear. After 30-60 minutes, the commotion dies down and the leftover scraps of dim aurora coalesce into very dim patches of longer-period modulated aurora, called *pulsating aurora.* During this spectacular auroral presentation, the magnetosphere has undergone a dramatic reconfiguration from a stretched-tail formation to more dipolar. The expansion phase is at an end.

Pulsating aurora is the dominant feature of the substorm recovery phase, extending into the morning sector, eastward of the initial substorm onset. To the west, the electrojet

dies down and quiet arcs form overhead once more. The auroral oval starts to contract and formations retreat poleward. This phase typically lasts for 1.5 hours until the magnetosphere returns to its initial steady state. If the IMF is still favorable, the tail may begin to load again during the recovery phase of the previous substorm, and the whole cycle begins anew.

4.3.2 Models of a Substorm

There are several models for magnetospheric reconfiguration during a substorm, the most well-developed of which is the *near-earth neutral line* (NENL) model (*McPherron et al.*, 1973; *Russell and McPherron*, 1973; *McPherron*, 1991). This model is quite consistent at explaining magnetospheric phenomena, but fails to incorporate some of the key ionospheric manifestations. Far downtail (100-200 R_E), the field lines form a *distant neutral line* (DNL), which is simply an X-line as discussed in Sec. 3.2 but quite inactive. With the expansion phase comes the stretching and thinning of the plasma sheet, and in this model a near-earth X-line forms from lobe magnetic pressure, much closer to the earth than the DNL (around 30 R_E).

The plasma encapsulated in closed loop field lines between the two X-lines is called a *plasmoid.* Reconnection begins slowly, then increasing in rate, until the explosive moment occurs that defines the breakup. The plasmoid gets pushed tailward as the NENL retreats down the tail. Eventually, in the recovery phase, the plasmoid is ejected out the back of the tail and joins the bulk solar wind. Now, the NENL has become the DNL and the arrangement is back to the initial quiet state.

Another prominent model is the *current sheet disruption* model (*Lui*, 1991a,b), whose basis lies in an attempt to explain inconsistencies seen by spacecraft nearer to earth during substorms. The model relies on the equivalent current system of the so-called *substorm current wedge*, that allows for current closure between the ionosphere and magnetosphere

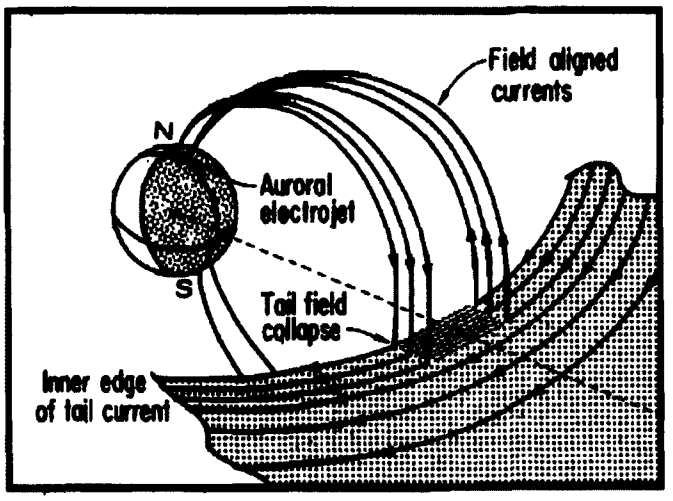

Figure 4-3: Equivalent current model called the substorm current wedge. Reprinted with permission from *McPherron et al.* (1973).

and accounts for real signatures of ground-based instrumentation (Fig. 4-3). In the inner magnetosphere, a thin current sheet is posited to form, under the same conditions as the NENL, but at a point much closer to earth around geosynchronous orbit at 6-7 R_E. Streaming ions then interact with the adiabatic drifting electrons and produce lower hybrid waves, which in turn creates an anomalous resistivity in the plasma sheet and disrupts the cross-tail current. The current thus diverts along the field lines of the substorm current wedge. The disruption moves radially outward and down the tail. This model accounts very well for the precise auroral conditions seen during a substorm. The two models, and others, are fervently debated to this day.

4.4 Magnetosphere-Ionosphere Coupling

Energy and momentum are exchanged between the magnetosphere and ionosphere through the various processes that have been discussed so far. The electric fields in the ionosphere are of course tied to the currents through Ohm's law. And the magnetospheric plasma convection is tied to the large-scale currents through collisions. The interesting part is how the magnetosphere couples into the ionosphere through current continuity and electric field

mapping. A change in any of the four fields/currents affects the other three completely.

A significant portion of the energy deposited in the ionosphere comes from the downward *Poynting flux* along field lines from the magnetosphere. In the atmosphere, this Poynting flux is dissipated via Joule heating by the Pedersen current (the Hall current is not dissipative since it is transverse to **E**). The exact rate of energy transfer into the ionosphere-thermosphere within the auroral zones is not known, but it is likely on the order of several to many erg/cm^{2}s. For comparison, the sunlit ionosphere receives approximately 0.5 erg/cm^{2}s from UV radiation above ~110 km. In fact, this energy deposition may be much more extensive than previously thought, an argument that will be presented in Sec. 5.5.

4.5 Observing the Aurora

Many techniques are employed to measure and record the aurora in every form. The aurora is primarily a visual phenomenon, and so optical techniques measuring intensity are the most common and widely-used methods of observation. These will be discussed at some length. However, there exist other measuring procedures. Much information has been gained using radar systems, specifically the *incoherent scatter radar* (ISR) modules. A radar beam is scattered off the electrons in the ionosphere and an echo is recorded when the signal bounces back to a dish antenna or antenna array. The resulting signal gives information about the temperatures of the ions and electrons, the electron density, the composition of ions and the bulk flow velocity of the plasma. ISR's exist at varying latitudes and longitudes, though the PFISR (modular ISR at Poker Flat, Alaska) and EISCAT (European ISR in northern Norway) stations are currently the most useful tools for observing the auroral ionospheric conditions. An ionospheric heating device is sometimes employed in the vicinity of ISR's to temporarily excite the ionosphere and observe "man-made" aurora for various studies.

For field measurements, arrays of ground magnetometers have populated the auroral

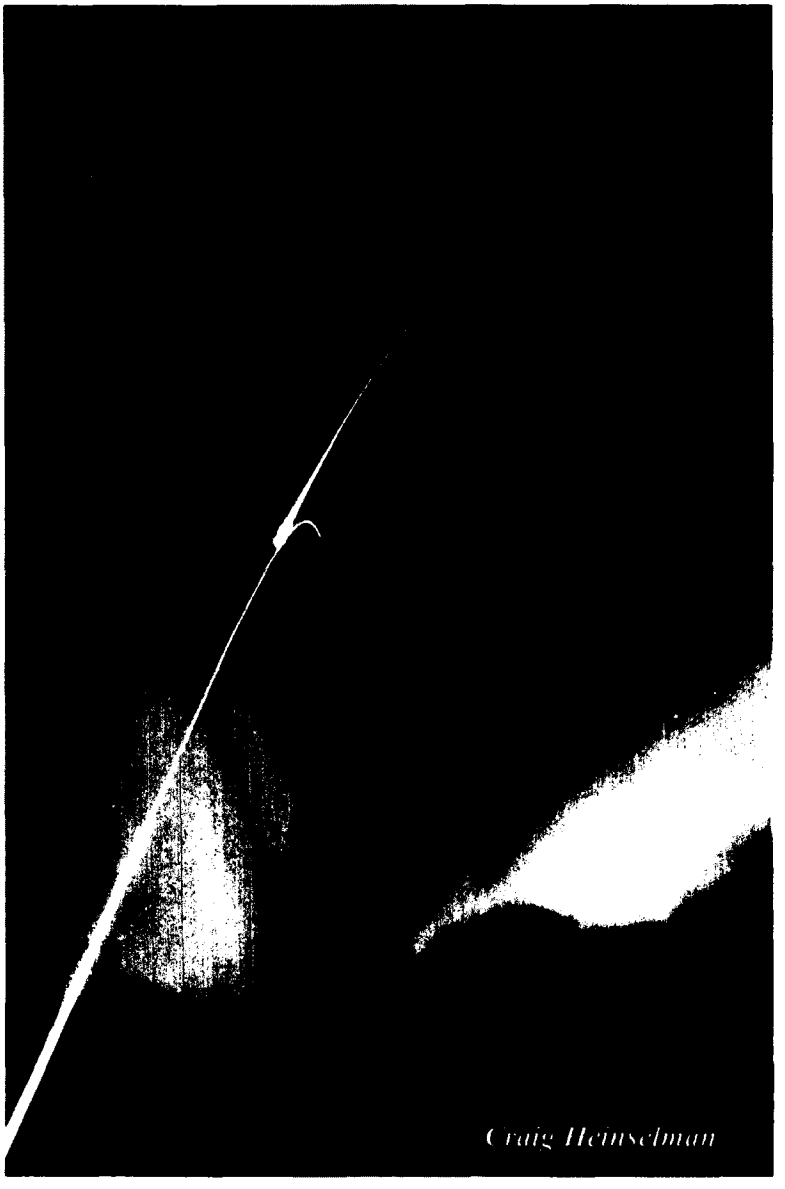

Figure 4-4: MICA sounding rocket launch from Poker Flat Rocket Range, Alaska on 18 February, 2012. The experiment, named Magnetosphere-Ionosphere Coupling in the Alfvén Resonator, was designed to measure the degree of such coupling and how it impacts auroral arcs. Photograph by Craig Heinselmen, SRI (included with permission).

zones since the time of arctic exploration, and have been a staple of auroral observation. More recently, deployable electric field booms have been used on sounding rocket and balloon missions. These consist of a pair of electrodes on long wire booms that unwind or otherwise deploy during flight. Magnetometers are also flown on these spacecraft, as well as satellites, for magnetic field determination. One such example of rocket-borne field measurements is the Cornell SIERRA-Class Subpayload, first used on the SIERRA experiment and subsequently launched on the SERSIO, ROPA, CASCADES2 and MICA sounding rockets. The payload contains a GPS receiver, one fluxgate magnetometer and the COWBOYS electric field instrument boasting two 6-m tip-to-tip electric field booms, shown in Fig. 4-5.

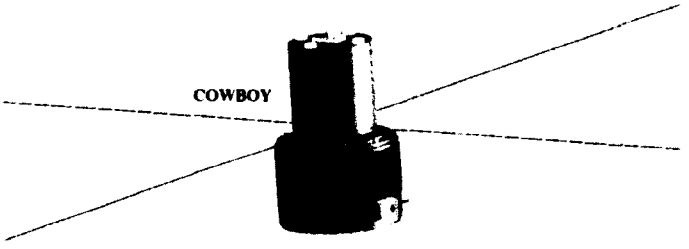

Figure 4-5: Schematic of the COrnell Wire Boom Yo-yo (COWBOY) electric field instrument. This design has an extensive heritage, having flown on the SIERRA, ROPA, CASCADES2 and MICA sounding rocket missions.

Particle detectors are utilized on both rocket and satellite experiments, and include such instruments as scintillators or solid state detectors to measure energy spectrums, retarding potential analyzers to measure thermal electrons, and electrostatic analyzers to measure fluxes within prescribed energy bands. Detectors flying directly through auroral excitation altitudes have provided invaluable *in-situ* data for studies of auroral processes. Instruments are able to measure energies from < 1 eV to 100's of keV, covering the entire range of precipitating auroral particles. Fig. 4-6 shows data from the CASCADES2 sounding rocket, including energy flux of precipitating particles seen on the Particle Free Flyer 1 (PFF1) during a discrete aurora event.

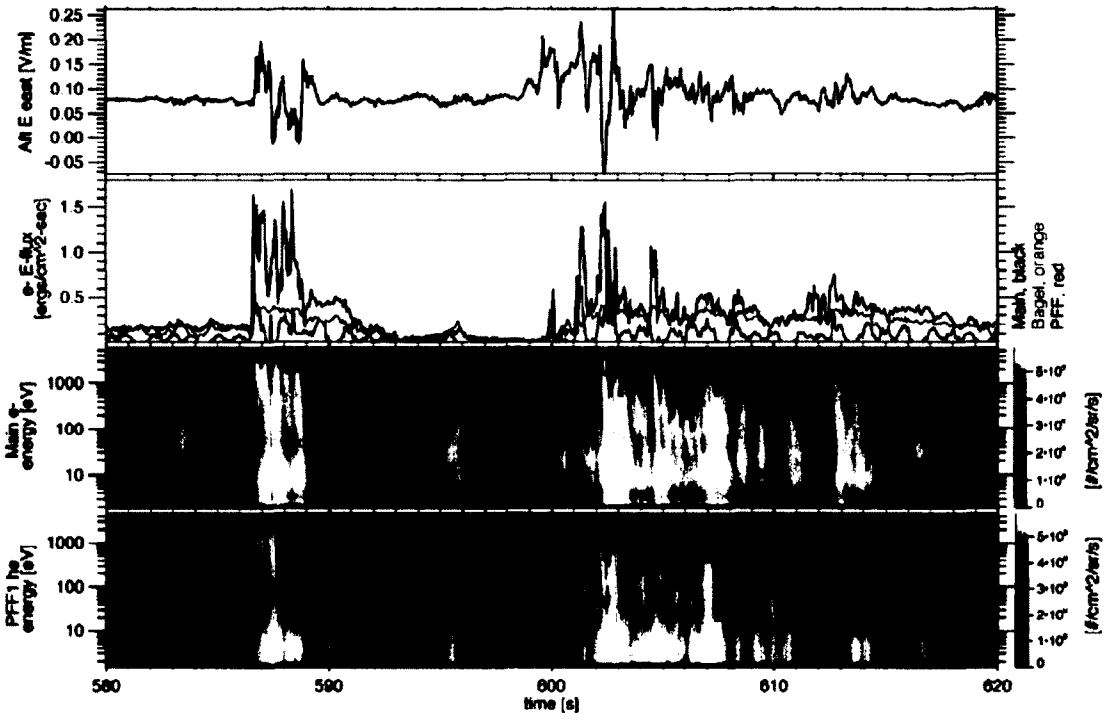

Figure 4-6: *In-situ* data from the CASCADES2 sounding rocket. For flight times from T + 580 s to T + 620 s, the top panel shows DC electric field data from the AFT subpayload. The second panel shows the integrated precipitating energy flux from the main payload and PFF1 electrostatic analyzers. The third panel shows the differential energy flux as seen on the main and the fourth the same from PFF1; the blue lines trace out the envelope of maximum acceleration energy. Reprinted with permission from *Lynch et al.* (2012).

Optical measurements make up the majority of observational data ever recorded pertaining to the aurora. Photometers are instruments that exploit the photoelectric effect through the use of photomultiplier tubes. By counting individual photons, and by making use of narrow-band filters, photometers can obtain precise intensity measurements for even the dimmest auroral emissions. Their noise levels depends highly on the operating temperature, with a higher signal-to-noise ratio obtained at low temperatures, making them ideal for arctic observing. Photometers are useful for the visible, near infrared and UV wavelength regions, and they can be employed as ground- or flight-based instruments.

Cameras and imager systems are widely used in addition to the aforementioned devices. Allsky cameras are designed to photograph 180° or more of the sky overhead, at varying rates and exposure times, with each frame transferred or stored digitally in modern times (Fig. 4-7). These systems are improved with the film and photography industries' never-ending progress in lens technology. To that end, smaller-field television cameras are also commandeered for scientific purposes. Image intensifiers and higher frame rates lend extra sensitivity to these instruments and make them fitting candidates for recording very dynamic and fine-scale auroral structures. During recent history, the *charge-coupled device* (CCD) detector has been the digital replacement for older film-based exposures. The photosensitive surface is many times more responsive than the human eye, and the architecture of the CCD means one can make much more precise interpretations of the resulting images than from traditional photographs.

4.5.1 UNH Rocket-borne Auroral Imager

The UNH auroral imager was designed (by A. Jaynes and P. Riley, UNH) utilizing a de-spun filtered CCD sensor with a medium-width FOV to image aurora onboard the RENU sounding rocket mission (Fig. 4-8). The imager was based on previous UNH imagers (designed

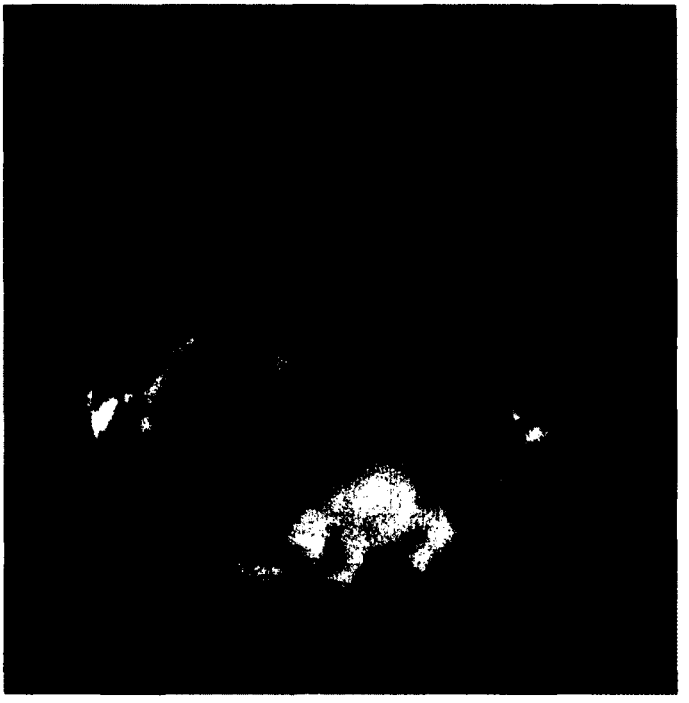

Figure 4-7: Example of an allsky camera image. Pulsating aurora is seen to fill the entire +180° field-of-view. Image included with permission by Robert Michell, SwRI.

by S. Jones, UNH) that were flown on both the ROPA (M. Lessard, PI, UNH, 2007) and CASCADES2 (K. Lynch, PI, Dartmouth, 2009) missions. The updated model was a similar, yet improved version of these earlier instruments. The RENU imager was positioned to look aft-ward and was intended to acquire 2D images of visible auroral emissions at 630 nm with a 26° field-of-view. The images would have provided a context for relating the in-situ RENU data to the aurora below. The imaging chip was an EMCCD (electron-multiplied CCD) with associated electronics that utilized double-correlated sampling to aid in noise reduction. The entire EMCCD was also drastically chilled in a dry environment using a thermo-electric cooler to further lower the noise floor that accompanies higher temperatures. The optical assembly consisted of a 25 mm standard mount CCTV lens with a low F-number (0.95), a narrow bandpass filter with peak transmission centered near 630 nm, and a high-sensitivity 512x512 EMCCD chip attached to custom electronics engineered by

P. Riley.

The rotation of the payload required that the imager be de-spun; the solution was to place part of the imager on a rotating platform such that the CCD was rotating counter to the rocket spin and was connected to the motor and telemetry link through a center slipring. This slipring allows the imaging CCD and its electronics boards to rotate at the same rate as the payload itself (yet in the opposite direction), while the rest of the imager remained stationary. The platform was set to spin at the roll rate of the payload, using a roll-rate sensor in a closed-loop feedback circuit. The instantaneous payload roll rate during flight does vary, though for slight blurring from such a disparity it is possible to de-blur the images in post-processing.

A tall baffle was designed (by A. Jaynes, Fig. 4-9) to block stray light due to the very high altitude of the rocket's planned apogee; looking back down at the aurora, it was desired that the images would not be contaminated by sunlight. The baffle consisted of many concentric rings within the baffle tube, each with a sharpened "knife-edge" interior rim. The knife-edge construction prevents photons that scatter off of the baffle edges from refracting down into the image plane itself. This greatly decreases the amount of stray light added to the image from outside the immediate field-of-view. The design was drawn from the few resources available on previously published optical baffle designs (*Lee et al.*, 2000; *Bucsela*, 1994).

The improved version of the UNH auroral imager was flown on the RENU sounding rocket in December 2010. The rocket motors developed an issue in flight and as a result, the nose cone was not properly ejected and the main payload forward instrument suite lost power just after turn-on. Though the aft and subpayload instruments remained operational, the apogee, spin dynamics, and trajectory were severely altered and there was essentially no useable data from the RENU mission main payload. However, we were fortunate to have a

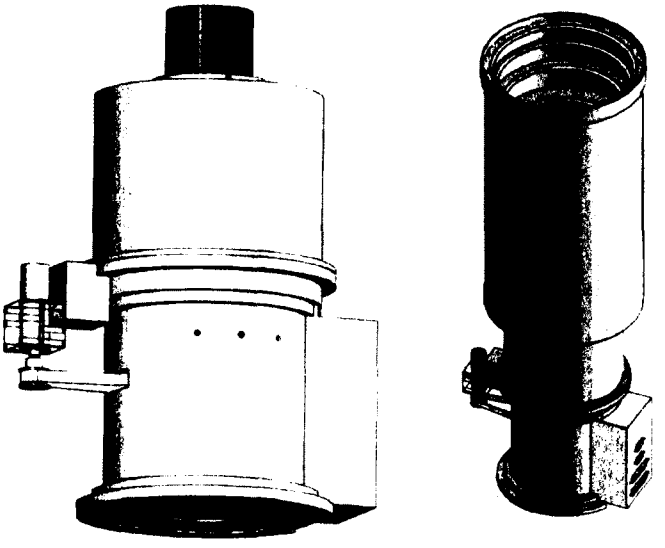

Figure 4-8: CAD drawing of the UNH auroral imager. On left, camera assembly with lens on top and de-spinning motor in the bottom half of the housing. On right, entire imager assembly with baffle attached over the lens. (Designed by A. Jaynes and P. Riley, UNH)

Figure 4-9: Off-center perspective of the UNH auroral imager baffle. The so-called "knife-edge" baffle rings can clearly be seen. This concentric ring geometry prevents stray photons from being refracted onto the image sensor surface below after scattering on the baffle edges.

mostly-identical flight spare of the imager on hand. This was brought to Poker Flat, Alaska during a subsequent rocket campaign and images of discrete aurora were captured from the ground, at lower than room temperatures. Fig. 4-10 shows one such image of a bright, discrete arc near zenith. Fine-scale curl structure can be seen along the arc boundary, as well as embedded within the arc itself. This image was taken at a much closer distance (from ground to ~100 km) than would have been on the payload (apogee of +450 km). Still one can see excellent structure of curls and luminosity striations. While this imager design has not yet been tested in flight, the images taken from the ground are a testament to the instrument's sensitivity and potential. With the proper amount of de-spinning and adequate cooling, which is all quite feasible, the imager should take similarly impressive pictures from onboard a rocket payload and provide excellent context for an auroral experiment.

Figure 4-10: Image frame taken by UNH auroral imager, from the ground, at Poker Flat Rocket Range, Alaska, February 2012. Fine-scale structure of curls and bands can be seen in this close-up of a bright, discrete arc.

CHAPTER 5

PULSATING AURORA

Pulsating aurora, the main subject of this thesis work, is a diffuse, patchy aurora that *Oguti and Watanabe* (1976) describe as on-off switching aurora. Pulsating aurora can be an impressive sight, or barely visible with the naked eye. As argued within this text, it has not been studied as thoroughly as deserved, and is likely a significant element in large-scale magnetosphere-ionosphere coupling. The pulsations have been previously linked exclusively to the substorm recovery phase, though we will see that this may be a somewhat outdated premise. In general, pulsating aurora is a less-studied auroral phenomenon and thus the source region, pulsation mechanism, and morphology determinants are still not well known.

5.1 Characteristics of Pulsating Aurora

Pulsating aurora is a distinct type of aurora, seen as irregularly-shaped, diffuse patches that are characterized by quasi-periodic brightness fluctuations of ~2-20 second periods, and horizontal sizes of a few to hundreds of kilometers (*Johnstone*, 1978). The temporal variation can change from one patch to the next, with nearby patches pulsating out of phase and independently of one another (*Omholt*, 1971; *Royrvik and Davis*, 1977; *Smith et al.*, 1980; *Duncan et al.*, 1981). The maximum power occurs in the frequency range of 0.05 to 0.15 Hz (*Jones*, 1974). The general brightness is only a few hundred R to a few kR at 428 nm, and normally occurs over a diffuse background (*Royrvik and Davis*, 1977).

Several other modulations are seen within auroral forms. *Flickering aurora* is a high-frequency (on the order of 10 Hz) modulation seen embedded within bright arcs and other forms, typically in the break-up phase. *Flaming aurora* is a upward or downward traveling modulation in zenith-viewed auroral forms. There are also traveling modulations observed along the edges of arcs in the break-up phase, which are known as *auroral waves* or *streaming* features. There occasionally may be some ambiguous overlap between these phenomena and pulsating aurora, but the focus of this work will be on pulsations with the typical characteristics of pulsating aurora. Thorough reviews of pulsating aurora have been published by *Davis* (1978); *Johnstone* (1978); *Davidson* (1990) and more recently by *Lessard* (2012).

5.1.1 Morphology

Pulsating patches at times appear in east-west aligned arcs, quasi-linear alignments or in a more random irregular distribution (*Royrvik and Davis*, 1977). *Sato et al.* (2002) reported these east-west lines of pulsating aurora to be immersed in a weak inverted-V precipitation, by comparing optical pulsations from the ground with FAST satellite data. *Thomas and Rothwell* (1979) report on wave-like propagations of pulsating patches along the meridional direction, with recurrent forms coming and going. And *Stenbaek-Nielsen and Hallinan* (1979) used a triangulation method to obtain thickness measurements of pulsating patches, recording vertical extents of 2 km or less.

The drift speed has been consistently measured to be on the order of 1 km/s in the morning sector, presumably at the $\mathbf{E} \times \mathbf{B}$ drift speed (*Davis*, 1978). However, *Swift and Gurnett* (1973) found that the pulsating form drift speed was lower than that of the measured convection eastward velocity.

Commonly, a 3 $\pm$1 Hz modulation of intensity is observed superimposed upon the pulsating aurora patches (*Oliven and Gurnett*, 1968; *Royrvik and Davis*, 1977; *Lepine et al.*,

1980; *Sandahl*, 1984; *Yamamoto*, 1988). Periods have been reported down to 0.1 s and up to 100 s by *Duncan et al.* (1981), but they observed periods between 5-10 s for a majority of their events.

5.1.2 Temporal and Spatial Distribution

A statistical study was done by *Kvifte and Pettersen* (1969) that showed the maximum probability of observing pulsating aurora was in the equatorward edge of the auroral oval, especially near 0600 MLT. This strong dependence on local time is not a unique finding. Many studies have shown pulsating aurora is far more common at or after magnetic midnight, and pulsations occur almost exclusively after local midnight (*Heppner*, 1954, 1958; *Victor*, 1965; *Cresswell and Davis*, 1966; *Omholt and Berger*, 1967). However, *Paulson and Shepherd* (1966) report pulsations at all times in almost all quiet forms, at 60° MLAT.

Berkey (1978) observed several instances of afternoon sector (1300-1600 MLT) pulsating aurora during a winter campaign at College, Alaska. Fig. 5-1 shows one such observation on 18 January, 1968. The experiment used a 4278 Å photometer to measure the intensity of the N_2^+ emission and a riometer to simultaneously monitor radio wave absorption. A riometer measures ionospheric absorption, or in other words, the amount of ionization present (which can be a proxy for auroral precipitation). In the figure, riometer signatures of pulsating aurora can be seen along the extent of the time interval (time increases from right to left in these panels). The photometer is turned on just after twilight, and is seen to be saturated until around 8° SDA (solar depression angle). As soon as the sky is dark enough to stabilize the photometer signal, a pulsating aurora signature is seen (and concurrently in the riometer), implying that the pulsations existed before the photometer was able to observe the fluctuations. The conclusion was that pulsating aurora does occur during the afternoon sector, a phenomenon that had not yet been well-documented.

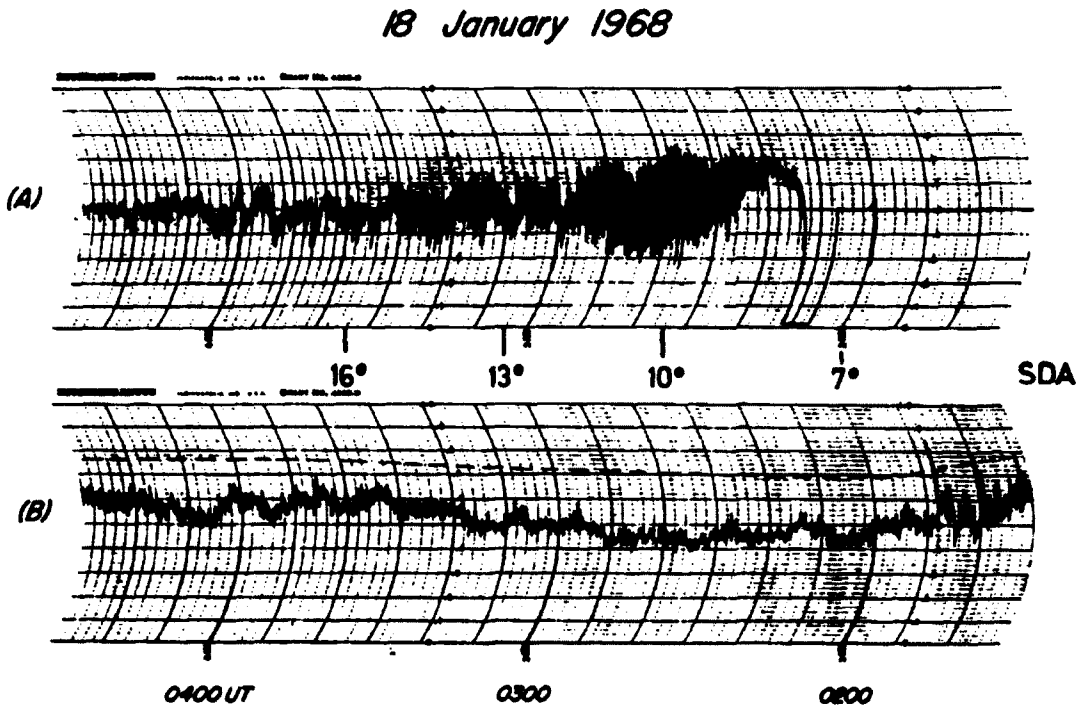

Figure 5-1: Plot showing riometer signatures of pulsating aurora (bottom panel) observed prior to photometer signatures (top panel). The photometer was turned on just after twilight, implying the pulsations existed in the afternoon sector. Time advances from right to left. Reprinted from *Berkey* (1978) with permission.

A statistical study was done by *Oguti et al.* (1981) of pulsating aurora during a solar maximum in 1980. They employed allsky cameras from five stations in Canada covering 61.5° to 74.3°, over the course of 34 nights. They found that there is a 30% probability occurrence of pulsating aurora near magnetic midnight, which increases dramatically to 100% near 0400 MLT. (Possibly this could extend further in MLT extent, but the cameras were forced to turn off at sunrise.)

Jones et al. (2011) used two Canadian allsky imagers (Gillam at 66.2° MLAT and Fort Smith at 67.4° MLAT) over the winter 2007-2008 season to complete a statistical study of pulsating aurora occurrences. The study found 74 pulsating aurora events and resulted in the following conclusions: (1) The source region of the pulsating electrons expands eastward for onsets in the pre-midnight sector. For post-midnight onsets, the progression is not as clear. This result disputes the link between substorm-injected electrons and pulsating aurora. (2) Although the most probable duration of a pulsating event is ~1.5 hours, the distribution includes many events lasting several hours or more. This finding has clear implications on the persistence of pulsating aurora (examined further by a related, subsequent study discussed in Sec. 5.5). (3) The occurrence rate increases to 60% in the morning sector, with onset especially likely (69%) just after substorm breakup.

5.2 Electron Precipitation in Pulsating Aurora

Pulsating aurora precipitation has been measured directly by many sounding rocket experiments, which found energies in the range of a few keV to several tens of keV (perhaps up to 100 keV), with stronger pulsations at energies around 30 keV and higher (*Bryant et al.*, 1969; *Whalen et al.*, 1971; *Bryant et al.*, 1975; *Sandahl et al.*, 1980; *Smith et al.*, 1980; *McEwen et al.*, 1981; *Yau et al.*, 1981; *Saito et al.*, 1992). However, *Sato et al.* (2002) reports observations of pulsating aurora electrons less than 5 keV. The Canadian pulsating

aurora rocket campaign (*McEwen et al.*, 1981) shows cases of pulsating electrons of surprisingly low energies, in the range of 1.5 keV to 1.8 keV over a single pulsating period. Much of this sounding rocket work has shown, through velocity dispersion analysis, that the source region of the pulsating aurora electrons lies in the equatorial magnetosphere (discussed in depth in the next section). Similar observations have been reported from satellite studies (*Frank et al.*, 1976; *Evans et al.*, 1987; *Sato et al.*, 2002).

There has been a strong assumed relation between substorms and pulsating aurora, due to a multitude of papers describing observations of pulsating aurora in the post-breakup recovery phase, e.g. *Akasofu* (1968), *Duthie and Scourfield* (1977). As such, several studies have focused on attempting to explain this link through high-energy, substorm-injected electrons (*Oguti and Watanabe*, 1976; *Akasofu*, 1977). More recently, this theory has been tested by studies seeking to show a magnetic conjugacy between pulsating aurora as seen on the ground and satellite observations of substorm-injected electrons in the equatorial magnetosphere (*Nemzek et al.*, 1995; *Suszcynsky et al.*, 1997).

Pulsating aurora modulations are often embedded in a larger swath of low-energy diffuse aurora. The precipitations are found to be from two entirely separate populations, although appearing simultaneously. More elaboration on this topic can be found in Sec. 7.1. One topic not discussed there is a link between pulsating aurora and diffuse proton precipitation, reported by *Viereck and Stenbaek-Nielsen* (1985). They found an apparent positive correlation between the diffuse Hβ emissions and the pulsating aurora period; the emissions increased in brightness as the pulsation period lengthened. The interpretation they give on this effect is that the proton flux gradually works to suppress the pulsations in the electron population. The authors also posit that there may be more than one process creating the pulsations (an insightful notion, that certainly should be more widespread). A major fraction of the pulsations seen were located equatorward of the proton aurora,

however, two pulsating events were observed within the region of the Hβ emissions.

5.3 Rocket- and Ground-based Source Region Studies

The source location of particles responsible for precipitating as pulsating aurora has been a long-standing question. The general position on this problem is that the source lies in the equatorial magnetosphere. This is due to a large body of work on the subject, coming to the conclusion from two methods: velocity dispersion analyses from sounding rocket experiments and conjugacy studies in both hemispheres.

Several velocity dispersion analyses have been performed on sounding rocket observations of energetic electrons in conjunction with auroral pulsations (*Bryant et al.*, 1975; *Yau et al.*, 1981). These studies showed that pulsating aurora is caused by energetic electrons (few to 10's of keV) (*McEwen et al.*, 1981; *Smith et al.*, 1980); the electrons are presumably precipitated by pitch angle diffusion into the bounce loss cone, and originate near the equatorial region of the magnetosphere (*Davidson*, 1986; *Huang et al.*, 1990; *Sandahl*, 1984). Characteristic pulsations from one such investigation are shown in Figure 5-2; here it is obvious that a one-to-one correlation exists between the optical pulsations in the aurora and the electron flux modulations measured in flight. The sounding rocket studies mentioned have consistently concluded that the electron populations must originate from geosynchronous orbit, perhaps as a result of scattering via VLF chorus or hiss (more details in the next section). This conclusion is based on examining the time delay in pulsations between the low- and high-energy electron populations and inferring a travel distance, which they found to be comparable to the length of the field line from the observation point out to the equatorial plane.

Investigations of magnetic conjugacy between pulsating aurora events have largely pointed to an equatorial source region (e.g. *Belon et al.* (1969); *Gokhberg et al.* (1970); *Stenbaek-*

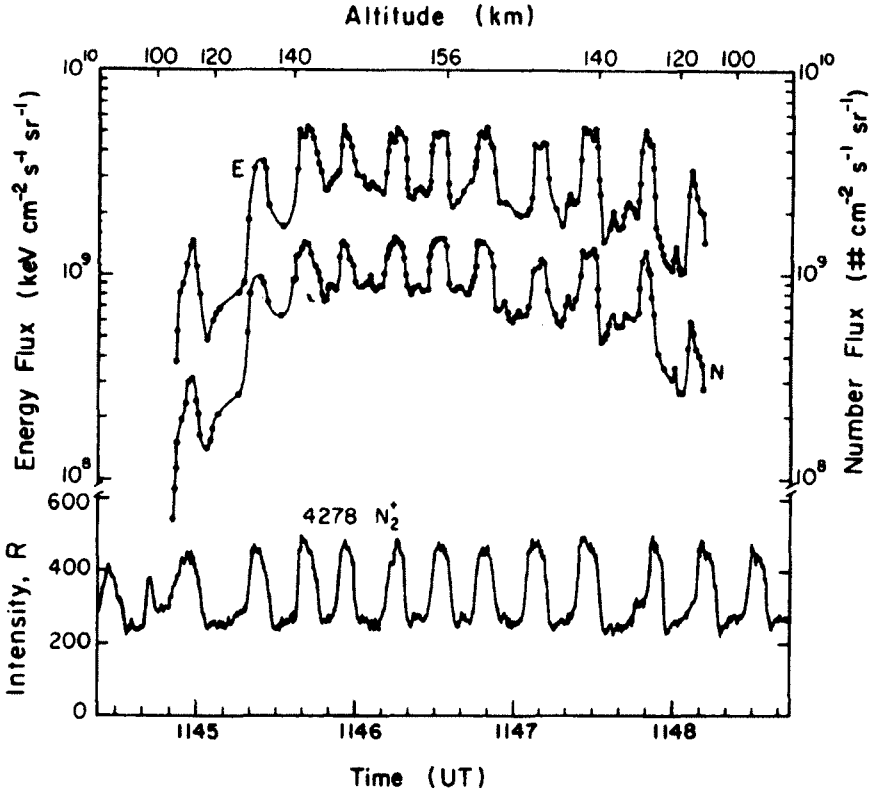

Figure 5-2: Electron fluxes observed from a sounding rocket (upper two traces) plotted with ground-based optical data (lower trace). Eleven distinct pulsations are shown in all traces. Reprinted from *McEwen et al.* (1981), with permission.

Nielsen et al. (1973), by observing pulsations simultaneously at two footpoints (one in each hemisphere) of the same field line, as deduced from theoretical magnetic modeling. This indicates the source mechanism is occurring at a point equidistant between the two observation points, i.e. the equatorial plane. Interestingly, some research reports on a lack of magnetic conjugacy (*Sato et al.*, 1998; *Watanabe et al.*, 2007), though the majority of work supports the conjugate observations. *Sato et al.* (2004), in part, explained this non-conjugacy by suggesting an ionospheric control of the pulsations, through oscillating electric fields. The role of the ionosphere in the pulsating aurora modulations is unclear, though much research implies there may be a source region near the equatorial magnetosphere and a secondary control mechanism closer to earth. This general topic will be considered further in Sec. 7.2.

There have been satellite examinations of the source region for pulsating aurora particles as well. We will delve into these in Ch. 6, where they become immediately relevant to our presented work on the same subject.

5.4 Wave-Particle Scattering Interaction

Pitch-angle diffusion is the standard theory for the generation of pulsating aurora precipitation, and wave-particle interactions are generally thought to be at the root of this process. Scattering via cyclotron resonance interaction (CRI) can result from different inception mechanisms, for which there are a plethora of theories.

One scattering theory is outlined by *Kennel and Petschek* (1966) and *Coroniti and Kennel* (1970a,b). When drifting electrons enter an interaction region, VLF wave growth occurs at the expense of electron perpendicular energy, thereby diffusing those electrons into the loss cone; next, hydromagnetic ULF waves act to modulate the growth of the VLF wave-particle resonance. This flux limiting effect could create periodic strong pitch angle

scattering events. Contradictory observations have been reported by *Oguti et al.* (1986) where they found no hydromagnetic waves in the equatorial magnetosphere conjugate to pulsating aurora. *Arnoldy et al.* (1982) also showed a lack of causality between magnetic pulsations and pulsating aurora, both observed from the ground.

Another current theory proposed by *Davidson* (1979, 1990) and developed within *Davidson and Chiu* (1991) invokes a nonlinear relaxation oscillator mechanism. This theory is essentially a constant cycle of refilling and dumping the loss cone through the following process: 1) trapped particles are lost through pitch-angle diffusion until 2) the electron distribution regains isotropy, thereby damping the waves and 3) the anisotropy increases in response to the changing pitch-angle diffusion rate and VLF wave growth is enhanced once more. The ratio of the strong diffusion lifetime, τ_S, to the relaxation time taken to refill the loss cone, τ_R, is theorized to be on the order of 10 or greater.

Additionally, a flow cyclotron maser (FCM) theory has been explored (*Tagirov et al.*, 1986; *Trakhtengerts et al.*, 1986; *Demekhov and Trakhtengerts*, 1994; *Trakhtengerts*, 1995). In this quasi-linear approach, drifting energetic electrons move into a region of dense cold plasma and generate the cyclotron maser, whereby VLF waves resonating within that flux tube scatter some of the electrons into the loss cone (Fig. 5-3). The "spent" electrons exit the interaction region and continue on their drift path with a more isotropic distribution. A new group of anisotropic electrons enters the region, sustaining the cyclical reaction.

Electrostatic ECH waves are also important for scattering auroral electrons (*Johnstone*, 1978). However, ECH waves only scatter electrons over a narrow range of pitch angles, and with energies from 100's of eV to a few keV. Upper-band chorus waves ($> 0.5\ \Omega_c$) scatter electrons in this same energy range, but are able to act on a much broader range of pitch angles. And lower-band chorus scatters electrons over broad pitch angles, with energies of a few to 100 keV. *Thorne et al.* (2010) compiled simultaneous observations of

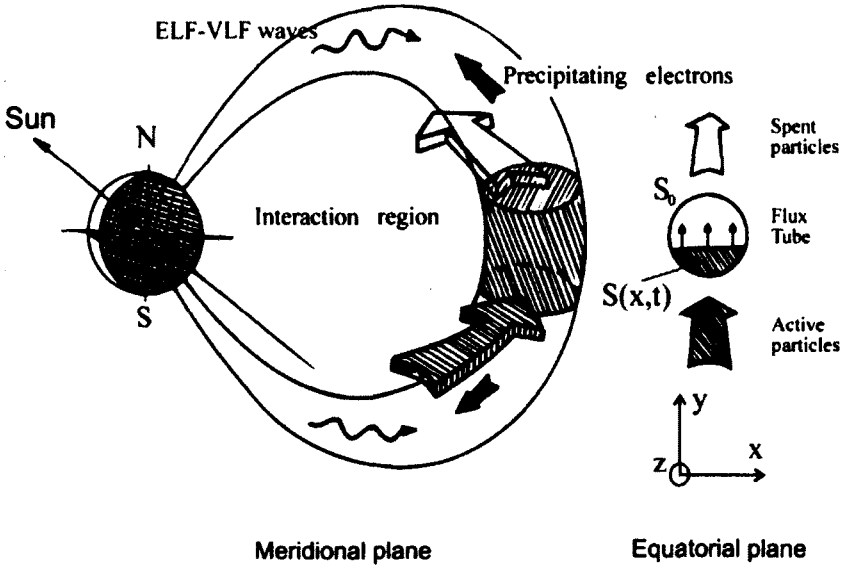

Figure 5-3: Schematic of the flow cyclotron maser generation of pulsating aurora. An anisotropic electron distribution drifts into the scattering region, diffuses into the loss cone via resonating VLF wave interaction, and then drifts out with a more isotropic distribution. Reprinted, with permission, from *Trakhtengerts and Rycroft* (2000).

low energy plasma sheet precipitation using the CRRESS satellite, and both ECH and chorus wave data from Polar. Their global statistics, in conjunction with their numerical model, led to the conclusion that chorus waves are accountable for the scattering of diffuse aurora electrons. And *Ni et al.* (2008) concluded the following: Lower-band chorus is the dominating scattering mechanism for higher energy (> 5 keV) electrons, while upper-band chorus is dominant for electrons with less than a few keV. Therefore, chorus is the much stronger candidate for the equatorial plane scattering that causes pulsating auroras.

VLF whistler-mode chorus waves are naturally occurring magnetospheric plasma waves that are distinguished as a discrete superposition of quasi-monochromatic emissions (*Sazhin and Hayakawa*, 1992). These wave bursts are generated near the magnetic equator (*Burtis and Helliwell*, 1969, 1976; *Russell and Holzer*, 1969; *Burton and Holzer*, 1974), and it is thought that their oscillating fields provide the mechanism for pitch angle scattering of energetic electrons into the loss cone (*Helliwell*, 1967; *Oliven and Gurnett*, 1968; *Rosenberg*

et al., 1971; *Tsurutani and Smith*, 1977). In Ch. 6, we will show how *Nishimura et al.* (2010) provide direct evidence that the modulation periods of chorus waves are indeed closely related to pulsating aurora. There we will also present our own work illustrating high correlations between equatorial region energetic electron fluxes and pulsating aurora periods.

There are just a few near-earth pulsation theories. In *Luhmann* (1979), a mechanism is submitted for pressure waves in the neutral atmosphere to drive pulsations in auroral luminosity. Poleward auroral arcs create acoustic gravity waves, which then generate these pressure waves and induce the pulsating aurora. And *Fedorov et al.* (2004) explore the interaction between Alfvén waves and the auroral acceleration region, wherein this interaction sets up oscillating field-aligned potential drops, causing the ULF modulation of energetic electrons. While investigation of near-earth elements is valuable, the overwhelming majority of work concentrates on the equatorial magnetosphere as the source for pulsating aurora electron modulation.

5.5 Widespread, Persistent Pulsating Aurora

Historically, pulsating aurora has been linked to substorm-injected electrons, and has been defined mainly as a recovery phase aurora. However, here we will present recent observations of the spatial and temporal extent of pulsating aurora that suggest this is a common, long-lasting and widespread auroral phenomenon that occurs without a necessary substorm precursor (*Jones et al.*, 2013).

Long-lasting pulsating aurora was observed on 11 February, 2008 using the THEMIS allsky imager array with stations located throughout Northern Canada and Alaska. The event lasted about 15 hours and, at its maximum observed spatial extent, spanned over 10 hours in MLT. In order to identify pulsating aurora at each location, both allsky images

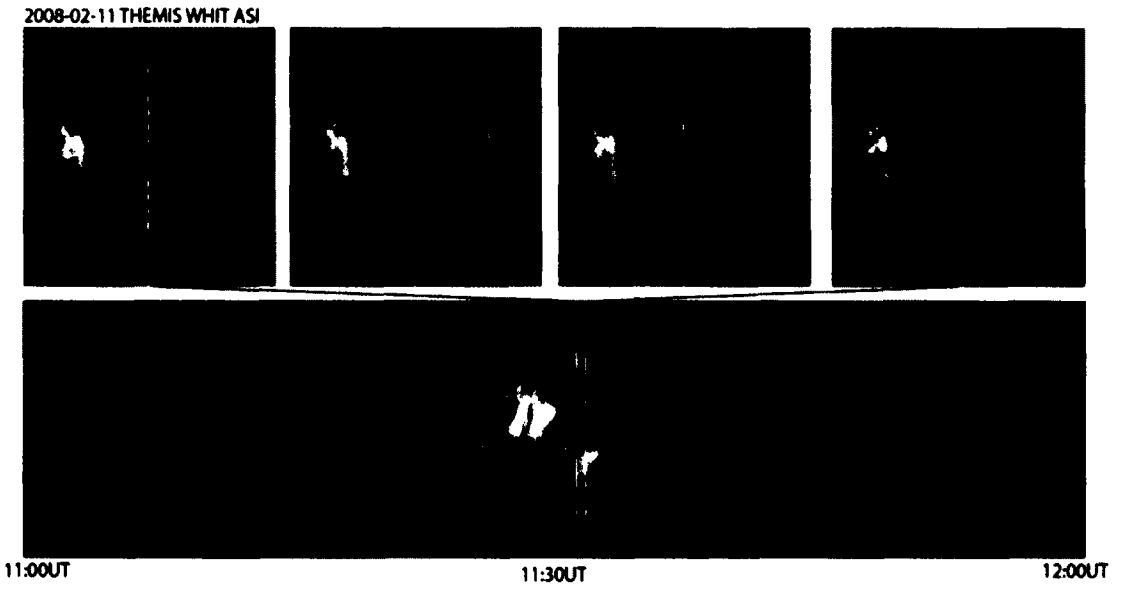

Figure 5-4: Allsky image frames and keogram showing typical pulsating aurora signatures. The thin bright lines in the keogram are representative of auroral pulsations. In the allsky images across the top, the encircled patch can be seen turning on and off between frames. Image courtesy of Emma Spanswick, University of Calgary.

and keograms were examined for typical signatures of these pulsations. Fig. 5-4 shows one example, from Whitehorse station, where pulsating aurora can be seen in the allsky frames across the top and thin striations signifying pulsating aurora can be seen in the keogram along the bottom. The white dashed lines through the allsky images show the pixel slice that was taken to create the keogram.

Mosaic images (and a movie) were created by projecting the THEMIS allsky images onto a geographic map of North America. The timeline of events is briefly described as follows. Discrete aurora begins before magnetic midnight (0340 UT) in the eastern stations, and expands westward. Next, pulsations begin in the eastern-most imagers, equatorward of the region where the discrete aurora first developed. The imagers turn on one-by-one in the west once nightfall occurs. By ~0430 UT, pulsating aurora covers almost the entire North American continent, from eastern Canada to Alaska. Several substorms come and

go over the next several hours. Each time, the localized pulsating aurora seems to be interrupted, or at least drowned out, by breakup aurora. When it returns, within the classical recovery phase, the pulsations are brighter, suggesting perhaps an energization by substorm-injected electrons. From 1000 UT, bright pulsating aurora is seen across the entire array (Fig. 5-5). The pulsations continue in the eastern-most camera until turn-off due to sunlight, implying the pulsations persisted into the daytime sector (though for how long is unknown). The cameras turn off one at a time across the array, with pulsations lasting until the last camera shuts off in western Alaska at 1715 UT. This event was one of several long-lasting events identified by examining 74 nights of clearly visible pulsating aurora over 7 months of allsky data from 2007-2008. Not only does our study show that pulsating aurora is likely not strictly a recovery phase phenomenon, it hints at the scope of large-scale energy deposition into the ionosphere through coupling with the magnetosphere via pulsating aurora precipitation.

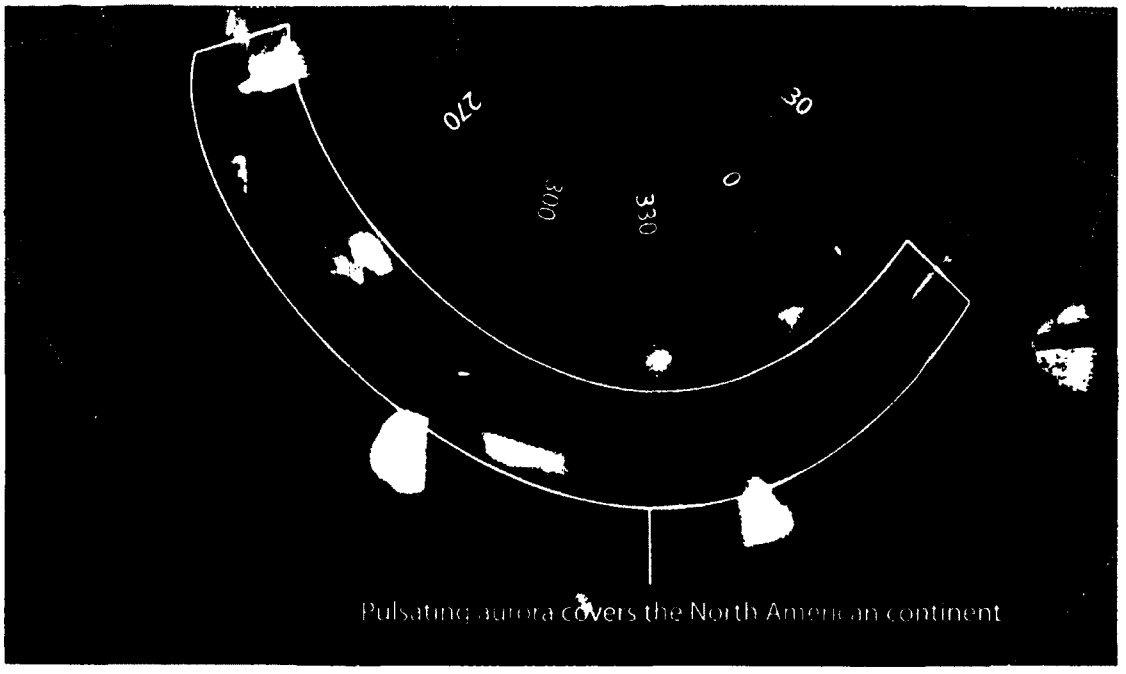

Figure 5-5: Pulsating aurora covers the entire continent of North America. The event lasted approximately 15 hours and covered a maximum span of over 10 hours MLT.

Chapter 6

Source Region of Pulsating Aurora in the Equatorial Magnetosphere

6.1 Recent Satellite-based Source Region Studies

While rocket- and ground-based studies of the source of pulsating aurora modulations were discussed thoroughly in Sec. 5.3, here we will review more recent work using satellite data. We have already touched on the paper by *Sato et al.* (2004), which determined the source region to be somewhere between the FAST satellite and the equatorial plane. However, they classify their pulsations as "east-west aligned band/arc type pulsations", which may have a different generation mechanism than more classical patchy pulsating aurora. *Miyoshi et al.* (2010) estimated the modulation source region to be near the equatorial plane, using a time-of-flight (TOF) model to analyze the energy dispersion of particle precipitation with data from the REIMEI satellite. The parameters derived from the TOF analysis (frequency of waves and vertical extent of modulation region) were consistent with previous statistical studies of whistler waves. *Nishiyama et al.* (2011) used two TOF models with REIMEI data to further examine the pulsating aurora source region. One model found the extent of

the generation region to be quite large, ranging continuously from MLAT -20° to 50°. The other model, which incorporated whistler waves, resulted in a much narrower region 11° off-equator. This study also found evidence that suggests perhaps upper-band chorus is the scattering mechanism for more near-earth modulations, while lower-band is responsible for equatorial plane scattering.

Specific correlations between equatorial lower-band chorus wave intensity and periods of pulsating aurora as observed from the ground were reported by *Nishimura et al.* (2010). Optical data was taken with an THEMIS allsky imager (Narsarsuaq station in Greenland) and wave frequency was observed with the THEMIS-A satellite. During a coordinated observation, high correlations were observed between the plasma wave modulations and the optical pulsations from the middle of a pulsating patch. At the highest coincidence point for this event, the two data sets were in agreement with a 0.88 cross-correlation coefficient (Fig. 6-1). A longer-duration chorus event at a later time was found to agree with a 0.71 cross-correlation coefficient. Also of note, ECH waves were reported to correlate well (0.73 coefficient) with an emergence of diffuse aurora, during which time no pulsations were present. The authors concluded that lower-band chorus in the near-equatorial region is responsible for modulating the pulsating aurora particles. This study was elaborated on and applied to magnetic field modeling in subsequent reports (*Nishimura et al.*, 2011a,b).

The dominant source of loss cone scattering for energetic equatorial electrons, which precipitate as pulsating aurora, has been explored but not yet clearly identified. Whatever the scattering mechanism, the source location of particles responsible for precipitating as pulsating aurora has been a long-standing question. In this study, we use simultaneous satellite- and ground-based data to show that there is a direct relationship between periods of energetic electron flux pulsations in space and pulsating aurora luminosity in the magnetically conjugate ionosphere. With high correlation coefficients linking the two data

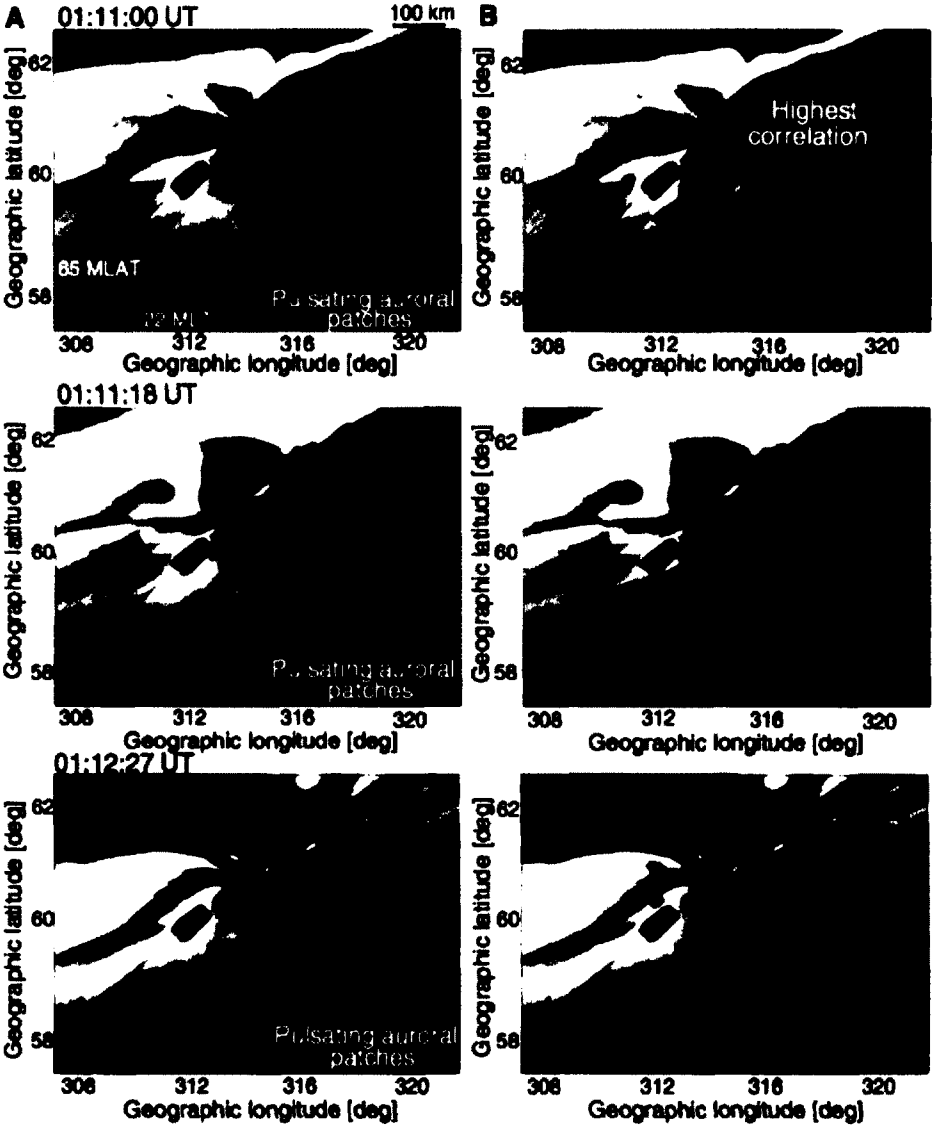

Figure 6-1: Cross-correlation analysis between equatorial chorus wave intensity and pulsating aurora periods. Column A shows where the pulsating patches appear within the image frames. Column B contains the correlation coefficients over-plotted on the frames as color contours. Maximum correlation value was 0.88. Reprinted from *Nishimura et al.* (2010), with permission.

sets, we present evidence that the source region of pulsating aurora lies in the equatorial magnetosphere.

6.2 Pulsating Event and Instrumentation

Observations of a typical pulsating aurora event were obtained on 15 March 2008, during relatively quiet geomagnetic conditions (K_p= 2-3), using the THEMIS All-Sky Imager (ASI) located at The Pas, Manitoba (TPAS) in northern Canada. Persistent pulsating aurora was present through the entire ASI field-of-view, covering an extent of ~1000 km in latitude and longitude at 110 km altitude, and image frames were obtained once every 3 seconds. Examples of 'on' and 'off' phases of pulsating patches from this data interval can be seen in Figure 6-2.

The geostationary (~6.6 R_E) GOES 13 satellite is located at 105° W, with magnetic midnight occurring at 0700 UT. The magnetic field line that threads the satellite location can be mapped down to the point where the field line intersects the ionosphere. This footprint, traced down to a 100 km altitude, maps to within the view of the TPAS ASI, as discussed in a subsequent section. The conjunction makes GOES 13 a prime candidate to look for electron populations in space, before they reach their destination in the ionosphere. In contrast to previous, spin-stabilized spacecraft (*Johnstone*, 1983; *Nemzek et al.*, 1995), GOES 13 is a three-axis-stabilized platform from which field-aligned particle observations can be made continuously for long periods of time. During the pulsating aurora event, simultaneous observations of electron fluxes (10's of keV) and magnetic fields were obtained from GOES 13, which was positioned just north of the geomagnetic equator at ~8° MLAT.

The Magnetospheric Electron Detector (MAGED) on GOES 13 consists of nine solid-state detector telescopes, whose fields-of-view are arranged in a crossed fan (Fig. 6-3). Each telescope reports electron fluxes in five energy channels: 30-50 keV, 50-100 keV, 100-

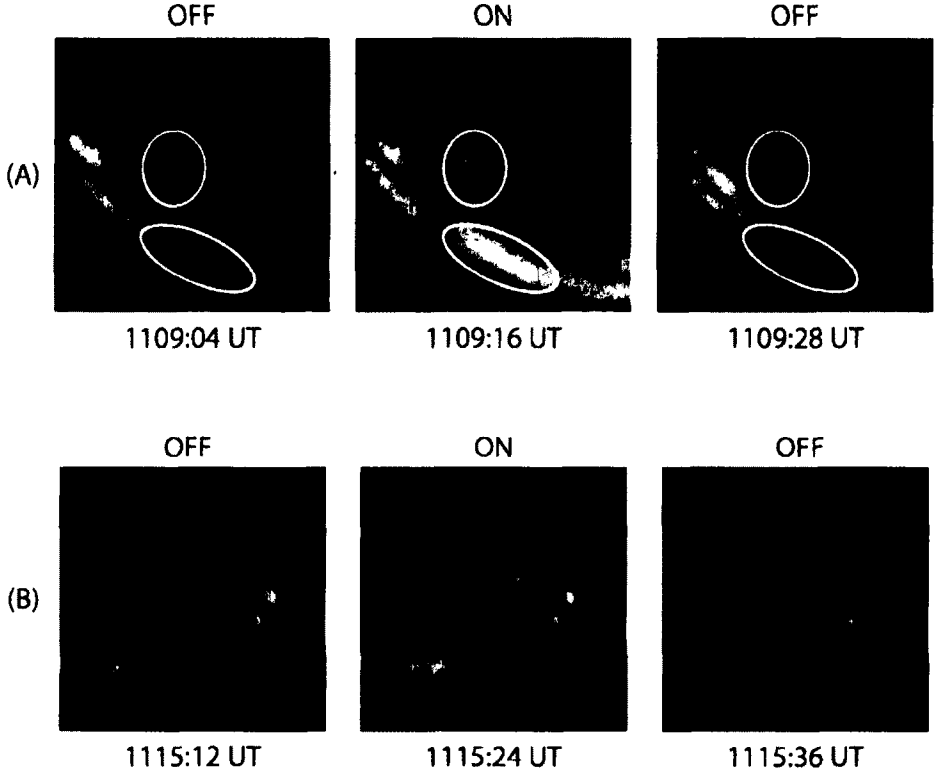

Figure 6-2: Two examples of sections of allsky imager frame sequences showing an off-on-off modulation of pulsating patches. (A) The top series spans 1109:04 UT to 1109:28 UT, and is taken from the lower left corner of the allsky images, or the north-east direction. The specific patches referred to are circled. (B) The bottom series spans 1115:12 UT to 1115:36 UT, at a later time than the series in (A), and taken from the bottom center in the due-north direction. The period for both series is approximately 24 seconds.

200 keV, 200-350 keV, and 350-600 keV, with accumulation periods of 2.048, 2.048, 4.096, 16.384, and 32.768 seconds, respectively. This analysis focuses on the 30-50 keV channel. The fields-of-view of the telescopes have a full-width-half-max of approximately 20°. The GOES 13 spacecraft can fly upright or inverted, which results in east-west and north-south swaps of field-of-view pairs, with the 0° telescope being invariant. For the duration of the event detailed in this study, the detector was in the inverted configuration. On-board compression of the electron flux data can result in quantization steps of as much as 6%. This, combined with the fields-of-view of the telescopes, limits the ability of the instrument to resolve small fluctuations.

On 15 March 2008, we observed periodic fluctuations of GOES 13 electron fluxes in the two lowest energy channels, covering 30-100 keV, intermittently in telescopes 6 and 9 (T6 and T9) between 0700 and 1500 UT. Reports on pulsations above 50 keV, such as we are reporting, are rare (*Sandahl et al.*, 1980; *Whalen et al.*, 1971). Figure 6-4 shows MAGED electron fluxes in the 30-50 keV and 50-100 keV channels from all nine telescopes, along with their associated time-varying pitch angles and magnetic field components. The pitch angles of the individual telescopes are determined from the relative direction of the particle velocities and the magnetic field measured by the GOES 13 magnetometer in the spacecraft body reference frame. In this inverted orientation, T9 is generally closest to zero pitch angle under geomagnetically quiet conditions. During disturbed periods, as the orientation of the magnetic field changes rapidly, the MAGED telescope pitch angles also change rapidly.

6.3 Methodology and Correlation Analysis

We present analysis of the 30-50 keV channel of T9 from 1100-1130 UT, as this energy channel and time span had the most notable pulsations. T9 was the MAGED telescope most closely field-aligned during this time and the only one that exhibited significant short-

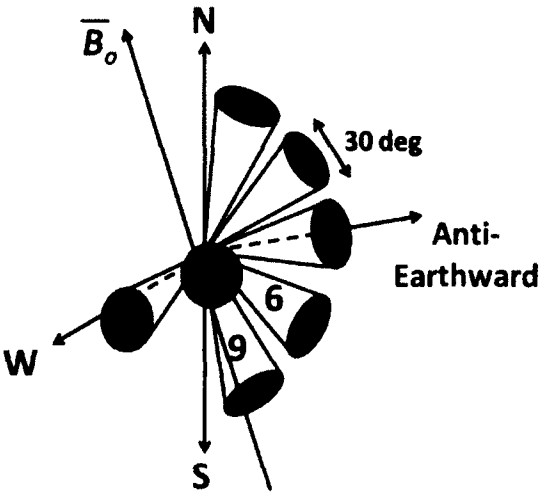

Figure 6-3: Schematic of GOES 13 MAGED telescope array, shown flying in inverted position, where T9 is most closely field-aligned.

term (< 1 min) flux variations. The TPAS ASI showed intense auroral pulsations during this time. Figure 6-5 shows concurrent line plots for both the pixel relative luminosity and the satellite particle flux. For this plot, the pixel sampled is one that has a high correlation coefficient during the time interval shown. The peaks in both data sets coincide closely. A sawtooth component is often evident in both data sets, which can possibly be interpreted as a loading and dumping cycle for the particle populations and may thus have implications for the theory of these specific wave-particle interactions. The theory of a nonlinear relaxation oscillator, detailed in Sec. 5.4, requires a similarly shaped particle flux modulation. Additionally, the average periods for both the pulsating aurora pixel luminosity and the GOES 13 flux measurements over the plot duration are ~22 seconds and ~24 seconds, respectively. Over the entire duration of the event, the average periods of both data sets vary from ~10-26 seconds. These matching characteristics are cited as further evidence that the pulsating aurora electron populations are originating from the same source region that GOES 13 is detecting in orbit. Fig. 6-6 shows the GOES 13 MAGED flux as

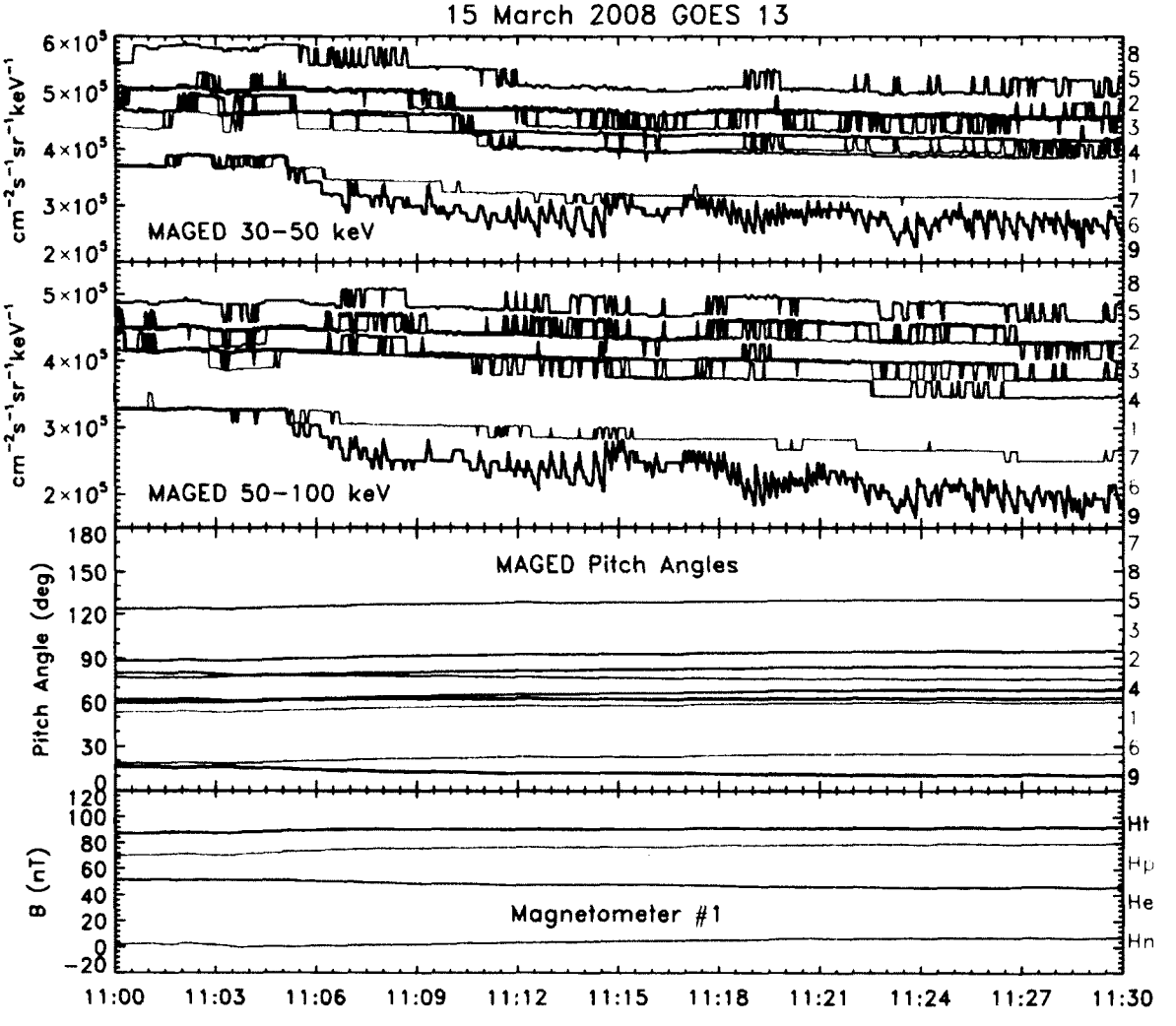

Figure 6-4: 15 March 2008, 1100-1130 UT, GOES 13 MAGED electron fluxes in the 30-50 keV and 50-100 keV channels from all nine telescopes, GOES 13 Magnetometer field components, and calculated pitch angles. The 30-50 and 50-100 keV channels in T9 (black trace), whose center is closest to zero pitch angle, are the only channels that exhibit significant short-term (<1 min) flux variations. The step changes in the fluxes measured by the other telescopes are due to on-orbit compression. The trace color matches the telescope number in the top three panels (as indicated in right axis).

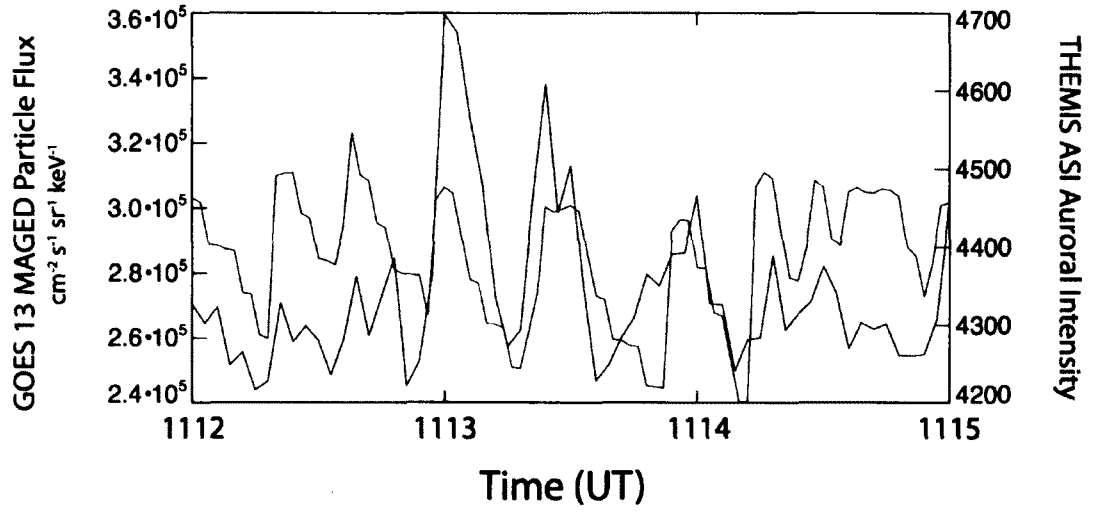

Figure 6-5: Over-plotted time series from 1112-1115 UT of THEMIS ASI pixel intensity (for high-correlation pixel) in blue and MAGED electron flux (for the 30-50 keV channel of T9) in red. Similarities in period and pulse shape are present.

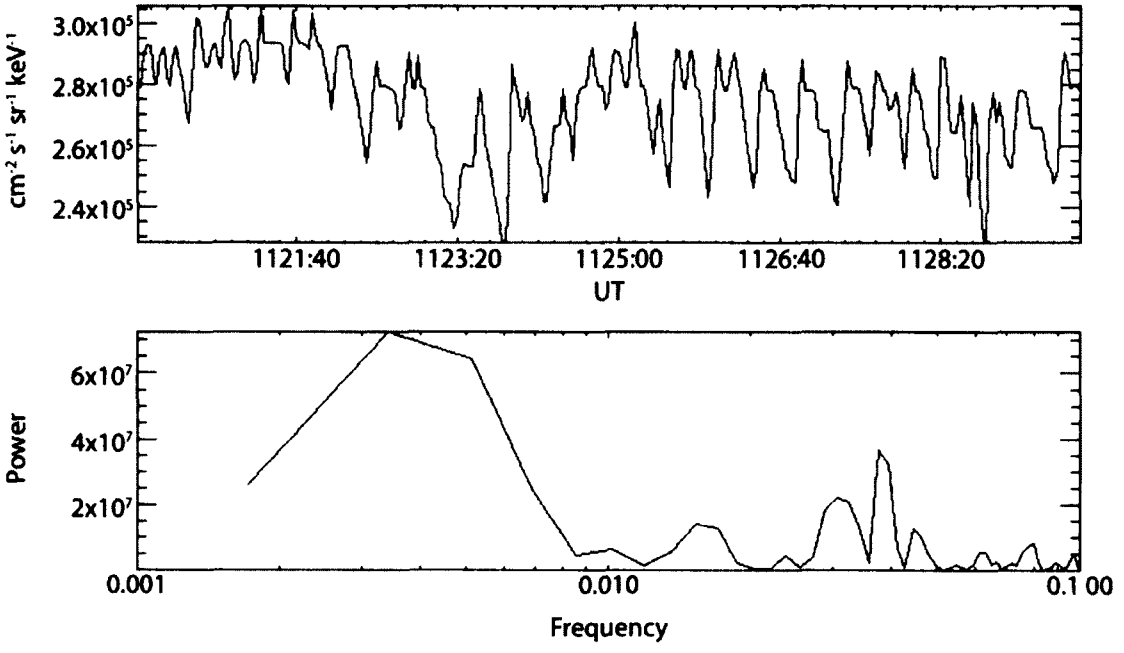

Figure 6-6: GOES 13 MAGED fluxes and FFT spectrum as a function of time from the 30-50 keV channel for T9 in the upper panel, spanning 1120 UT to 1130 UT. The spectral peak at ~38 mHz corresponds to a ~26 s pulsation period over this interval.

a function of time from the 30-50 keV channel for T9 in the upper panel (from 1120 UT to 1130 UT.) The lower panel shows the corresponding FFT spectrum, resulting in a frequency versus wave power plot. The FFT spectral peak occurs at ~38 mHz, indicating a ~26 s period. Also of note are the peak shapes apparent in this figure. The sawtooth shape of the pulsations is evident, as well as a double peak feature, the cause of which is not known.

6.3.1 Cross-Correlation Results

In order to numerically determine the similarities between the two data sets, we computed an array of the cross-correlation coefficients between the pixel luminosity for each individual pixel in the ASI and the flux measurements from GOES 13. The THEMIS ASI images consist of an array of 256 by 256 pixels. After compiling 600 images over 30 minutes of data, with 20 images per minute, we sampled all 65,536 pixels contained in each image to correlate with the GOES 13 signal. The number of images used varied with the time interval of the individual correlation. Correlation intervals examined were in the 3 to 5 minute range; due to the fluctuation period being tens of seconds, more than a minute of data was necessary to determine an accurate correlation value for a given pixel. And for longer than 5 minute intervals, the pulsating patch would often have drifted out of view of the pixel by the end of the interval. Since our data span just 30 minutes, intervals were overlapped such that numerous correlations could be computed within the data set. For example, for a 3 minute correlation interval, the first interval would range from 1105-1108 UT, the second from 1106-1109 UT, the third from 1107-1110 UT and so on, resulting in a total of twenty-seven intervals to cover the total 30 minutes of measurements.

For each time increment, we generated a contour plot and overlaid it on a single THEMIS ASI image (generally one displaying the patches "on", as seen in Panel B of Fig. 6-7) showing correlation coefficient trends. The fluctuation periods of the two data sets are

highly correlated during various times, indicating a one-to-one response for certain patches. The first plot of Figure 6-7, panel A, shows a contour plot for a 5 minute time interval, with areas of over 0.85 correlation coefficient values in red, spanning the time range 1104-1109 UT. The maximum correlation value for this time interval is 0.92. Note that the regions of high correlation drop off to lower values as the contours move outward, as would be expected. Each contour plot has a white cross indicating the one pixel of maximum correlation at that time. Panel C is a contour plot for a shorter correlation interval of 2 minutes, and shows less widespread high correlations, yet still has a high maximum correlation value at 0.81. Panel D shows a contour plot of the time interval 1119-1124 UT, and illustrates how the high correlations have diminished during these later times. This is likely due to the intensified footpoint motion during this time, as discussed below in Sec. 6.4. Fig. 6-8 shows a zoomed-in detail view of the high correlation regions in Panels A and C of Fig. 6-7.

6.3.2 Time Lag Between Data Sets

We built a variable time lag into the analysis in order to determine the optimal time difference to produce the best correlation coefficients. The two data sets were each interpolated down to 1-second time steps to allow better control on lag shifts. The data shown in Figure 6-7 is for a lag time of 0 seconds. Depending on the correlation interval examined, a lag of 0-1 seconds gave the highest overall correlation values. Prior experimental measurements of total round-trip electron bounce times from the Echo 7 sounding rocket were found to be $\sim$2 +/-1 s for the highest energy (30 keV) electrons reported (*Nemzek et al.*, 1992). Since a total round-trip travel time should be four times the expected lag time between our two data sets, and our energy range was higher in scope than the Echo 7 experiment, our estimated lag time is agreeable with experimental results.

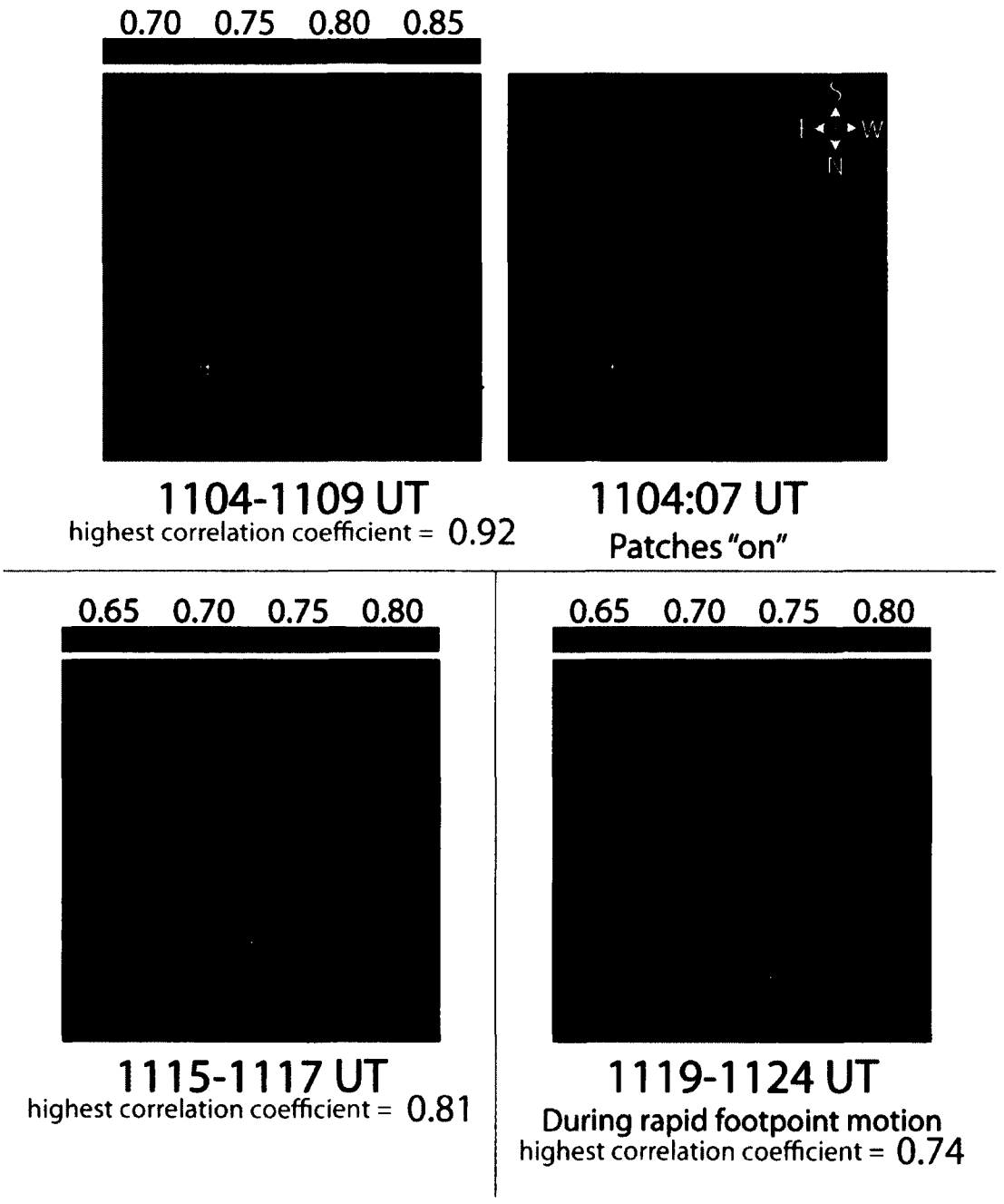

Figure 6-7: Correlation coefficient contour plots of GOES 13 flux data with THEMIS all-sky PA intensity. **Top row:** Panel A shows contour plot of correlation coefficients overlaid on the corresponding all-sky image for a correlation interval of 5 minutes, from 1104 to 1109 UT. Panel B shows the patches in their "on" phase, to compare with the contour plot that partially obscures the patches. Maximum correlation value is 0.92, marked by a white cross. **Bottom row:** Panel C is for a shorter correlation time of 2 minutes, showing less correlation during a shorter interval, but still with a high maximum correlation value (0.81), again marked by a white cross. Panel D is for a later time, with a correlation interval of 5 minutes, and shows a drop in correlation values and scope, potentially due to rapid footpoint motion. Maximum correlation value is only 0.74.

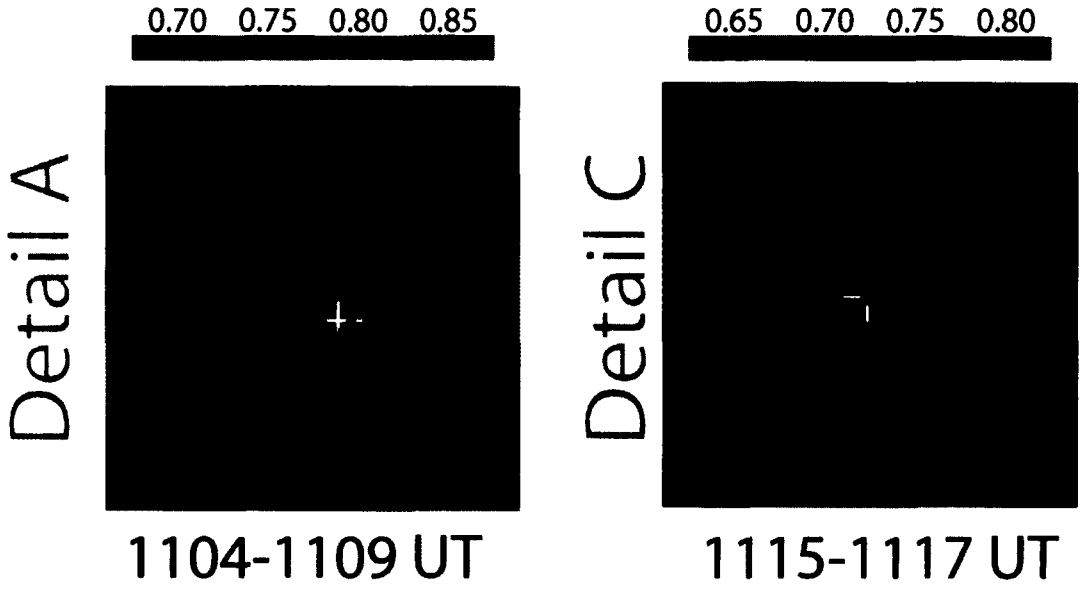

Figure 6-8: Detailed view of the high correlation regions from Panels A and C in Fig. 6-7. As above, the white cross marks the pixel of maximum correlation (0.92 in Detail A and 0.81 in Detail C).

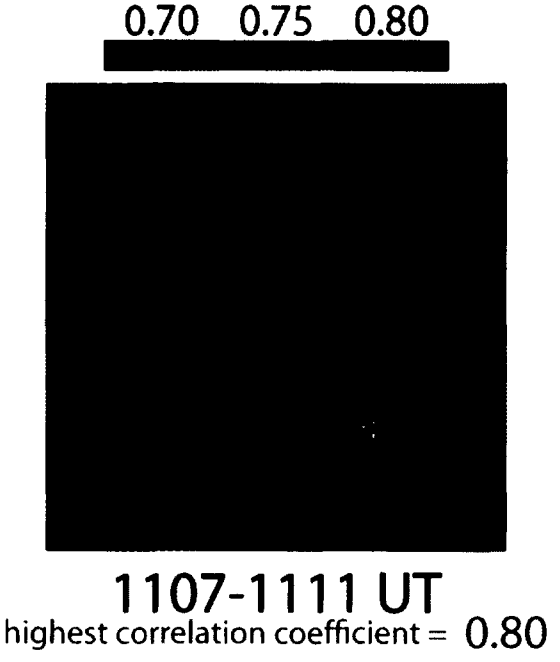

Figure 6-9: An additional contour plot covering the four-minute correlation interval 1107-1111 UT, showing correlations ranging from 0.7 to 0.8. The white cross marks the highest correlation pixel, having a value of 0.80.

Note that the data from the satellite uses a corrected timestamp. The 30-50 keV channel has a time resolution of 2.048 s, which is the time necessary for both the accumulation period and sample spacing. The spacecraft also requires time to read out the data at the end of accumulation period. The timestamp for all data points is corrected by 3.072 s earlier, to place the time precisely in the middle of the accumulation period. This allows us to establish an accurate temporal relationship between the electron flux and the pulsating aurora.

6.4 Satellite Footpoint Motion and Mapping Discussion

The location of the GOES 13 satellite during this observation period has been traced to a 100 km altitude in the northern hemisphere using the TS05 model (*Tsyganenko and Sitnov*, 2005) based on calculations of the satellite's location using its two-line elements, and using OMNI solar wind data as input. (For this hour, K_p = 3+, v_{SW} = 619 km/s, B_z (GSM) = -0.5 nT, B_y (GSM) = 3.2 nT.) Although it is traditionally used as a storm-time model for the inner magnetosphere, TS05 has been shown to be the most accurate model for geosynchronous orbit at all disturbance levels (*Huang et al.*, 2008). By assuming that the auroral emissions observed in the ASI come from ~100 km altitude, we can map the ASI images onto geographic coordinates in order to determine the set of pixels that contains the mapped GOES 13 footprint. From the model calculations, we find that the northwest quadrant of the image (the lower right-hand section) contains the set of pixels that has been mapped most closely to the footprint of the equatorial GOES 13 location. However, the mapped region of pixels does not coincide directly with any high-correlation locations.

Figure 6-10 depicts the time evolution of the modeled Northern hemisphere footprint of the satellite between 1100 and 1130 UT on the day of our event. Towards the end of the 30 minute window, the mapped footpoint behaved erratically. There was a dramatic shift in footpoint location from 1115-1130, throughout the time of high pulsations at GOES 13. By

examining the TS05 drivers, we offer the following explanation for this shift. The beginning of the interval corresponds to the period of Bz < 0 starting near 0730 UT and ending soon after 1115 UT. This would suggest that the shift in location is related to a decrease in Region 1 and 2 currents as well as, to a lesser degree, the tail current and partial ring currents (assuming the latter at dusk) as Bz turns northward. The disappearance of meaningful correlation values after 1116 UT is likely due to the rapid footpoint motion of the field line within the viewing area of the ASI.

In the event presented, we see a strong correlation between pulsating aurora modulations and equatorial electron flux pulsations at GOES 13 while it is located along a field line over a region of widespread pulsating aurora on the ground. However, the shape and scope of the interaction region providing the scattering cannot be determined, limiting the ability to pin down the field line footprint location based on this data set alone. There are several pulsating patches that are candidates for a footpoint match, and there are other optical patches whose oscillations are clearly uncorrelated with the GOES 13 electron flux variations. Those patches absent of correlation may be supplied with particles from a distinct but nearby source region. We can presume that the interaction region is nebulous in structure, not uniform, and will therefore likely feed certain field lines but not others in the same vicinity.

6.5 Loss Cone Coverage and Implications

Another result we report is the preliminary quantification of loss cone coverage of each telescope and how it changed in response to magnetospheric dynamics. This analysis is discussed in detail below. The field line intersecting the satellite location changed shape during our time interval, which allowed us to examine the fluctuations seen in T6 and T9, and compare those to the telescope response functions as the field line stretched from one

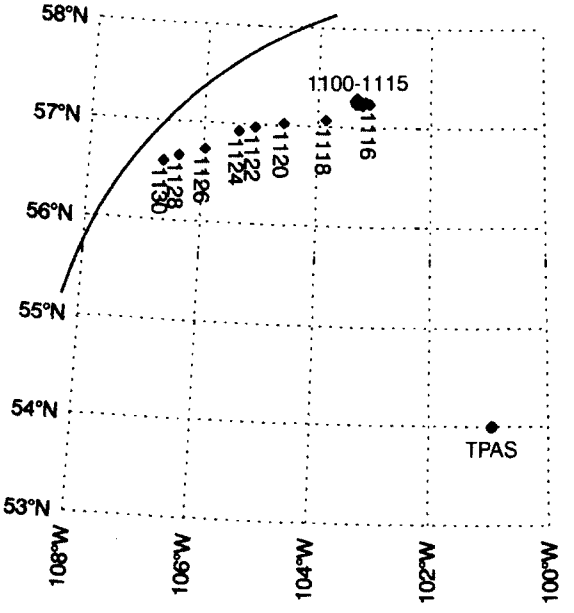

Figure 6-10: Northern hemisphere footpoint of the field line threading GOES 13 between 1100 and 1130 UT. The field line tracing has been performed using the TS05 model with OMNI solar wind data as input. These locations lie in the northwest quadrant of the field-of-view of the THEMIS TPAS ASI. At 1115, the foot of the field line lies just west of Reindeer Lake in Saskatchewan; at 1130, the foot of the field line lies ~200 km southwest.

orientation to another.

6.5.1 Telescope Response Function Calculation

The first step in determining the fraction of the measured flux that could lie within the loss cone is to assume a flat distribution in pitch angle within an individual telescope FOV and to integrate over the telescope response accordingly. In order to quantify the pitch angle coverage of the MAGED telescopes, the two-dimensional telescope response is transformed into pitch angle coordinates following the method of *Selesnick and Blake* (2000). Since the central pitch angle of each telescope varies with the magnetic field orientation, this transformation is recalculated for every consecutive pitch angle distribution.

The count rate R_{ik} in telescope k at energy i is related to the differential flux as follows:

$$R_{ik} = \int\int j(E_i, \theta, \varphi) A_k(E_i, \theta, \varphi) d\Omega dE$$

where $A(E, \theta, \varphi)$ is the effective area (cm^2) of the detector at particle kinetic energy E and direction (θ, φ). By attributing the differential flux to an energy $\bar{E}$ within a bandpass of equivalent width δE, assuming the flux is gyrotropic (symmetric with respect to the direction of the magnetic field), and treating the effective area as cylindrically symmetric about the telescope axis (a good approximation for MAGED), the above integral equation can be simplified. Knowing the central pitch angle, the effective area can be transformed numerically from a function of telescope angle θ_t to a function of pitch angle and gyrophase angle. The telescope response function G_k (cm^2 radians), a function of pitch angle, is calculated by integrating the transformed effective area over gyrophase angle:

$$G_k(\bar{E}_i, \alpha) = \sin(\alpha) \int_0^{2\pi} A_k \left[\bar{E}_i, \theta_t(\alpha, \beta)\right] d\beta$$

It is defined from 0 to 180 degrees pitch angle, and is identically zero at 0 and 180 degrees, due to the $\sin(\alpha)$ factor, and positive in between. The subscript k indicates the number of the telescope. These response functions provide the key to understanding the behavior of the MAGED fluxes.

6.5.2 Central Pitch Angles and Corresponding Flux Observations

The following discussion concerns the extended period after 1100 UT when fluctuations were observed in T9. The central pitch angles are shown in Figure 6-4 and the telescope response functions are shown in Figure 6-11. The central pitch angle of T9 decreased steadily between 1100 and 1120 UT. At 1100:30 UT, the contribution from the loss cone ($\sim$2.5°) to the T9 count rate was 0.0%. By 1106:30, the contribution was 0.4%, and structured fluctuations began to appear in the flux observations. (See Fig. 6-12 where telescope response function and fluxes are plotted concurrently.) Between 1114 and 1135, the contribution ranged from 1.4% to 2.5%. The fluctuations tapered off after 1140 UT. The fluctuations in T6 were of the order of the quantization level throughout this period. Assuming the fluctuations appeared at 1107 due to the change in the telescope central pitch angle rather than a change in the magnetospheric dynamics, the lower pitch-angle limit of the T6 response function at this time indicated that the flux variations in T9 were occurring over pitch angles below $\sim$10°. For example, the large fluctuations at 1126-1127 UT represented 17% of the flux, which corresponded to the T9 response function integrated over pitch angles below 7°. Therefore, a region of phase space much larger than the nominal loss cone was being repeatedly depleted and filled. This region will be more fully characterized, with error bars due to quantization effects, in future work. The response functions are consistent with the fluctuations only appearing in a telescope that overlaps the loss cone, and analysis of the functions promises to allow us to constrain the portion of the pitch angle distribution

that is causing the fluctuations in the observed 30-100 keV electron fluxes.

6.6 Magnetic Field Observations

During the time intervals on 15 March 2008 when pulsations in the 30-100 keV electron fluxes were observed, no coherent ULF wave activity was observed by the GOES 13 magnetometer. In the H_p component (in the direction perpendicular to the satellite's orbital plane), there was a small level of interference from spacecraft current sources that places an upper limit of a few tenths of a nanoTesla, larger than the amplitude sampling resolution, to the ability to readily detect coherent wave amplitudes in this axis. This observation is consistent with the results of *Oguti et al.* (1986), who compared pulsating auroral observations in Canada with magnetic field observations on GOES 2 and GOES 3 (which made electron flux measurements only above 2 MeV). In the absence of the 30-100 keV electron flux measurements, the conjugacy of the older GOES satellites and the pulsating aurora was estimated using magnetic field models. In the nine time intervals (11.3 hours total) that they examined, *Oguti et al.* (1986) found that the amplitude of all fluctuations with periods less than 40 seconds was less than 0.6% of the total field. The GOES 2 and GOES 3 magnetometers had a 3.06-s reporting period and a resolution of 0.2 nT, while the GOES 13 three-axis fluxgate magnetometer has a 0.512-s sampling period and an amplitude sampling resolution of 0.03 nT.

With no clear source identified, and consisting of successions of rising tones (*Sazhin and Hayakawa*, 1992), chorus emissions in the magnetosphere are notoriously enigmatic. Within the confines of the analysis presented here, lacking coherent magnetic field data from the spacecraft, we are not able to determine the nature of the waves in the interaction region. However, based on the vast body of work already mentioned on the statistics and modeling of whistler-mode chorus wave location and relation to pulsating aurora, chorus is

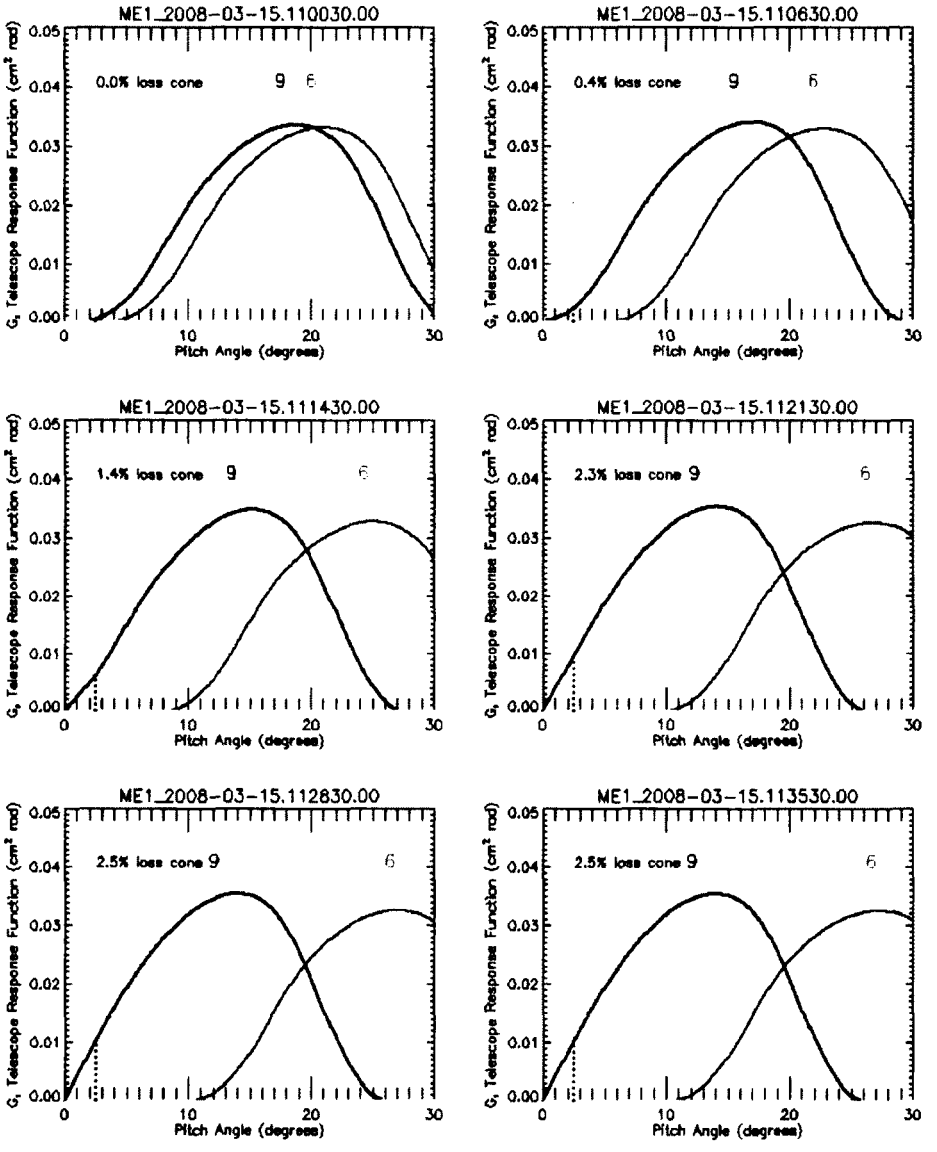

Figure 6-11: Telescope response functions for GOES 13 MAGED T6 and T9, 1100:30-1135:30 UT, 15 March 2008. During this period, the FOV of T9 overlaps the loss cone. The percent contribution from the loss cone to the telescope count rate increases from 0.0% to 2.5% during this period.

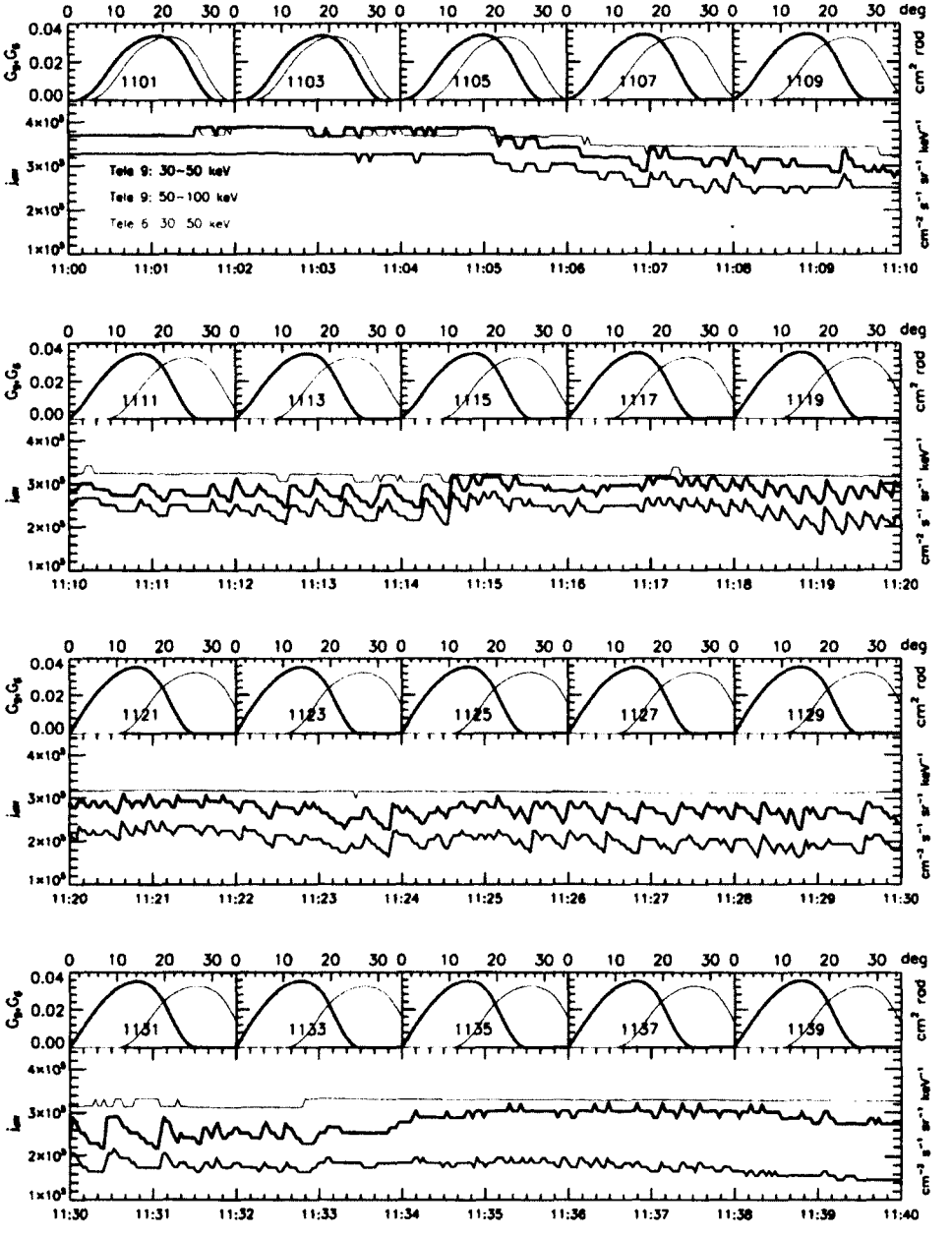

Figure 6-12: GOES 13 MAGED electron fluxes (j_{diff}) and telescope response functions (G), 1100-1140 UT. In the top rows of each panel, the telescope pitch-angular response functions as a function of pitch angle are shown every two minutes for T9 (black) and T6 (blue). The bottom rows of each panel show the 30-50 keV fluxes from T9 (black) and T6 (blue) plotted along with the 50-100 keV fluxes from T9 (red). Note that fluctuations are only appearing in a telescope that overlaps the loss cone (assuming a 2.5° loss cone).

a likely candidate for the pulsating aurora pitch angle scattering mechanism. Furthermore, the periods observed in this study correspond well to chorus wave packet repetition periods. An illustration of the theoretical scattering process is presented here for consideration (Fig. 6-13).

6.7 Conclusions and Further Study

Widespread pulsating aurora was observed on 15 March 2008 in the THEMIS TPAS ASI. During this time, over a shorter interval, pronounced short-term electron flux modulations in the 30-100 keV range were observed using the MAGED telescope on the geosynchronous GOES 13 satellite. The cross-correlation analysis of periodic fluctuations seen in both the GOES 13 electron flux measurements and the intensity of pulsating aurora in the THEMIS ASI, from 1100-1130 UT, shows regions of high correlation between the two phenomena. This result suggests that there is a strong relationship between frequencies of equatorial electron flux pulsations and pulsating aurora luminosity in the corresponding ionospheric magnetic footprint.

Another result obtained from this study was the preliminary quantification of loss cone coverage of each telescope and how it changed in response to magnetospheric dynamics. In short, the fluctuations only appear in a telescope that overlaps the loss cone; this may allow a better determination of the extent of the pitch angle distribution that is causing these fluctuations, and therefore the size of the loss cone.

A logical extension of this type of observation would include conjunctions with satellites able to resolve the plasma waves, such as THEMIS, in order to correlate electron fluxes, chorus, and pulsating aurora simultaneously. Additional information about the cold plasma density in the active flux tube would also serve to illuminate the theory behind the pulsations. This study is consistent with both the flow cyclotron maser and relaxation oscillator

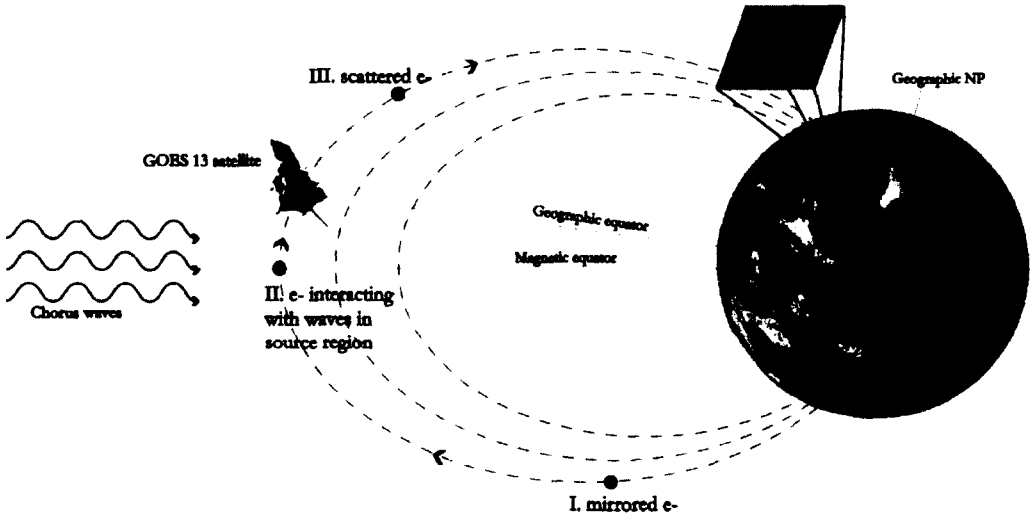

Figure 6-13: Conceptual drawing of the potential chorus scattering mechanism that drives pulsating aurora. I. Trapped energetic electrons bounce between mirror points along closed field lines. II. Incident chorus waves generated in the vicinity of the equatorial magnetosphere serve to scatter electrons into the loss cone in a periodic fashion. III. The scattered electrons precipitate in the ionosphere where the allsky imager sees them as auroral pulsations. GOES 13, sitting just off the magnetic equator, sees the energetic electron flux as the pitch angle diffusion process is taking place.

theories presented in Sec. 5.4.

The general correlation technique detailed in this study may be adapted to serve as a validity check on current mapping models, though clearly there exists some ambiguity in determining the exact location of the field line footprint. In addition to magnetic mapping constraints, this data set serves to strengthen our overall understanding of pulsating aurora and truly confirms the conjecture that a source region of pulsating aurora modulated electrons lies in the equatorial magnetosphere.

CHAPTER 7

PULSATING AURORA MORPHOLOGY WITHIN THE CONTEXT OF DIFFUSE AURORA

Pulsating aurora almost always appears within a region of diffuse aurora. This well-documented paradigm has led to confusion as to the nature of pulsating aurora. The idea that pulsating aurora evolves from diffuse aurora, and originates from the same mechanism, had been a common misconception. Studies over the past 40 years, however, illuminate this error. Yet there is no denying a relationship between the two auroral types. One of the outstanding problems of auroral physics is the precise characterization of this connection.

7.1 Relationship Between Pulsating Aurora & Diffuse Aurora

Perhaps the first study that strived to disentangle the mechanisms governing these related types of aurora was *Brown et al.* (1976). The basis of their study was the use of triangulated measurements to determine auroral emission heights of various auroral forms. A pair of imagers were placed along a 10-km baseline and analyzing observations to obtain an estimate

of the auroral lower border. They determined a median altitude of 92 km for pulsating aurora, with a total range of 82-105 km. The energy required for such lower borders is 10's of keV to 60 keV, consistent with measurements made by *Rosenberg et al.* (1971) and in a whole host of measurements done since that time. Using these conclusions, together with a PhD dissertation by *Royrvik* (1976), *Brown et al.* (1976) drew up this classic picture of the vertical extents of pulsating, diffuse and discrete auroras (Fig. 7-1). It depicts a layer of soft electron diffuse aurora, comprised of ~1 keV electrons, sitting at an altitude above (and wholly separate from) the region of higher-energy pulsating aurora precipitation in the range of 30-60 keV. Thus, the ground observer sees pulsating aurora occurring "over" the diffuse aurora, obscuring the dim layer; and consequently, the pulsating aurora appears embedded in a field of surrounding diffuse aurora.

Since then, many authors describe observing pulsating aurora within a non-pulsating diffuse background (*Royrvik and Davis*, 1977; *Stenbaek-Nielsen and Hallinan*, 1979). Furthermore, this soft electron background often appears first, with pulsations emerging seem-

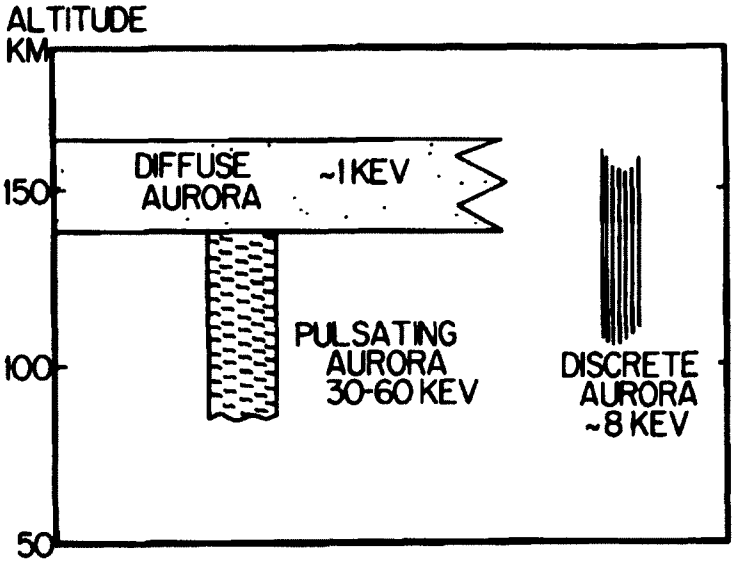

Figure 7-1: Schematic showing the spatial geometry between pulsating, diffuse, and discrete aurora. Reprinted, with permission, from *Brown et al.* (1976).

ingly from within the diffuse structure (*Smith et al.*, 1980; *McEwen et al.*, 1981; *Sandahl*, 1984). In particular, the *Stenbaek-Nielsen and Hallinan* (1979) paper reports evidence for non-collisional thermalization for pulsating aurora precipitation, based on the small vertical thickness of the patches. This insinuates that there is some local, ionospheric effect (potentially a wave-particle interaction) responsible for exciting the auroral modulations (more discussion in the following section, 7.2).

Evans et al. (1987) further characterized this diffuse background as a combination of backscattered and secondary electrons, in addition to a phase mixing element caused by the transit of electrons between conjugate mirror points. This background is a natural consequence of the higher-energy modulated pulsating aurora precipitation, and thus occurs within the framework of the pulsating aurora mechanism; which leads to the conclusion that pulsating aurora is a driver of diffuse aurora. The model described was based on measurements of energy spectra in morningside aurora from the NOAA 6 satellite. The observations indicated modulated electron intensities from several keV to 10's of keV, with an additional constant background of electron with energies down to < 1 keV. The authors lament the fact that current VLF wave generation theories did not explain the precipitation fluctuations in the range of 5-20 keV. Another interesting result derived from their simulations in the study was that the energy fluxes during the minimum of the pulsation (or the 'off' phase) were 10% of the fluxes for the pulsation maximum, leading to the assertion that the pulsations do not turn completely off, except perhaps during long pulsation periods. In a subsequent segment (Sec. 7.4.1), we report on observations of pulsating aurora where the entire diffuse background is temporarily eliminated after the pulsation period ends.

Diffuse and pulsating aurora are both theorized to occur through pitch angle scattering as a result of cyclotron resonance interactions in the equatorial magnetosphere. The modulation of the pulsating aurora is then achieved through one of the mechanisms described

in Sec. 5.4. Just as there are many competing theories for the types of waves that cause pulsating aurora, the specific CRI that scatters plasma sheet electrons as diffuse aurora is not known.

Whistler-mode chorus waves can scatter diffuse aurora through resonance with plasma sheet electrons (*Villalon and Burke*, 1991; *Inan et al.*, 1992; *Ni et al.*, 2008); a theory that has the potential for tying in well to pulsating aurora generation mechanisms. However, it has been shown that ECH waves resonate with plasma sheet electrons as well (*Horne and Thorne*, 2000; *Horne et al.*, 2003). Furthermore, *Meredith et al.* (2009) showed that both ECH and chorus likely contribute to diffuse aurora. Essentially, both scattering mechanisms are implicated in the generation of diffuse aurora. Though there are different characteristics associated with each; ECH waves are more unstable within regions of cold plasma and chorus requires a larger temperature anisotropy.

Clearly, a comprehensive theory of pulsating aurora formation must include a diffuse aurora component that belies an understanding of the relationship between the two types of precipitation. This has been lacking from current theoretical considerations.

7.2 Role of the Ionosphere

The role that the ionosphere plays in the formation and structure of pulsating and diffuse aurora has remained one of the larger unanswered questions in auroral physics. Does the ionosphere further modulate or constrain the scattered electrons that come from the equatorial region of the magnetosphere? Or does the ionosphere itself take the dominant role in some pulsating auroras? Does it act as the passive television screen or have active control on the generation processes? The assumption of a completely passive ionosphere is almost certainly a misjudgment. Yet defining the conditions under which the ionosphere or the magnetosphere is the dominant party is not an easy task; within a nonlinear system, it is a

hard mystery to untangle.

The paper referred to earlier by *Stenbaek-Nielsen and Hallinan* (1979) scratches the surface of just such an issue. They determined that the very short vertical extent (2 km or less) of the observed pulsating patches is less than the scale height of the atmosphere and therefore could not be produced by the traditional collisional process of excitation and emission by precipitating particles. The study used a stereo television system to triangulate the lower border altitudes of auroral forms, finding a surprisingly thin extent for pulsating patches, closer to what *Størmer* (1955) called "horizontal pulsating surfaces". In place of the standard collisional theory, the authors suggest a local wave-particle interaction in the ionosphere that would generate the modulations. Wave growth could increase at the expense of a mono-energetic electron beam, thereby transferring energy to ambient electrons that then would ionize atmospheric constituents. This novel proposition has yet to be confirmed, but observations of thin patches have been reported since (*Kaila et al.*, 1989; *Kaila and Rasinkangas*, 1989; *Wahlund et al.*, 1989; *Bösinger et al.*, 1996). In contrast, both *Størmer* (1955) and *Hallinan et al.* (1985) report pulsating aurora with much greater vertical extent, perhaps signifying that the thin patches are not ubiquitous among all forms of pulsations.

The spatial characteristics of pulsating aurora also may point to an ionospheric input. *StenbaekNielsen* (1980) succinctly reviews these spatial tendencies that indicate an ionospheric contribution. First, there is the express lack of shear motion in pulsating auroral observations. The precipitating electrons do not shear with the E×B drift motion, as is observed in discrete aurora through boundary vortices. Second, there is often a persistence of geometry in pulsating patch shapes. If the precipitating electrons did indeed originate from hot magnetospheric plasma, there would be a smearing observed in the patch shape, due to gradient and curvature drift motion. Instead, patches can persist for several to many pulsation periods, and have sharply defined boundaries or small-scale intricate shapes, which

we will show next in our study on filtered pulsating aurora (Sec. 7.3). In response to this known geometry persistence, *Oguti* (1976) proposed that regions of cold plasma from the ionosphere may act to create the pattern of patch shape, yet the particles still originate from the equatorial region. They likened the process to a computer recalling memory from storage. *StenbaekNielsen* (1980) further suggested not just island of cold plasma, but columns extending up from the ionosphere. This would be more consistent with barium releases exhibiting a faster drift velocity than pulsating patches below (*Swift and Gurnett*, 1973; *Wescott et al.*, 1976).

7.3 Filtered Allsky Images at 4278 Å & 5577 Å

The aim of this study was to use the simultaneous filtered images of pulsating aurora to examine the intensity ratio between the 5577 Å green line and the 4278 Å blue line emission for a small area of pixels; the results were then compared to an earlier study of pulsating aurora energies. However, we also observed excellent events of patch geometry persistence during the course of the study.

An experiment called Multi-Spectral Observatory Of Sensitive EMCCDs (MOOSE), designed by M. Samara and R. Michell of SwRI, consists of five low-light imagers intended to apply to a wide range of optical imaging science. Each of the imagers allows for a range of angular FOVs, and uses an Andor DU-888 Electron Multiplying CCD. For this preliminary study of pulsating aurora, we used two imagers, located at the same observation point near Poker Flat Research Range, Alaska ($\sim$ 65.4° MLAT), filtered at 4278 Å and 5577 Å respectively, each supplying images at a frame rate of 3 Hz.

We assume that the 5577 Å atomic oxygen emission, O[I], represents the bulk of the diffuse aurora emission while the 4278 Å molecular nitrogen emission, N_2^+, is present mainly as the pulsating aurora emission. These assumptions are based on the observed height dis-

tributions of the two types of aurora (pulsating aurora almost invariably occurring at lower altitudes than diffuse aurora) and the altitude dependency of the atmospheric constituents (the N_2^+ occupying a lower layer than O). Figure 7-2 shows a false color image of a series of filtered images taken during a dynamic pulsating aurora event. The time between sequential images is 30 seconds (an arbitrary interval), with the total time range spanning 1241:05 UT to 1243:05 UT.

7.3.1 Filtered Imager Preliminary Results

The pulsating aurora events detailed here were observed on 26 September 2011. To illustrate the concept of geometry persistence, we present two image sequences from an extremely dynamic portion of pulsations (Figs. 7-3 and 7-4). The first figure shows a sequence of 6 full pulsation periods, over 21 seconds, from 1301:41 UT to 1302:02 UT. Strikingly similar patch shapes endure through all 6 image frames. The second figures shows a progression of 4 full pulsation periods, over 28 seconds, from 1307:26 UT to 1307:54 UT. Again, the same patch geometries remain for all four frames. Also note the sharp, well-defined boundaries at

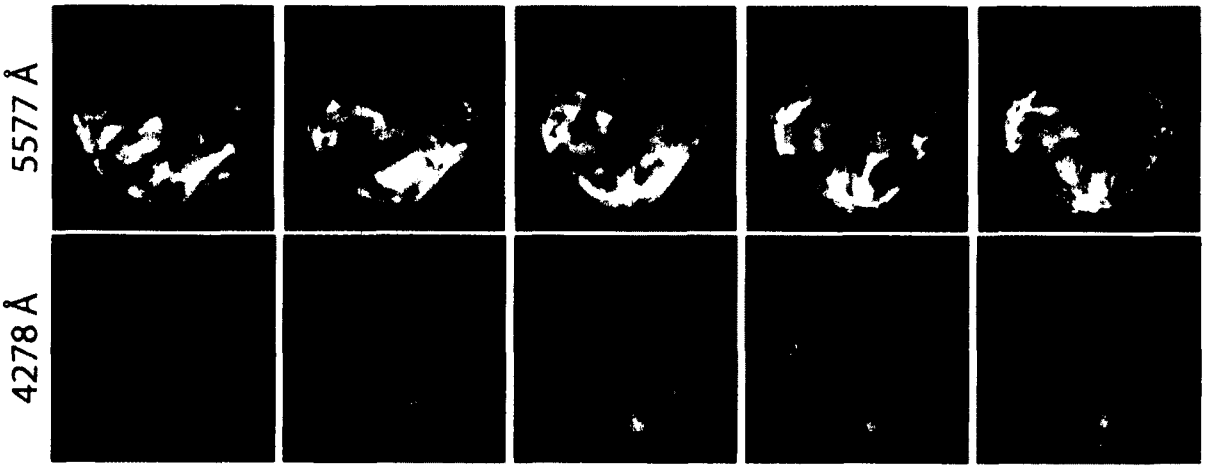

Figure 7-2: A time series in both the 5577 Å and 4278 Å filtered images, taken of a dynamic pulsating aurora event on 26 September 2011. The images span 1241:05 UT to 1243:05 UT, with the time between images being 30 seconds. False color is added for effect.

the patch edges. These are arguably prime examples of ionospherically-controlled pulsating aurora. One other thing of significance is the period times. In this study, we see periods of 4-7 seconds, which is measurably shorter than the periods we found for the source region study in Ch. 6 which were on the order of 20 seconds. Pulsating auroras of shorter periodicity are generally classified as having a near-earth source (e.g. *Johnstone* (1971)), while those with longer periodicity are cited as being magnetospheric in origin (as detailed in the preceding chapters).

The ratios of common emission lines in aurora can be used to infer the characteristic energy for Maxwellian distributions (*Rees and Luckey*, 1974; *McEwen and Bryant*, 1978). Due to the difference in species altitude of molecular nitrogen and atomic oxygen, this specific ratio is dependent on height. In particular, *McEwen and Bryant* (1978) measured the I(5577 Å)/I(4278 Å) column emission ratio. They found the change in characteristic

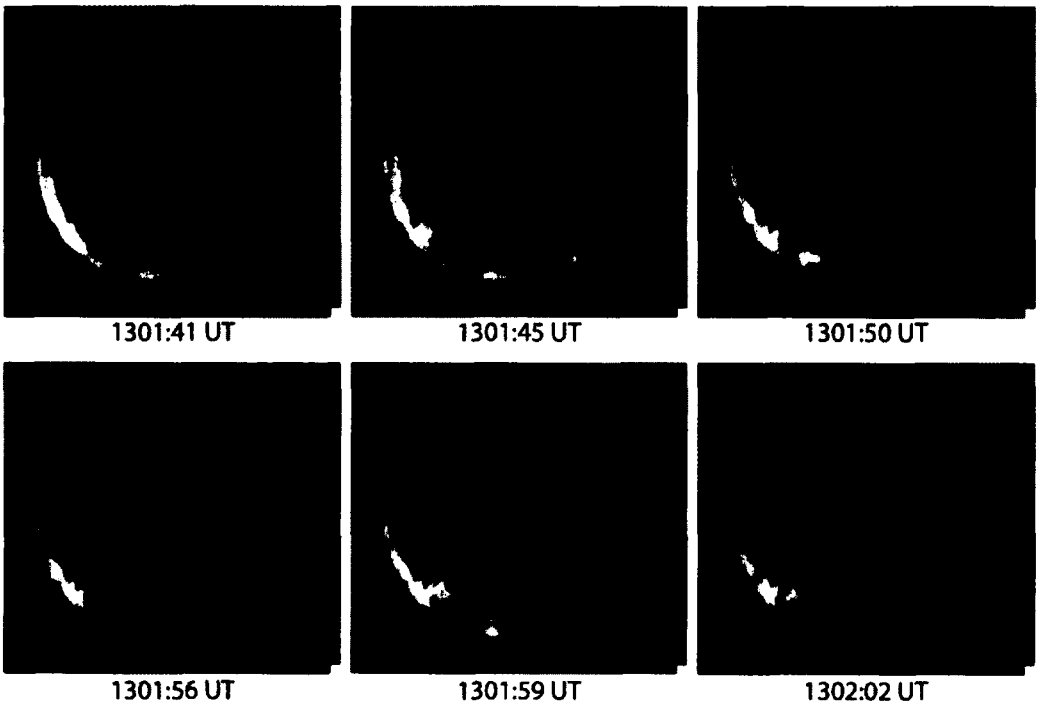

Figure 7-3: Dynamic pulsating aurora showing persistence of patch geometry through 6 periodic cycles, spanning 21 seconds.

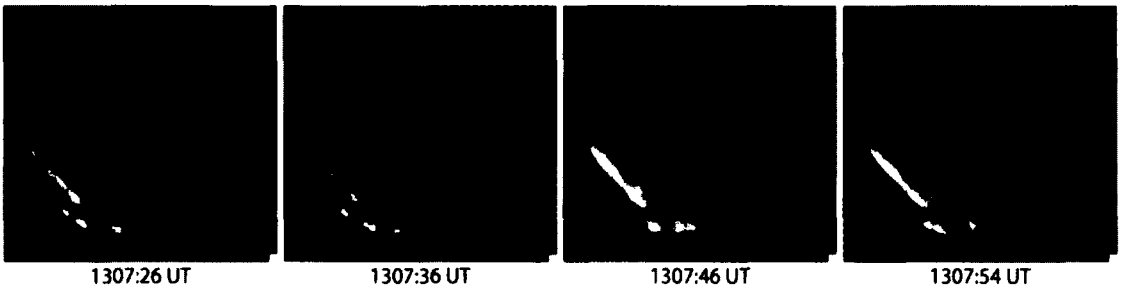

Figure 7-4: A second example of dynamic pulsating aurora showing persistence of patch geometry through 4 periodic cycles, spanning 28 seconds.

energy to jump from 2.2 to 2.6 keV in one pulsating auroral form, and from 2.6 to 4.0 keV in another more active event. Their results are consistent with the sounding rocket study conclusions showing characteristic energies of a few keV, and Maxwellian spectral distributions. Here, we follow a similar scheme by estimating the I(5577 Å)/I(4278 Å) ratio during pulsating aurora events using the filtered allsky images. The spectral temperature increases as the intensity of the emitted light increases, which manifests as a changing ratio during one pulsation. A noticeable decrease in this ratio is generally observed at the peak 'on' phase of a pulsation. If we assume the diffuse aurora energy spectrum remains uniform, this implies that the pulsating aurora energy is variable during the interval of one pulsation, reaching a maximum within the peak.

The following figures show line plots of various pixels from near the center of several pulsating patches within the imager FOVs (Figs. 7-5, 7-6). We only take patches appearing within the central portion (~30%) of the allsky imagers, to gain a better integrated column emission estimate, without the distortion present when the angle of inclination decreases. The plots give relative pixel intensities for both the 5577 Å and 4278 Å filters as well as the intensity ratio between the two. Unfortunately, absolute intensities for the filtered images was not available before the publication of this thesis. Calibration data to achieve raw intensities will further advance the relevance of the results given here. However, the

observations reported here agree completely with *McEwen and Bryant* (1978) and others, showing marked decreases in the intensity ratio during the peak 'on' phase of a pulsation. This is depicted well in Figs. 7-5 and 7-6, where the ratio minimums are seen clearly at the times listed in the captions. With the addition of calibrated intensities, the characteristic energies can easily be computed using the method of *Rees and Luckey* (1974), and this study will have a greater leverage for comparison with earlier results. We also see a slight time dispersion between the emission onsets. The 4278 Åpulsating aurora precedes the 5577 Ådiffuse aurora emission by ~0.7-0.75 s. Unfortunately, the lifetime of the atomic oxygen emission is precisely 0.7 s, so any velocity dispersion will be difficult to untangle from a lifetime effect. Further observation is necessary to determine the cause of the onset delay. However, if related to transit time, this dispersion will be able to identify the source region of the diffuse aurora.

7.4 Churchill Pulsating Aurora Observations

In this section, we present a separate set of observations, taken from a field study at the Churchill Northern Studies Center (68.8° MLAT) in Manitoba, Canada on 15 March 2002. The data is owned by D. Knudsen of the University of Calgary (also participated in data collection). The camera operator and experiment designer was T. Trondsen of the University of Calgary. S. Jones of NASA Goddard aided in data collection and digitization. The data is presented here with the permission of all mentioned.

The recordings were taken using a ITT F4588 Generation III Intensified white-light CCD camera, with an approximately 10° narrow field-of-view, pointed along the local magnetic zenith. The image frames were recorded at the NTSC standard video framerate of 29.97 frames per second, and then digitized through a VGA digitizer to 640x480 pixel images. Over an extended time interval (approximately one hour), diffuse aurora was pervasive

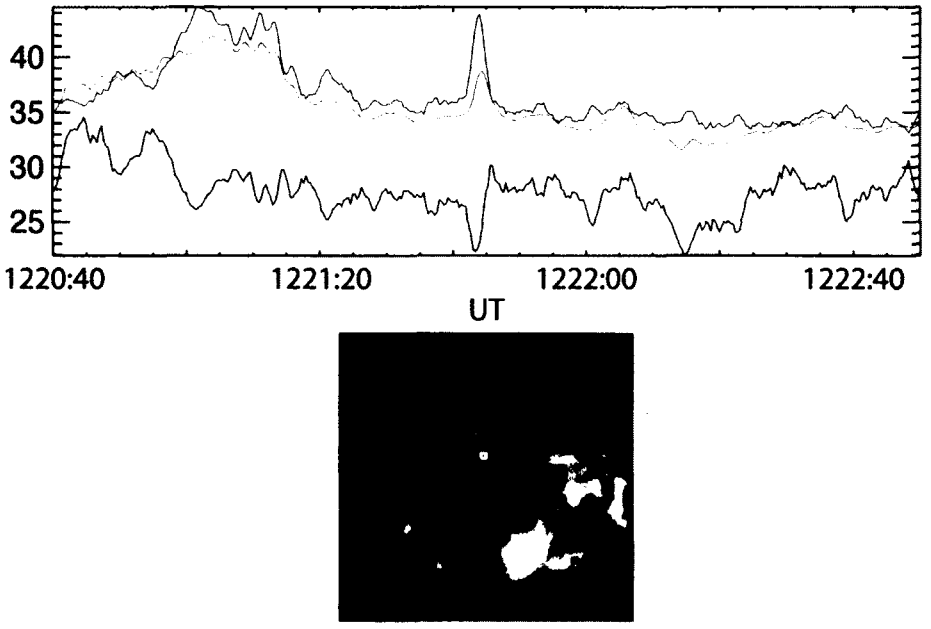

Figure 7-5: Time series showing three traces from a pulsating aurora event: green trace is 5577 Å intensity, blue trace is 4278 Å intensity and black trace is the I(5577 Å)/I(4278 Å) ratio. Dramatic decreases in ratio can be seen when pulsations reach a maximum, clearly evident near 1221:00 UT and 1221:43 UT. Allsky picture shows the location of the pixel region sampled for this plot.

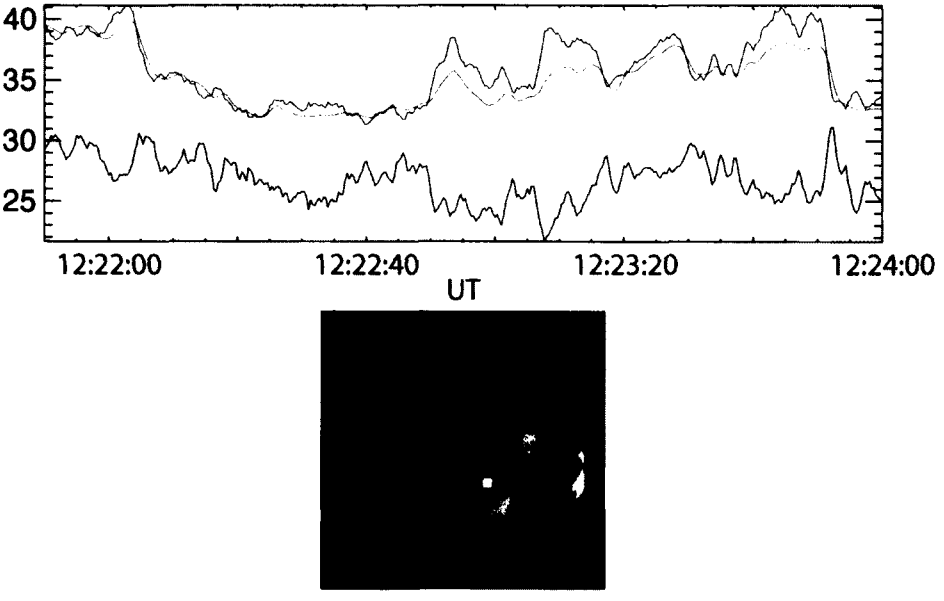

Figure 7-6: Same as Fig. 7-5, except decreases in ratio are most clearly present at 1222:02 UT, 1222:53 UT and 1223:08 UT.

throughout the view of the imager, interrupted periodically by transient pulsating patches. These patches would appear for several pulsation periods, the pulsations would often maximize and then abruptly stop, after which time the non-pulsating diffuse background would be 'erased' from its nominal level to the noise level of the imager (indicating no light emissions present). After several seconds, the diffuse background would refill gradually to its pre-pulsation level. Typically, the pulsations would then start again and the process would be repeated.

Also during the time interval, black auroral forms were observed in stark contrast to the normally described black aurora. Typically, black aurora is seen as black arcs or bands, often on the boundary of discrete auroral forms, and are known to be upgoing electrons in a downward-directed field-aligned current. Only scant observations of black aurora holes or spots have been reported (*Oguti*, 1975; *Royrvik*, 1976). The forms recorded in our study included very elongated ropes, rings and irregular patches, all with non-uniform drift speeds and directions. On several nights throughout the field campaign, many black auroral forms were observed to drift into zenith from one direction, rotate or otherwise evolve shape, and drift away in a completely nonlinear direction. The black aurora occurred against both a diffuse and pulsating background. Analysis of these drift directions is part of future research, but is not included in this dissertation. However, a brief depiction of these perplexing forms begs a mention. Fig. 7-7 shows several frames containing several distinctive black auroral forms.

7.4.1 The Diffuse Aurora Eraser

The series of frames in Figs. 7-8 and 7-9 attempt to show two examples of a diffuse aurora eraser. The sequence in still frames does not entirely convey the dynamics, but it is an adequate proxy for video in this case. The contrast has been artificially increased in all

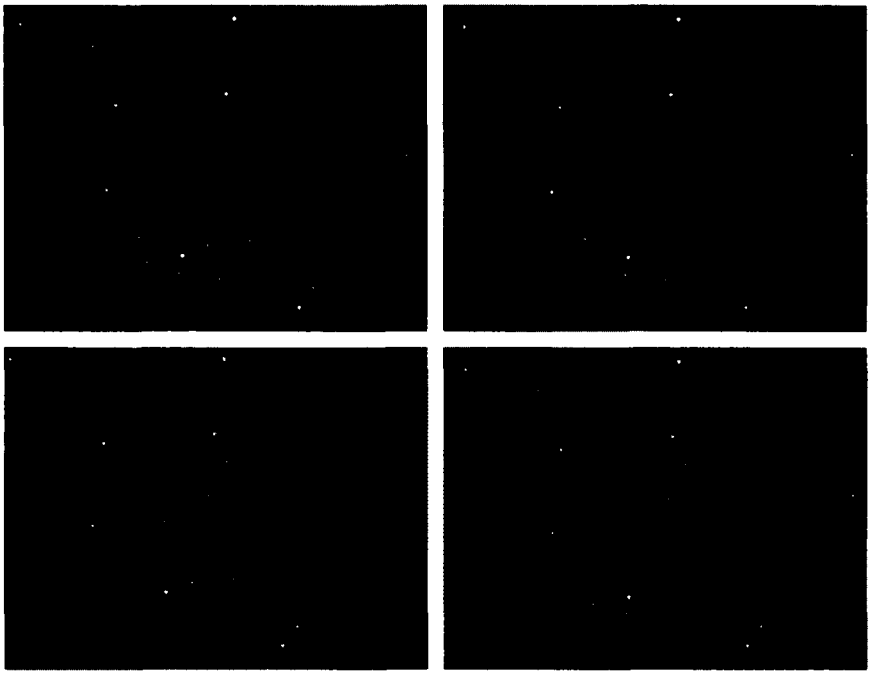

Figure 7-7: Black aurora forms embedded within diffuse and pulsating aurora. Recorded between 0540 and 0620 UT on 15 March 2002.

images for clarity. In these images, geographic north is towards the top and east is towards the left. In Fig. 7-8, the images shown are at three unequal intervals. In frame (a), the bright patch in the center of the FOV is pulsating aurora with a diffuse background. Frame (b) shows the diffuse aurora eraser; the pulsations have stopped for the lower half of the frame, and additionally erased the diffuse background. Note the sharp boundary at the lower edge of the bright patch. By frame (c), 9 seconds later, the diffuse aurora has started to refill the erased portion. Fig. 7-9 is perhaps easier to see. This sequence shows frames at a constant 2-s cadence. The FOV is filled with diffuse aurora in frame (a), with just a very small east-west band pulsating, approximately 2/3 from the bottom of the frame, in an east-west alignment. In frame (b) it is easy to spot the band that had been pulsating; the pulsations have stopped and the diffuse eraser episode begins. By frame (c) the band is a distinct black stripe, at a noticeably lower intensity than the diffuse

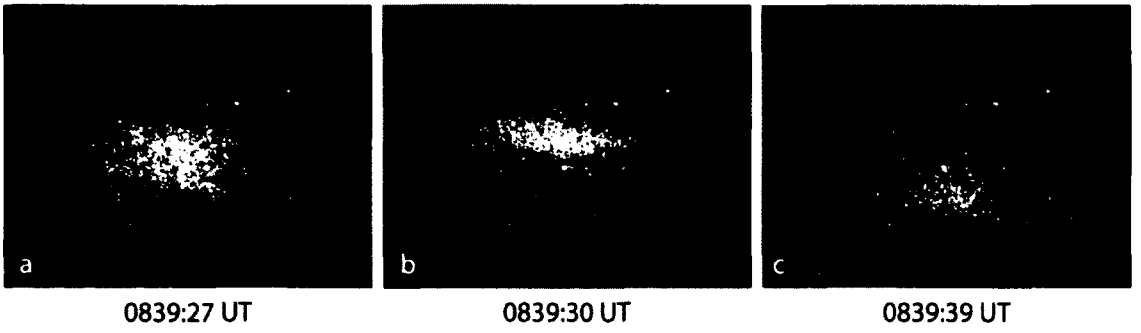

Figure 7-8: First example of a diffuse aurora event. Pulsations in (a) erase the diffuse background when they stop in (b) to lower than background levels. The last image (c) shows this region beginning to refill to a nominal non-pulsating level.

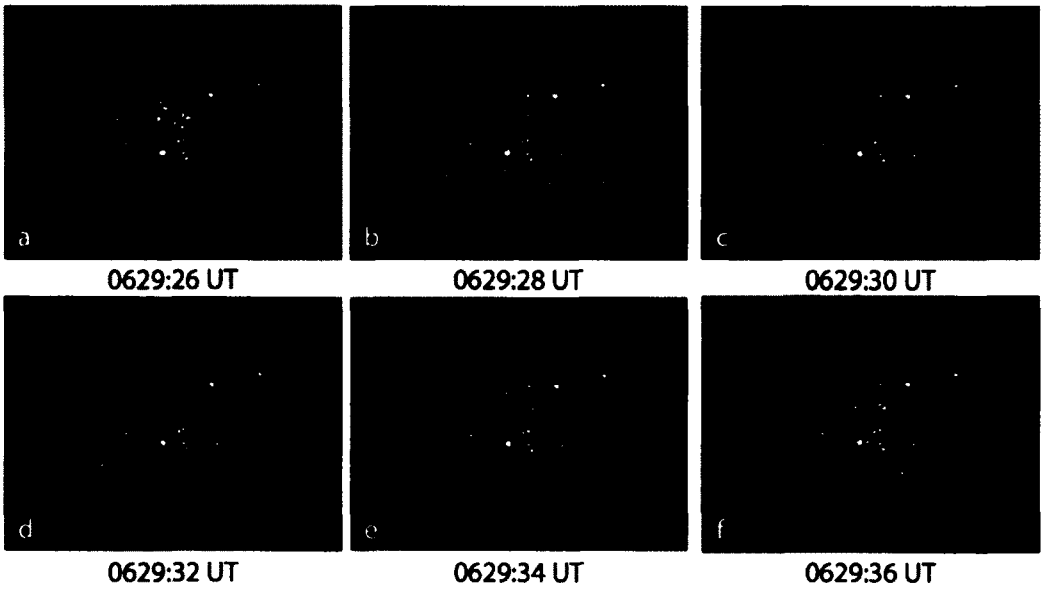

Figure 7-9: Second example of a diffuse aurora event. Pulsations appear in a thin elongated patch in (a). When the pulsations stop in (b), the region is erased of the diffuse background, continuing in (c). In (e)-(f), the background levels start to return to non-pulsating status.

background surrounding it. Frame (d) shows the eraser region perhaps starting to refill, which progresses through frames (e) and (f). By the last frame, the stripe is not yet up to the nominal diffuse background level.

It is useful to examine one or several pixels from in the midst of these diffuse aurora eraser episodes. Fig. 7-10 displays time series plots of three separate pixel regions, as a function of relative intensity. Locations were chosen from within pulsating patch that exhibited the diffuse aurora eraser. Groups of four pixels were averaged together, to average the pixel intensity as an approximate low-pass filter. The total time spans 90 seconds, from 940 UT to 1110 UT. The pulsations (3-4 s periods) can be seen at the start of the time series. At around 1005 UT, a single intense pulsation is clearly seen in each pixel region. Immediately after this pulsation, the intensity drops sharply down to levels below the 'off' phase of the pulsation (what could be considered an approximation of the diffuse background). Gradually, the background level returns to nominal, with the pulsations continuing until after the end of the plot.

One of the main goals of this study was to determine an estimate for the refilling time constant, τ_r, after the pulsation(s) erased the diffuse aurora; we define this refilling time constant as the time taken from when the diffuse background begins to fill in until it reaches the pre-pulsation nominal brightness. Evaluating this parameter can help to determine the physical processes involved in the diffuse aurora eraser. A superposed epoch analysis was performed using pixels from several different eraser patches at various times throughout the data set. Figure 7-11 shows this result. Each color trace corresponds to a different eraser event; three separate events were identified and used for this plot. From the events coded by green and orange, three pixels each were taken from varying spatial locations within the patch. From the events coded by blue, two pixels were used. The plot spans about 90 seconds of total time, with the 0 mark centered on the eraser epoch time. The solid

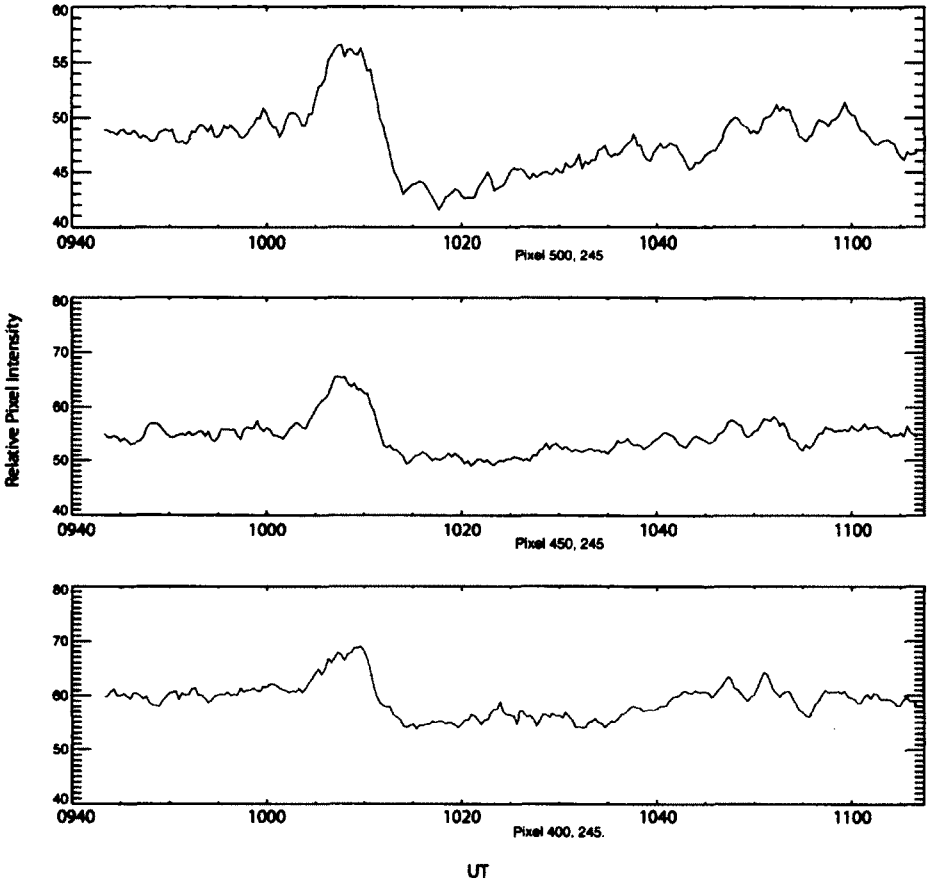

Figure 7-10: Time series of three pixel region from within a diffuse aurora eraser pulsating patch. The eraser characteristic is apparent at approximately 1012 UT, when the background levels drop to far below that of the pulsation 'off' phase.

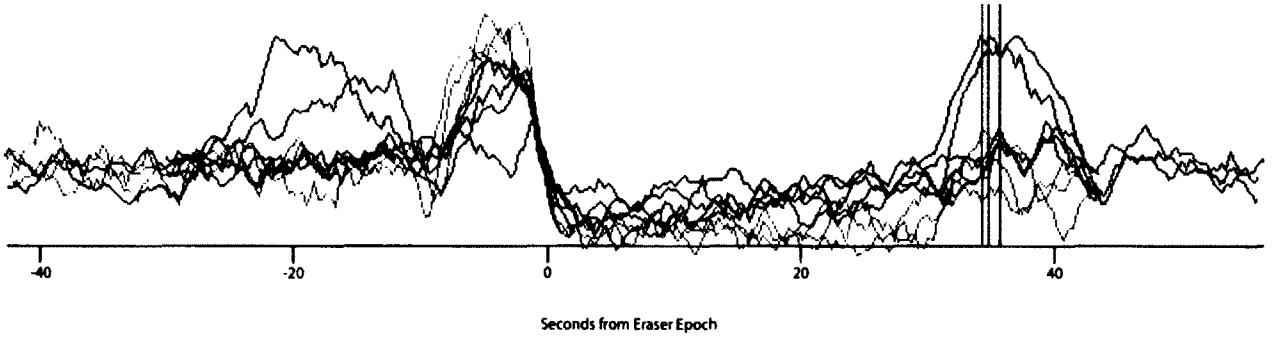

Figure 7-11: A superposed epoch analysis centered on the diffuse aurora eraser start times for several different eraser events (coded by color). The vertical lines represent the approximate end of refilling time (time required for the diffuse aurora background to return to nominal levels) for each respective colored event. The total time spans ~90 seconds, with the average refilling time constant, τ_r, of 34.9 seconds.

vertical color-coded lines indicate approximations of when the background diffuse aurora had refilled to nominal levels; this could be interpreted as marking the end of the refilling time. The time constant varies slightly between events, with each value as follows: for orange, $\tau_r \approx 34.3$ s; for blue, $\tau_r \approx 34.8$ s; for green, $\tau_r \approx 35.7$ s. We shall discuss the significance of these values in the discussion (Sec. 7.5.2).

7.5 Discussion & Preliminary Conclusions

7.5.1 Filtered Pulsating Aurora Discussion

Several events were presented illustrating the distinct persistence of geometry of the pulsating aurora shapes from filtered imager data obtained on 26 September 2011, near Poker Flat, Alaska. The patches show sharp boundaries and remain in approximately the same location with the same geometry for a series of pulsation periods. There is no smearing observed which would indicate gradient and curvature drift and point to a magnetospheric source of plasma modulation. This result supports the theories of *Oguti* (1976) and *Sten-*

baekNielsen (1980), which call for islands or columns of cold ionospheric plasma to damp the precipitation mechanism.

The results from this study are in agreement with work done on emission ratios for aurora with Maxwellian temperature spectra. Specifically, the ratio of atomic oxygen emission line at 5577 Å to the molecular nitrogen emission line at 4278 Å shows an explicit decrease in amplitude during the maxima of a pulsation period. Examples of this are shown using the same pulsating aurora event as was used to show the geometry persistence.

The availability of absolute intensities will serve to quantify the results obtained even further. Additionally, the possibility of tomography studies using two or more imagers separated by ~10 km baselines promises to add significantly to the debate. By triangulating the images of auroral forms, lower border altitudes can be gained, which would doubtlessly be invaluable to a study in this vein. It is relevant to note that the pulsation periods in this study are on the lower range of typical pulsating aurora periods. It has been implied that the smaller periods are related to near-earth source regions, while the longer periods are related to magnetospheric source regions. Adding the characteristic energies and lower border altitudes of these observed auroral forms may aid in delineating two (or more) disparate types of pulsating aurora, with different modulation generation mechanisms.

7.5.2 Diffuse Aurora Eraser Discussion

The diffuse aurora eraser constitutes an interesting problem. The pulsation and diffuse background luminosity drop off dramatically, but the refilling time back up to the nominal diffuse level is much more gradual, with a time constant, τ_r, estimated here to be approximately 35 seconds. *Hosokawa et al.* (2010) compared electron densities from EISCAT with optical pulsating aurora and found distinct density peaks in line with optical auroral pulse peaks. The electron density jumps up immediately with the patch 'on' phase. However, the

decay time down to background levels after the patch turns 'off' was found to be on the order of 5-10 s. This is similar timing to our time constant presented here. They also detected a marked increase in the height-integrated Hall conductance during the 'on' phases.

Schlegel and Füllekrug (2002) determined a conductance profile using MSIS (*Mass-Spectrometer-Incoherent-Scatter*) model parameters, and estimating the conductance directly from the observed electron density. The model incorporates 11 years of EISCAT electron density profiles and the MSIS95 neutral atmosphere model. They derived a conductance function that depends only on the scale height of the conductivity profile at 84 km (H) and the conductivity value at 84 km (10^A),

$$\sigma_{\parallel}(h) = 10^{(h-84km)/H+A} \tag{7.1}$$

We can use this profile to perform a check on our time constant. The simplest model of the diffuse aurora eraser is one of electron injections from the pulsating patch forming a downward electric field. This field will reflect back the diffuse aurora drizzle, assuming the potential is near -1 keV, which thus inhibits the diffuse aurora. Invoking continuity, we can show the following progression,

$$\sigma \nabla \mathbf{E} = -\frac{d\rho}{dt} \tag{7.2}$$

From there, we can easily get

$$\rho = \rho_0 \, e^{-\frac{t}{\tau}} \tag{7.3}$$

where τ, our time constant, equals ϵ_0/σ. For a time constant of, say, just 1 second (far less than the observed τ_r in this study), then $\sigma \approx \epsilon_0 = 10^{-11}$. Using the conductance profile from *Schlegel and Füllekrug* (2002), this puts the altitude of the pulsating aurora emission at around 40 km. An even longer τ would push that altitude further down, thus the results are not consistent with the physical picture.

This points to perhaps a wave-particle interaction local to the ionosphere, as suggested by *Stenbaek-Nielsen and Hallinan* (1979). There is also the possibility of some suppression mechanism acting simultaneously on both scattered particle populations in the equatorial region, however this would be a difficult theoretical scenario to solve, due to the complications discussed previously. Further research in this area is required to make a more robust statement about the processes at work. The intriguing interplay between diffuse and pulsating aurora needs to be taken into account during any theoretical discussion concerning pulsation mechanisms and the wave-particle interactions involved.

CHAPTER 8

CONCLUSIONS

This dissertation attempts to tell a larger story about the nature of pulsating aurora in terms of the source mechanisms responsible for generating the characteristic temporal fluctuations, as well as the relationship between pulsating aurora, diffuse aurora and the ionosphere. Typically, auroral studies focus on discrete aurora, favored highly over the diffuse precipitation; yet, here we offer insight into the diffuse and pulsating populations that may, in fact, comprise a larger part of the energy transfer during magnetosphere-ionosphere coupling. The general implications of this work can be summarized as follows:

- The conjecture made by multiple sounding rocket studies, that the source region of typical pulsating aurora modulations lies in the equatorial magnetosphere, has been confirmed with the results presented in Chapter 6. We present, for the first time, *in-situ* particle data in the magnetosphere identifying this source region of pulsating aurora.

- We also offer a technique for quantification of loss cone coverage using GOES 13 particle flux measurements. The progression of this work involves a better determination of the conjugate ionospheric footprint tied to the electron pulsations observed in space. Studies of this type will certainly prove invaluable when used as magnetic field mapping constraints.

- Some types of pulsating aurora (perhaps a small subset) may require a source region closer to earth, either located within the ionosphere or controlled by ionospheric parameters, as supported by the work in Chapter 7.

- An integral part of the pulsation theory is the inclusion of diffuse aurora. Pulsating aurora exhibits an intriguing morphology in the context of diffuse aurora and it should therefore not be omitted from the theoretical framework.

We began this thesis with a summary of the basic plasma and magnetospheric physics that govern the aurora. From there, a basic primer on aurora was offered, as well as recent optical techniques developed to image the aurora from new vantage points via sounding rockets. Next, we detailed the history of pulsating aurora research, including searches for the source region, ionospheric considerations, and the connection between pulsating aurora and the diffuse plasma sheet precipitation. Also included in Chapter 5 were the results of a case study (*Jones et al.*, 2013) on the large-scale temporal and spatial persistence of a pulsating aurora event. The sections up to this point were used essentially to set the stage for the main work presented in Chapters 6 and 7. A good story requires a thorough introduction. The principal conclusions of these studies are detailed next.

8.1 Source Region of Pulsating Aurora

In this study, we use simultaneous satellite- and ground-based data to show that there is a direct relationship between periods of energetic electron flux pulsations in space and pulsating aurora luminosity in the magnetically conjugate ionosphere. These measurements confirm a long-standing hypothesis concerning the source of pulsating aurora electrons in the equatorial magnetosphere. Using the three-axis spin-stabilized GOES 13 satellite, we were able to observe *in-situ*, for the first time, the source of pulsating aurora electrons at their magnetospheric origin.

The GOES 13 MAGED electron detector observed structured, short-term fluctuations on 15 March 2008. The electron pulsations were seen at energies ranging from 30-100 keV, with average periods of ~24 seconds. At a coinciding time, pulsating aurora was observed using a THEMIS allsky imager at The Pas, Manitoba, with average periods of ~22 seconds. The ionospheric footprint of the GOES 13 satellite during the interval 1100 UT to 1130 UT was estimated to lie within the field-of-view of the ASI. Using a cross-correlation technique to compare the electron flux modulations with the auroral pulsations, we discovered high correlations for the portion of the time interval when the magnetic footprint was nearly stationary. The appearance of high (>0.8) correlation values indicates a non-trivial association and led to the conclusion that we had identified a magnetospheric source region of pulsating aurora modulations using *in-situ* satellite measurements.

We also report on a technique for quantifying the loss cone coverage for the particle detector telescope, a useful first step in determining the pitch angle distribution of the pulsating particles. Finally, we suggest that this and similar studies be used to put much-needed observational constraints on magnetic field line models. The work in this chapter was adapted from *Jaynes et al.* (2013).

8.2 Connection Between Pulsating Aurora & Diffuse Aurora

Next, we presented studies of two different pulsating aurora events that illuminated the relationship between pulsating aurora, diffuse aurora, and the ionosphere. First, we offered data taken on 26 September 2011 from a pair of allsky imagers filtered at 4278 Å and 5577 Å respectively. The main goal of this study was to explore the ratio of intensities between the atomic oxygen emission line and the molecular nitrogen emission line to examine the relative energy spectra of diffuse and pulsating aurora. We show evidence from our data set that there is a marked decrease in the I(5577 Å)/I(4278 Å) emission ratio during an auroral

pulsation maxima, indicating an energy variance during one pulsation, which stands in agreement with *McEwen and Bryant* (1978). We additionally observed a slight dispersion between emission onset times. The significance may relate to velocity dispersion of the different electron energies, but is not resolved within the limitations of this study.

A secondary result was the observation of persistent geometries for the pulsating patch boundaries. This result serves as further evidence to support a non-passive ionosphere, as proposed by *Oguti* (1976), *StenbaekNielsen* (1980) and others. The gradient and curvature drift smearing effects one would expect to see if looking at a magnetospheric-based phenomenon were not present. This may be cause for a re-examination of pulsating aurora classifications.

In a second pulsating aurora study, we showed data from Churchill, Manitoba recorded on 15 March 2002, using a narrow-field intensified CCD camera. The analysis identifies a process dubbed the diffuse aurora eraser, whereby a pulsating patch stop pulsating and effectively erases the diffuse background behind it, leaving an 'empty' space. Eventually, this region is refilled to nominal background levels, and thus defined by a refilling time constant, τ_r. We present several series of images, depicting the steps of the diffuse aurora eraser. A superposed epoch analysis was performed to better quantify τ_r, with a resulting average of $\approx$ 35 s. This value does not appear to fit well into the current theoretical framework, although not all wave-particle interactions have been adequately explored.

8.3 The Enigmatic Pulsating Aurora

As often is the case, a long-standing physical quandary is not solved overnight. It is the aim of this dissertation to contribute to the discussion concerning the nature of the enigmatic pulsating aurora.

In the correlation study that identified a source region that is magnetospheric in origin,

the pulsating aurora observed was of the 'classic' variety - with pulsation periods spanning 10's of seconds. In the diffuse/pulsating aurora studies, the pulsations observed were much shorter - with periods on the order of a couple to several seconds. These studies carried evidence for a source region more ionospheric in origin. Perhaps, the reason for differing opinions on the location of the source region may come down to the fact that there are disparate processes involved in creating pulsating aurora. After all, a quick review of the small-scale morphology of pulsating aurora reveals many varied configurations of timescale, shape and occurrence patterns.

Pulsating aurora nearly always occurs within a bed of diffuse aurora. This, alone, is good justification for incorporating existing diffuse aurora theory into the theory of auroral pulsations. This fundamental observation, together with supportive data reported in this research, calls for a re-evaluation of current pulsating aurora theory and classification, and how diffuse aurora fits into that context.

The more we learn about the topics discussed in this dissertation, the closer we come to disentangling the complex web of fields, waves, particles and lights that culminate in the nightly scene of the aurora.

BIBLIOGRAPHY

Akasofu, S.-I. (1964), The development of the auroral substorm, *Planetary and Space Science*, *12*, 273, doi:10.1016/0032-0633(64)90151-5.

Akasofu, S. I. (Ed.) (1968), *Polar and Magnetosphere Substorms*, *Astrophysics and Space Science Library*, vol. 11.

Akasofu, S. I. (1977), Magnetospheric substorms, *Quarterly Journal of the Royal Astronomical Society*, *18*, 170–187.

Arnoldy, R. L., K. Dragoon, L. J. Cahill, S. B. Mende, and T. J. Rosenberg (1982), Detailed correlations of magnetic field and riometer observations at L= 4.2 with pulsating aurora, *J. Geophys. Res.*, *87*(A12), 10,449.

Belon, A., J. Maggs, T. Davis, K. Mather, N. Glass, and G. Hughes (1969), Conjugacy of visual auroras during magnetically quiet periods, *J. Geophys. Res.*, *74*(1), 1–28.

Berkey, F. T. (1978), Observations of pulsating aurora in the day sector auroral zone, *Planetary and Space Sciences*, *26*, 635, doi:10.1016/0032-0633(78)90097-1.

Bösinger, T., K. Kaila, R. Rasinkangas, P. Pollari, J. Kangas, V. Trakhtengerts, A. Demekhov, and T. Turunen (1996), An EISCAT study of a pulsating auroral arc: simultaneous ionospheric electron density, auroral luminosity and magnetic field pulsations., *Journal of Atmospheric and Terrestrial Physics*, *58*, 23–35.

Brown, N. B., T. N. Davis, T. J. Hallinan, and H. C. Stenbaek-Nielsen (1976), Altitude of pulsating aurora determined by a new instrumental technique, *Geophys. Res. Lett.*, *3*(7), 403–404, doi:10.1029/GL003i007p00403.

Bryant, D., M. Smith, and G. Courtier (1975), Distant modulation of electron intensity during the expansion phase of an auroral substorm, *Planetary and Space Science*, *23*(5), 867–878, doi:10.1016/0032-0633(75)90022-7.

Bryant, D. A., G. M. Courtier, and A. D. Johnstone (1969), Modulation of auroral electrons at large distances from the Earth., *Journal of Atmospheric and Terrestrial Physics*, *31*, 579–592.

Bucsela, E. J. (1994), Two daytime observations of atomic nitrogen emissions in the thermosphere., Ph.D. thesis, The University of Michigan.

Burtis, W. J., and R. A. Helliwell (1969), Banded chorus - a new type of VLF radiation observed in the magnetosphere by OGO 1 and OGO 3, *J. Geophys. Res.*, *74*(11), 3002–3010, doi:10.1029/JA074i011p03002.

Burtis, W. J., and R. A. Helliwell (1976), Magnetospheric chorus: Occurrence patterns and normalized frequency, *Planetary and Space Science*, *24*, 1007–1024, doi:10.1016/0032-0633(76)90119-7.

Burton, R. K., and R. E. Holzer (1974), The origin and propagation of chorus in the outer magnetosphere, *J. Geophys. Res.*, *79*(7), 1014–1023, doi:10.1029/JA079i007p01014.

Coroniti, F. V., and C. F. Kennel (1970a), Electron precipitation pulsations, *J. Geophys. Res.*, *75*, 1279, doi:10.1029/JA075i007p01279.

Coroniti, F. V., and C. F. Kennel (1970b), Auroral micropulsation instability, *J. Geophys. Res.*, *75*, 1863, doi:10.1029/JA075i010p01863.

Cresswell, G. R., and T. N. Davis (1966), Observations on pulsating auroras, *J. Geophys. Res.*, *71*(13), 3155–3163, doi:10.1029/JZ071i013p03155.

Davidson, G. (1979), Self-modulated VLF wave-electron interactions in the magnetosphere: a cause of auroral pulsations, *J. Geophys. Res.*, *84*(A11), 6517–6523.

Davidson, G. (1986), Pitch angle diffusion in morningside aurorae, 1. the role of the loss cone in the formation of impulsive bursts of precipitation, *J. Geophys. Res.*, *91*(A4), 4413–4427, doi:10.1029/JA091iA04p04413.

Davidson, G. (1990), Pitch-angle diffusion and the origin of temporal and spatial structures in morningside aurorae, *Space Science Reviews*, *53*(1), 45–82.

Davidson, G., and Y. Chiu (1991), An unusual nonlinear system in the magnetosphere: A possible driver for auroral pulsations, *J. Geophys. Res.*, *96*(A11), 19,353.

Davis, T. (1978), Observed characteristics of auroral forms, *Space Science Reviews*, *22*(1), 77–113.

Demekhov, A., and V. Trakhtengerts (1994), A mechanism of formation of pulsating aurorae, *J. Geophys. Res.*, *99*(A4), 5831–5841.

Duncan, C. N., F. Creutzberg, R. L. Gattinger, F. R. Harris, and A. Vallance Jones (1981), Latitudinal and temporal characteristics of pulsating auroras, *Canadian Journal of Physics*, *59*, 1063–1069, doi:10.1139/p81-140.

Duthie, D. D., and M. W. J. Scourfield (1977), Aurorae and closed magnetic field lines, *Journal of Atmospheric and Terrestrial Physics*, *39*, 1429–1434.

Evans, D., G. Davidson, H. Voss, W. Imhof, J. Mobilia, and Y. Chiu (1987), Interpretation of electron spectra in morningside pulsating aurorae, *J. Geophys. Res.*, *92*(A11), 12,295.

Fedorov, E., V. Pilipenko, M. Engebretson, and T. Rosenberg (2004), Alfvén wave modulation of the auroral acceleration region, *Earth, Planets, and Space*, *56*(7), 649–662.

Frank, L. A., N. A. Saflekos, and K. L. Ackerson (1976), Electron precipitation in the postmidnight sector of the auroral zones, *J. Geophys. Res.*, *81*, 155–167, doi: 10.1029/JA081i001p00155.

Gokhberg, M. B., B. N. Kazak, O. M. Raspopov, V. K. Roldugin, V. A. Troitskaya, and V. I. Fedoseyev (1970), Pulsating auroras at conjugate points, *Geomagnetism and Aeronomy*, *10*, 289.

Hallinan, T. J., H. C. Stenbaek-Nielsen, and C. S. Deehr (1985), Enhanced aurora, *J. Geophys. Res.*, *90*, 8461–8475, doi:10.1029/JA090iA09p08461.

Helliwell, R. A. (1967), A theory of discrete VLF emissions from the magnetosphere, *J. Geophys. Res.*, *72*(19), 4773–4790, doi:10.1029/JZ072i019p04773.

Heppner, J. P. (1954), Time sequences and spatial relations in auroral activity during magnetic bays at College, Alaska, *J. Geophys. Res.*, *59*, 329–338, doi: 10.1029/JZ059i003p00329.

Heppner, J. P. (1958), Satellite Geomagnetic Measurements, in *Scientific Uses of Earth Satellites*, edited by J. A. van Allen, p. 234.

Horne, R. B., and R. M. Thorne (2000), Electron pitch angle diffusion by electrostatic electron cyclotron harmonic waves: The origin of pancake distributions, *J. Geophys. Res.*, *105*(A3), 5391–5402, doi:10.1029/1999JA900447.

Horne, R. B., R. M. Thorne, N. P. Meredith, and R. R. Anderson (2003), Diffuse auroral electron scattering by electron cyclotron harmonic and whistler mode waves during an isolated substorm, *J. Geophys. Res.*, *108*, 1290, doi:10.1029/2002JA009736.

Hosokawa, K., Y. Ogawa, A. Kadokura, H. Miyaoka, and N. Sato (2010), Modulation of ionospheric conductance and electric field associated with pulsating aurora, *J. Geophys. Res.*, *115*(A03201), doi:10.1029/2009JA014683.

Huang, C.-L., H. E. Spence, H. J. Singer, and N. A. Tsyganenko (2008), A quantitative assessment of empirical magnetic field models at geosynchronous orbit during magnetic storms, *J. Geophys. Res.*, *113*(A12), A04208, doi:10.1029/2007JA012623.

Huang, L., J. Hawkins, and L. Lee (1990), On the generation of the pulsating aurora by the loss cone driven whistler instability in the equatorial region, *J. Geophys. Res.*, *95*(A4), 3893–3906, doi:10.1029/JA095iA04p03893.

Inan, U. S., Y. T. Chiu, and G. T. Davidson (1992), Whistler-mode chorus and morningside aurorae, *Geophys. Res. Lett.*, *19*, 653–656, doi:10.1029/92GL00402.

Jaynes, A. N., M. R. Lessard, J. V. Rodriguez, E. Donovan, T. M. Loto'aniu, and K. Rychert (2013), Source region of pulsating aurora modulations in the equatorial magnetosphere, *J. Geophys. Res.*, In review.

Johnstone, A. (1978), Pulsating aurora, *Nature*, *274*, 119–126, doi:10.1038/274119a0.

Johnstone, A. D. (1971), Correlation between electron and proton fluxes in postbreakup aurora, *J. Geophys. Res.*, *76*, 5259, doi:10.1029/JA076i022p05259.

Johnstone, A. D. (1983), The mechanism of pulsating aurora, *Annales Geophysicae*, *1*, 397–410.

Jones, A. (1974), *Aurora*, Geophysics and Astrophysics Monographs, Kluwer Academic Pub.

Jones, S. L., M. R. Lessard, K. Rychert, E. Spanswick, and E. Donovan (2011), Large-scale aspects and temporal evolution of pulsating aurora, *J. Geophys. Res.*, *116*(A3), A03,214, doi:10.1029/2010JA015840.

Jones, S. L., M. R. Lessard, K. Rychert, E. Spanswick, E. Donovan, and A. N. Jaynes (2013), Persistent, widespread pulsating aurora: a case study, *J. Geophys. Res.*, In review.

Kaila, K., and R. Rasinkangas (1989), Coordinated photometer and incoherent scatter radar measurement of pulsating arcs with high time resolution, *Planetary and Space Science*, *37*(5), 545–553.

Kaila, K., R. Rasinkangas, P. Pollari, R. Kuula, J. Kangas, T. Turunen, and T. Bösinger (1989), High resolution measurements of pulsating aurora by EISCAT, optical instruments and pulsation magnetometers, *Advances in Space Research*, *9*(5), 53–56.

Kelley, M. (2009), *The Earth's Ionosphere: Plasma Physics and Electrodynamics*, International Geophysics Series, Academic Press.

Kennel, C. F., and H. E. Petschek (1966), Limit on stably trapped particle fluxes, *J. Geophys. Res.*, *71*, 1.

Kivelson, M. G., and C. T. Russell (1995), *Introduction to Space Physics*, Cambridge University Press.

Kvifte, G. J., and H. Pettersen (1969), Morphology of the pulsating aurora, *Planet. Space Sci.*, *17*, 1599–1607, doi:10.1016/0032-0633(69)90148-2.

Lee, Y. S., Y. H. Kim, Y. Yi, and J. Kim (2000), A baffle design for an airglow photometer onboard the Korea Sounding Rocket-III, *Journal of the Korean Astronomical Society*, *33*, 165–172.

Lepine, D., D. Bryant, and D. Hall (1980), A 2.2-Hz modulation of auroral electrons imposed at the geomagnetic equator, *Nature*, *286*, 469–471.

Lessard, M. R. (2012), A Review of Pulsating Aurora, in *Auroral Phenomenology and Magnetospheric Processes: Earth and Other Planets, Washington DC American Geophysical Union Geophysical Monograph Series*, vol. 197, edited by A. Keiling, E. Donovan, F. Bagenal, and T. Karlsson, pp. 55–68, doi:10.1029/2011GM001187.

Luhmann, J. G. (1979), Auroral pulsations from atmospheric waves, *J. Geophys. Res.*, *84*, 4224–4228, doi:10.1029/JA084iA08p04224.

Lui, A. T. Y. (1991a), A synthesis of magnetospheric substorm models, *J. Geophys. Res*, *96*(A2), 1849–1856, doi:10.1029/90JA02430.

Lui, A. T. Y. (1991b), Extended consideration of a synthesis model for magnetospheric substorms, in *Magnetospheric Substorms, Washington DC American Geophysical Union Geophysical Monograph Series*, vol. 64, edited by J. R. Kan, T. A. Potemra, S. Kokubun, and T. Iijima, pp. 43–60, doi:10.1029/GM064p0043.

Lynch, K. A., D. Hampton, M. Mella, B. Zhang, H. Dahlgren, M. Disbrow, P. M. Kintner, M. Lessard, E. Lundberg, and H. C. Stenbaek-Nielsen (2012), Structure and dynamics of the nightside poleward boundary: sounding rocket and ground-based observations of auroral electron precipitation in a rayed curtain, *J. Geophys. Res.*, *117*(A16), A11202, doi:10.1029/2012JA017691.

McEwen, D. J., and D. A. Bryant (1978), Optical-particle characteristics of pulsating aurora, *Journal of Atmospheric and Terrestrial Physics*, *40*, 871–876, doi:0021-9169/78/0701-0871.

McEwen, D. J., E. Yee, B. A. Whalen, and A. W. Yau (1981), Electron energy measurements in pulsating auroras, *Canadian Journal of Physics*, *59*, 1106–1115, doi:10.1139/p81-146.

McPherron, R. L. (1991), Physical processes producing magnetospheric substorms and magnetic storms., in *Geomagnetism*, edited by J. A. Jacobs, pp. 593–739.

McPherron, R. L., C. T. Russell, and M. P. Aubry (1973), Satellite studies of magnetospheric substorms on August 15, 1968: 9. Phenomenological model for substorms, *J. Geophys. Res.*, *78*(16), 3131–3149, doi:10.1029/JA078i016p03131.

Meredith, N. P., R. B. Horne, R. M. Thorne, and R. R. Anderson (2009), Survey of upper band chorus and ECH waves: Implications for the diffuse aurora, *J. Geophys. Res.*, *114*(A7), n/a–n/a, doi:10.1029/2009JA014230.

Miyoshi, Y., Y. Katoh, T. Nishiyama, T. Sakanoi, K. Asamura, and M. Hirahara (2010), Time of flight analysis of pulsating aurora electrons, considering wave-particle interactions with propagating whistler mode waves, *J. Geophys. Res.*, *115*(A10), A10,312, doi:10.1029/2009JA015127.

Nemzek, R., P. Malcolm, and J. Winckler (1992), Comparison of Echo 7 field line length measurements to magnetospheric model predictions, *J. Geophys. Res.*, *97*(A2), 1279–1287, doi:10.1029/91JA02658.

Nemzek, R., R. Nakamura, D. Baker, R. Belian, D. McComas, M. Thomsen, and T. Yamamoto (1995), The relationship between pulsating auroras observed from the ground and energetic electrons and plasma density measured at geosynchronous orbit, *J. Geophys. Res.*, *100*(A12), 23,935–23,944, doi:10.1029/95JA01756.

Ni, B., R. M. Thorne, Y. Y. Shprits, and J. Bortnik (2008), Resonant scattering of plasma sheet electrons by whistler-mode chorus: Contribution to diffuse auroral precipitation, *Geophys. Res. Lett.*, *35*(11), L11,106, doi:10.1029/2008GL034032.

Nishimura, Y., J. Bortnik, W. Li, R. M. Thorne, L. R. Lyons, V. Angelopoulos, S. B. Mende, J. W. Bonnell, O. L. Contel, C. Cully, R. Ergun, and U. Auster (2010), Identifying the driver of pulsating aurora, *Science*, *330*(6000), 81–84, doi:10.1126/science.1193186.

Nishimura, Y., J. Bortnik, W. Li, R. M. Thorne, L. R. Lyons, V. Angelopoulos, S. B. Mende, J. Bonnell, O. Le Contel, C. Cully, R. Ergun, and U. Auster (2011a), Estimation of magnetic field mapping accuracy using the pulsating aurora-chorus connection, *Geophys. Res. Lett.*, *38*, L14110, doi:10.1029/2011GL048281.

Nishimura, Y., J. Bortnik, W. Li, R. M. Thorne, L. Chen, L. R. Lyons, V. Angelopoulos, S. B. Mende, J. Bonnell, O. Le Contel, C. Cully, R. Ergun, and U. Auster (2011b), Multievent study of the correlation between pulsating aurora and whistler mode chorus emissions, *J. Geophys. Res.*, *116*(A15), A11221, doi:10.1029/2011JA016876.

Nishiyama, T., T. Sakanoi, Y. Miyoshi, Y. Katoh, K. Asamura, S. Okano, and M. Hirahara (2011), The source region and its characteristic of pulsating aurora based on the Reimei observations, *J. Geophys. Res.*, *116*(A15), A03226, doi:10.1029/2010JA015507.

Oguti, T. (1975), *Metamorphoses of Aurora*, Memoirs of National Institute of Polar Research: Aeronomy, National Institute of Polar Research.

Oguti, T. (1976), Recurrent auroral patterns, *J. Geophys. Res.*, *81*, 1782–1786, doi: 10.1029/JA081i010p01782.

Oguti, T., and T. Watanabe (1976), Quasi-periodic poleward propagation of on-off switching aurora and associated geomagnetic pulsations in the dawn, *Journal of Atmospheric and Terrestrial Physics*, *38*, 543–551.

Oguti, T., S. Kokubun, K. Hayashi, K. Tsuruda, S. Machida, T. Kitamura, O. Saka, and T. Watanabe (1981), Statistics of pulsating auroras on the basis of all-sky TV data from five stations. I - Occurrence frequency, *Canadian Journal of Physics*, *59*, 1150–1157, doi:10.1139/p81-152.

Oguti, T., K. Hayashi, T. Yamamoto, J. Ishida, T. Higuchi, and N. Nishitani (1986), Absence of hydromagnetic waves in the magnetospheric equatorial region conjugate with pulsating auroras, *J. Geophys. Res.*, *91*(A12), 13,711.

Oliven, M. N., and D. A. Gurnett (1968), Microburst phenomena: 3. an association between microbursts and VLF chorus, *J. Geophys. Res.*, *73*(7), 2355–2362, doi: 10.1029/JA073i007p02355.

Omholt, A. (1971), *The optical aurora*, Physics and chemistry in space, Springer-Verlag.

Omholt, A., and S. Berger (1967), The occurrence of auroral pulsations in the frequency range 0.01-0.1 c/s over Tromsø, *Planet. Space Sci.*, *15*, 1075, doi:10.1016/0032-0633(67)90174-2.

Paulson, K. V., and G. G. Shepherd (1966), Fluctuations in brightness from quiet-form auroras, *Canadian Journal of Physics*, *44*, 837, doi:10.1139/p66-070.

Rees, M. H., and D. Luckey (1974), Auroral electron energy derived from ratio of spectroscopic emissions. I - Model computations, *J. Geophys. Res.*, *79*, 5181–5186, doi: 10.1029/JA079i034p05181.

Rosenberg, T. J., R. A. Helliwell, and J. P. Katsufrakis (1971), Electron precipitation associated with discrete Very-Low-Frequency emissions, *J. Geophys. Res.*, *76*(34), 8445–8452, doi:10.1029/JA076i034p08445.

Royrvik, O. (1976), Pulsating aurora: Local and global morphology, Ph.D. thesis, Alaska Univ., College.

Royrvik, O., and T. Davis (1977), Pulsating aurora: Local and global morphology, *J. Geophys. Res.*, *82*(29), 4720–4740, doi:10.1029/JA082i029p04720.

Russell, C. T., and R. E. Holzer (1969), OGO 3 observations of ELF noise in the magnetosphere, 1. spatial extent and frequency of occurrence, *J. Geophys. Res.*, *74*(3), 755–777, doi:10.1029/JA074i003p00755.

Russell, C. T., and R. L. McPherron (1973), The magnetotail and substorms, *Space Science Reviews*, *15*, 205–266, doi:10.1007/BF00169321.

Saito, Y., S. Machida, M. Hirahara, T. Mukai, and H. Miyaoka (1992), Rocket observation of electron fluxes over a pulsating aurora, *Planetary and Space Science*, *40*(8), 1043–1054, doi:10.1016/0032-0633(92)90033-K.

Sandahl, I. (1984), Pitch angle scattering and particle precipitation in a pulsating aurora: An experimental study, *Tech. rep.*, Kiruna Geophysical Institute, Sweden.

Sandahl, I., L. Eliasson, and R. Lundin (1980), Rocket observations of precipitating electrons over a pulsating aurora, *Geophys. Res. Lett.*, *7*(5), 309–312, doi: 10.1029/GL007i005p00309.

Sato, N., M. Morooka, K. Minatoya, and T. Saemundsson (1998), Nonconjugacy of pulsating auroral patches near L= 6, *Geophys. Res. Lett.*, *25*(20), 3755–3758.

Sato, N., D. Wright, Y. Ebihara, M. Sato, Y. Murata, H. Doi, T. Saemundsson, S. Milan, M. Lester, and C. Carlson (2002), Direct comparison of pulsating aurora observed simultaneously by the FAST satellite and from the ground at Syowa, *Geophys. Res. Lett.*, *29*(21), 37–1.

Sato, N., D. Wright, C. Carlson, Y. Ebihara, M. Sato, T. Saemundsson, S. Milan, and M. Lester (2004), Generation region of pulsating aurora obtained simultaneously by the FAST satellite and a Syowa-Iceland conjugate pair of observatories, *J. Geophys. Res*, *109*(A10201), doi:10.1029/2004JA010419.

Sazhin, S., and M. Hayakawa (1992), Magnetospheric chorus emissions: A review, *Planetary and Space Science*, *40*(5), 681–697, doi:10.1016/0032-0633(92)90009-D.

Schlegel, K., and M. Füllekrug (2002), A D-region conductivity model from EISCAT VHF measurements, *Annales Geophysicae*, *20*, 1439–1445, doi:10.5194/angeo-20-1439-2002.

Selesnick, R. S., and J. B. Blake (2000), On the source location of radiation belt relativistic electrons, *J. Geophys. Res.*, *105*(A2), 2607–2624, doi:10.1029/1999JA900445.

Smith, M. J., D. A. Bryant, and T. Edwards (1980), Pulsations in auroral electrons and positive ions, *Journal of Atmospheric and Terrestrial Physics*, *42*, 167–178.

Stenbaek-Nielsen, H., and T. Hallinan (1979), Pulsating auroras: Evidence for noncollisional thermalization of precipitating electrons, *J. Geophys. Res.*, *84*(A7), 3257–3271.

Stenbaek-Nielsen, H., T. Davis, and N. Glass (1972), Relative motion of auroral conjugate points during substorms, *J. Geophys. Res.*, *77*(10), 1844–1858.

Stenbaek-Nielsen, H. C., E. M. Wescott, T. N. Davis, and R. W. Peterson (1973), Differences in auroral intensity at conjugate points, *J. Geophys. Res.*, *78*, 659–671, doi: 10.1029/JA078i004p00659.

StenbaekNielsen, H. (1980), Pulsating aurora: The importance of the ionosphere, *Geophys. Res. Lett.*, *7*(5), 353–356.

Størmer, C. (1955), *The polar aurora*, International monographs on radio, Clarendon Press.

Suszcynsky, D., J. Borovsky, M. Thomsen, D. McComas, and R. Belian (1997), Coordinated ground-based and geosynchronous satellite-based measurements of auroral pulsations, *Proceedings of SPIE*, *3237*, 2.

Swift, D., and D. Gurnett (1973), Direct comparison between satellite electric field measurements and the visual aurora, *J. Geophys. Res.*, *78*(31), 7306–7313.

Tagirov, V. R., V. I. Trakhtengerts, and S. A. Chernous (1986), The origin of pulsating auroral spots, *Geomagnetism and Aeronomy*, *26*, 600–604.

Thomas, R. W., and P. Rothwell (1979), A latitude effect in the periodicity of auroral pulsating patches, *Journal of Atmospheric and Terrestrial Physics*, *41*, 1179–1184.

Thorne, R. M., B. Ni, X. Tao, R. B. Horne, and N. P. Meredith (2010), Scattering by chorus waves as the dominant cause of diffuse auroral precipitation, *Nature*, *467*, 943–946, doi: 10.1038/nature09467.

Trakhtengerts, V., and M. Rycroft (2000), Whistler-electron interactions in the magnetosphere: new results and novel approaches, *Journal of Atmospheric and Solar-Terrestrial Physics*, *62*(17-18), 1719–1733.

Trakhtengerts, V. I., V. R. Tagirov, and S. A. Chernous (1986), A flow-through cyclotron maser and pulsed VLF emission, *Geomagnetism and Aeronomy*, *26*, 99–106.

Trakhtengerts, V. Y. (1995), Magnetosphere cyclotron maser: Backward wave oscillator generation regime, *J. Geophys. Res.*, *100*, 17,205–17,210, doi:10.1029/95JA00843.

Tsurutani, B. T., and E. J. Smith (1977), Two types of magnetospheric ELF chorus and their substorm dependences, *J. Geophys. Res.*, *82*(32), 5112–5128, doi: 10.1029/JA082i032p05112.

Tsyganenko, N. A., and M. I. Sitnov (2005), Modeling the dynamics of the inner magnetosphere during strong geomagnetic storms, *J. Geophys. Res.*, *110*(A03208), doi: 10.1029/2004JA010798.

Victor, L. J. (1965), Correlated auroral and geomagnetic micropulsations in the period range 5 to 40 seconds, *J. Geophys. Res.*, *70*, 3123–3130, doi:10.1029/JZ070i013p03123.

Viereck, R., and H. Stenbaek-Nielsen (1985), Pulsating aurora and hydrogen emissions, *J. Geophys. Res.*, *90*(A11), 11,035.

Villalon, E., and W. J. Burke (1991), Near-equatorial pitch angle diffusion of energetic electrons by oblique whistler waves, *J. Geophys. Res.*, *96*, 9655–9667, doi:10.1029/91JA00444.

Wahlund, J., H. Opgenoorth, and P. Rothwell (1989), Observations of thin auroral ionization layers by EISCAT in connection with pulsating aurora, *J. Geophys. Res.*, *94*(A12), 17,223.

Watanabe, M., A. Kadokura, N. Sato, and T. Saemundsson (2007), Absence of geomagnetic conjugacy in pulsating auroras, *Geophys. Res. Lett.*, *34*(15), L15,107, doi: 10.1029/2007GL030469.

Wescott, E., H. Stenbaek-Nielsen, T. Davis, and H. Peek (1976), The Skylab barium plasma injection experiments, 1. Convection observations, *J. Geophys. Res.*, *81*(25), 4487–4494.

Whalen, B. A., J. R. Miller, and I. B. McDiarmid (1971), Energetic particle measurements in a pulsating aurora, *J. Geophys. Res*, *76*(4), 978–986, doi:10.1029/JA076i004p00978.

Yamamoto, T. (1988), On the temporal fluctuations of pulsating auroral luminosity, *J. Geophys. Res.*, *93*(A2), 897–911.

Yau, A. W., B. A. Whalen, and D. J. McEwen (1981), Rocket-borne measurements of particle pulsation in pulsating aurora, *J. Geophys. Res.*, *86*(A7), 5673–5681, doi: 10.1029/JA086iA07p05673.